THE PROCEEDINGS OF
THE PHYSICAL SOCIETY

Section A

VOL. 65, PART 5 | 1 May 1952 | No. 389 A

On the Use of a Random Parameter in Combinatorial Problems

BY C. DOMB
Clarendon Laboratory, Oxford

MS. received 17th December 1951

ABSTRACT. Many problems in probability connected with n events occurring randomly in space can be substantially simplified by dealing first with an indefinite number of events distributed in a Poisson series. A combinatorial problem arising in cosmic-ray counting discussed recently by Schrödinger provides a good example, and several properties of the corresponding distribution are derived. A generalization of this problem is considered, and the method is also applied to the random division of a line.

§1. INTRODUCTION

IN a recent note Schrödinger (1951) has considered a combinatorial problem arising in connection with cosmic-ray counters when the possibility of more than one event occurring in each counter is allowed for. This is one of a class of problems in which it is substantially simpler to consider the number of events occurring as indefinite, and distributed in a Poisson series. The solution when the number of events is fixed can then readily be derived as a corollary, and properties such as the mean and mean square deviation can be simply deduced.

§2. THE COSMIC-RAY PROBLEM

The problem put to Schrödinger was as follows:

I. A tray of r equal counters is exposed to a cosmic-ray shower and hit by $n\,(\geqslant 1)$ rays. A particular ray hits one, and only one, counter, and the probability of its hitting any particular counter is $1/r$. What is the probability of precisely m counters going off?

We shall consider the following alternative problem:

II. Cosmic rays occur randomly in space and time, the mean number passing through a tray of r equal counters in a given time being λ. Each ray hits one, and only one, counter. What is the probability of precisely m counters going off?

Denote the probability in I by $w(n;\, r,\, m)$, and in II by $W(\lambda;\, r,\, m)$. The solution of I can easily be derived from II. It is well known that in II the probability of precisely n rays passing through the counters is $e^{-\lambda}\lambda^n/n!$. Hence,

we can divide $W(\lambda; r, m)$ into mutually exclusive cases in which precisely n rays have passed through, and write identically

$$W(\lambda; r, m) = \sum_{n=0}^{\infty} e^{-\lambda} \frac{\lambda^n}{n!} w(n; r, m). \qquad \ldots\ldots(1)$$

Thus, if we expand $W(\lambda; r, m)e^{\lambda}$ as a power series in λ we can obtain $w(n; r, m)$.

The solution of II is very straightforward since the counters are independent. The probability of no ray passing through a particular counter is equal to $\exp(-\lambda/r)\,(=q)$. The probability of one or more rays passing through is $[1-\exp(-\lambda/r)]\,(=p)$. The probability of m counters going off is

$${}^{r}C_m p^m q^{r-m} \qquad \left({}^{r}C_m \equiv \frac{r!}{m!\,(r-m)!}\right) \qquad \ldots\ldots(2)$$

and the distribution is binomial.

The practical problem, to estimate λ or p from m, is a straightforward problem of binomial estimation. As pointed out by Schrödinger, there is a difficulty in deriving an estimate when $m=r$. It is clear that in this case, if we set some arbitrary probability limit, the only conclusion we can reasonably draw is that $q<q_0$ or $\lambda>\lambda_0$. In statistical terminology we would say that the upper confidence limit has become infinite.

To derive Schrödinger's solution from (2) we must expand

$${}^{r}C_m(1-e^{-\lambda/r})^m(e^{-\lambda/r})^{r-m}\,e^{\lambda} = {}^{r}C_m(e^{\lambda/r}-1)^m \qquad \ldots\ldots(3)$$

as a power series in λ, and pick out the coefficient of $\lambda^n/n!$. This is easily seen to be

$${}^{r}C_m \sum_{t=0}^{m} {}^{m}C_{m-t}(-1)^t \frac{(m-t)^n}{r^n} = \frac{r!}{r^n(r-m)!} \sum_{t=0}^{m} (-1)^t \frac{(m-t)^n}{t!(m-t)!}, \qquad \ldots\ldots(4)$$

which is equivalent to eqn. (6) of Schrödinger's paper. It is clear from (3) that the series (4) is identically zero if $n<m$.

The moments and moment generating functions can be derived in an analogous manner. Denoting, for example, the moment generating functions for the distributions I and II by $f(n; r, \theta)$ and $F(\lambda; r, \theta)$ respectively, we have

$$\left.\begin{aligned} f(n; r, \theta) &= \sum_{m=0}^{\infty} w(n; r, m)\, e^{m\theta} \\ \text{and} \qquad F(\lambda; r, \theta) &= \sum_{m=0}^{\infty} W(\lambda; r, m)\, e^{m\theta}. \end{aligned}\right\} \qquad \ldots\ldots(5)$$

Hence, from (1)

$$F(\lambda; r, \theta) = \sum_{n=0}^{\infty} e^{-\lambda} \frac{\lambda^n}{n!} f(n; r, \theta), \qquad \ldots\ldots(6)$$

and a corresponding result holds for any of the moments. In particular, since for I

$$\left.\begin{aligned} \bar{m} &= rp = r(1-e^{-\lambda/r}), \\ \text{and} \qquad \overline{m^2} &= r^2p^2 + rpq = r^2(1-e^{-\lambda/r})^2 + re^{-\lambda/r}(1-e^{-\lambda/r}), \end{aligned}\right\} \qquad \ldots\ldots(7)$$

we deduce that, for II

$$\left.\begin{aligned} \bar{m} &= r[1-(1-1/r)^n], \\ \text{and} \quad \overline{m^2} &= r^2[1-2(1-1/r)^n + (1-2/r)^n] + r[(1-1/r)^n - (1-2/r)^n]. \end{aligned}\right\} \qquad \ldots\ldots(8)$$

Needless to say it would have been a much more complicated matter to have derived (8) directly from (4).

§ 3. THE DISTRIBUTION OF CLUSTERS

A natural generalization which suggests itself is to divide the counters into groups through which exactly k rays have passed. Let us denote the probability that there are m counters of this type by $w_k(n; r, m)$ for I, and $W_k(\lambda; r, m)$ for II. Clearly

$$\left.\begin{aligned} w(n; r, m) &= \sum_{k=1}^{\infty} w_k(n; r, m), \\ W(\lambda; r, m) &= \sum_{k=1}^{\infty} W_k(\lambda; r, m). \end{aligned}\right\} \quad \ldots\ldots(9)$$

The solution of II is binomial as before, except that now the probability of k rays passing through a particular counter is $\exp(-\lambda/r)(\lambda/r)^k/k!\,(=p_k)$. Hence,

$$W_k(\lambda; r, m) = {}^rC_m p_k{}^m q_k{}^{r-m} \qquad (q_k = 1-p_k). \qquad \ldots\ldots(10)$$

Expanding $e^{\lambda} W_k(\lambda; r, m)$ as before we find that $w_k(n; r, m)$ is the coefficient of $\lambda^n/n!$ in

$${}^rC_m \frac{\lambda^{km}}{r^{km}(k!)^m}\left[e^{\lambda/r} - \frac{\lambda^k}{r^k k!}\right]^{r-m} \qquad \ldots\ldots(11)$$

which, after a little simplification, gives

$$\frac{r!}{r^n m!}\sum_{t=0}^{\tau}(-1)^t \frac{(r-m-t)^{n-km-kt}}{t!\,(r-m-t)!}\,\frac{1}{(k!)^{t+m}}\,\frac{n!}{(n-km-kt)!} \qquad (n \geqslant km) \quad \ldots\ldots(12)$$

(where $n \geqslant km$ and τ is the integral part of $n/k-m$).

Again the mean and mean square of the $W_k(\lambda; r, m)$ distribution are given by

$$\left.\begin{aligned} \bar{m} &= \frac{r}{k!}\left(\frac{\lambda}{r}\right)^k e^{-\lambda/r}, \\ \overline{m^2} &= \frac{r^2}{(k!)^2}\left(\frac{\lambda}{r}\right)^{2k} e^{-2\lambda/r} + \frac{r}{k!}\left(\frac{\lambda}{r}\right)^k e^{-\lambda/r}\left[1 - \frac{1}{k!}\left(\frac{\lambda}{r}\right)^k e^{-\lambda/r}\right]. \end{aligned}\right\} \quad \ldots\ldots(13)$$

Proceeding as before, we deduce the corresponding moments of the $w_k(n; r, m)$ distribution,

$$\left.\begin{aligned} \bar{m} &= \frac{rn!}{k!\,(n-k)!}\left(\frac{1}{r}\right)^k\left(1-\frac{1}{r}\right)^{n-k}, \\ \overline{m^2} &= \frac{r(r-1)n!}{(n-2k)!\,(k!)^2}\left(\frac{1}{r}\right)^{2k}\left(1-\frac{2}{r}\right)^{n-2k} + \frac{rn!}{k!\,(n-k)!}\left(\frac{1}{r}\right)^k\left(1-\frac{1}{r}\right)^{n-k}. \end{aligned}\right\} \quad .(14)$$

The task of deriving these moments directly would have been even more formidable than before.

A number of authors have considered the problem of the distribution of aggregates in a random set of points (Silberstein 1945, Berg 1945, Mack 1948). The definition of an aggregate was as follows: a region of given size and shape is moved all over the total length or area, and any set of k points falling within the region constitutes a k-aggregate. It is clear on this definition that any point may belong to several different aggregates, and for some purposes this may not be satisfactory. The present problem suggests an alternative possibility of dividing the total length or area arbitrarily into r cells, the number of points falling into each cell constituting an aggregate. The distribution of aggregates is then given by eqns. (12) and (14) above.

§4. THE RANDOM DIVISION OF A LINE

Suppose n points are taken at random on a line of length l. They subdivide the line into $(n+1)$ intervals $x_1, x_2 \ldots . x_{n+1}$, and problems connected with the distribution of intervals have been discussed by many writers (see Moran 1947 for references). The method described in the present paper was first used for problems in which each point is the left-hand end-point of an interval of fixed length (Domb 1946). It can readily be applied to several other problems of a similar type. We always consider the associated problems in which events occur randomly on the line the mean number per unit length being λ; the probability of n events occurring on the line is then $\exp(-\lambda l)(\lambda l)^n/n!$. Let us first apply the method to the determination of the probability distribution of the length of the first interval x_1. For the associated problem we have

$$\left.\begin{aligned} W(\lambda; x_1)\,dx_1 &= \lambda e^{-\lambda x_1}\,dx_1 \quad & x_1 \leqslant l, \\ &= e^{-\lambda l} & x_1 = l. \end{aligned}\right\} \qquad \ldots\ldots(15)$$

Hence, expanding $W(\lambda; x_1)\, e^{\lambda l}$ as before, we find

$$w(n; x_1)\,dx_1 = \frac{n(l-x_1)^{n-1}}{l^n}\,dx_1 = \frac{n}{l}\left(1-\frac{x_1}{l}\right)^{n-1} dx_1 \quad \begin{pmatrix} n \geqslant 1 \\ x_1 \leqslant l \end{pmatrix}. \qquad \ldots\ldots(16)$$

It is clear that the second line of (15) can be ignored if we are interested in $n \geqslant 1$. Similarly, if we require the joint probability distribution of the first r intervals, we have

$$\begin{aligned} &W^{(r)}(\lambda; x_1, x_2 \ldots . x_r)\,dx_1 \ldots . dx_r \\ &\qquad = \lambda^r e^{-\lambda(x_1 + \ldots . + x_r)}\,dx_1 \ldots . dx_r \quad (x_1 + \ldots . x_r < l) \qquad \ldots\ldots(17) \end{aligned}$$

and hence

$$\begin{aligned} &w^{(r)}(n; x_1 \ldots . x_r) \\ &= \frac{n(n-1)\ldots .(n-r+1)}{l^r}\left(1-\frac{x_1+x_2+\ldots . x_r}{l}\right)^{n-r} \quad (n \geqslant r). \qquad \ldots\ldots(18) \end{aligned}$$

The moment generating function $F(\lambda; \theta_1)$ of the $W(\lambda; x_1)$ distribution is

$$e^{l(\theta_1-\lambda)} + \int_0^l \lambda e^{-x_1(\lambda-\theta_1)}\,dx_1 = \frac{\lambda}{\lambda-\theta_1}[1-e^{-l(\lambda-\theta_1)}] + e^{l(\theta_1-\lambda)}. \qquad \ldots\ldots(19)$$

Hence, using an expansion analogous to (6),

$$f(n; \theta_1) = \frac{n!}{l^n {\theta_1}^n}\left[e^{l\theta_1} - 1 - l\theta_1 - \frac{l^2{\theta_1}^2}{2!} \ldots . - \frac{l^{n-1}{\theta_1}^{n-1}}{(n-1)!}\right], \qquad \ldots\ldots(20)$$

and in particular

$$\overline{x_1} = \frac{l}{(n+1)}, \quad \overline{x_1^2} = \frac{l^2 2!}{(n+1)(n+2)}, \quad \overline{x_1^r} = \frac{l^r r!}{(n+1)\ldots .(n+r)}. \qquad \ldots\ldots(21)$$

We can proceed similarly to determine the correlations between successive intervals. For example, in the Poisson problem, for a line of indefinite length x_1 and x_2 are uncorrelated. The finite length of the line only introduces a correlation when less than two events occur. Hence, if we ignore this latter possibility and proceed as before, our results will be correct if $n \geqslant 2$. For the Poisson distribution with a line of indefinite length we have the very simple result

$$\overline{x_1^r} = \frac{r!}{\lambda^r} \qquad \overline{x_1^r x_2^s} = \frac{r!\,s!}{\lambda^{r+s}}. \qquad \ldots\ldots(22)$$

Thus, for the case of n points we deduce that

$$\left.\begin{aligned} \overline{x_1 x_2} &= \frac{l^2}{(n+1)(n+2)}, \\ \overline{x_1{}^r x_2{}^s} &= \frac{r!\,s!}{(r+s)!}\,\overline{x_1{}^{r+s}} = \frac{r!\,s!\,l^{r+s}}{(n+r)\ldots(n+r+s)} && (n \geqslant 2), \\ x_1{}^{r_1}\ldots x_t{}^{r_t} &= \frac{r_1!\ldots r_t!}{(r_1+\ldots r_t)!}\,\overline{x_1{}^{r_1+\ldots r_t}} = \frac{r_1!\ldots r_t!\,l^{r_1+\ldots r_t}}{(n+1)\ldots(n+r_1+\ldots r_t)} && (n \geqslant t). \end{aligned}\right\} \quad (23)$$

ACKNOWLEDGMENT

The author is indebted to the University of Oxford for the award of an I.C.I. Fellowship.

REFERENCES

Berg, W. F., 1945, *Phil. Mag.*, **36**, 337.
Domb, C., 1947, *Proc. Camb. Phil. Soc.*, **43**, 329.
Mack, C., 1948, *Phil. Mag.*, **39**, 778.
Moran, P. A. P., 1947, *J. R. Statist. Soc.*, **9**, 92.
Schrödinger, E., 1951, *Proc. Phys. Soc.* A, **64**, 1040.
Silberstein, L., 1945, *Phil. Mag.*, **36**, 319.

The Range of Tensor Forces in the Deuteron Ground State

By D. G. PADFIELD
Department of Mathematics, Durham Colleges in the University of Durham

Communicated by N. Kemmer ; *MS. received* 15*th October* 1951

ABSTRACT. A set of nuclear parameters (ranges and depths of potential wells) yielding the established values of the binding energy, quadrupole moment and magnetic moment of the deuteron, and consistent with the other experimental data relevant to the ground state of the neutron–proton system has been found.

§ 1. INTRODUCTION

The ground state of the neutron–proton system is of particular interest in the study of nuclear forces for the following reasons: it is a state of a two-particle system, so the analytical difficulties characteristic of many-body problems do not arise, and the complication of many-body forces is also avoided; it is a *stable* nuclear state, so several different types of experimental data are available; and its several properties formerly led investigators to incompatible estimates of the range of the neutron–proton force.

The main data relevant to the neutron–proton interaction are:

(1) The binding energy E of the deuteron ($E \simeq 2{\cdot}23$ Mev).
(2) The quadrupole moment Q of the deuteron ($Q \simeq 2{\cdot}76 \times 10^{-27}$ cm^2).
(3) The magnetic moment μ of the deuteron ($\mu = 0{\cdot}8565$ n.m.).
(4) Neutron–proton scattering cross sections and angular distributions.
(5) Cross section for photodisintegration, and cross section for the converse process of deuteron formation by proton–neutron collision.

Of these, the first two can be determined quite accurately from experiment, and are also quite satisfactorily derivable from theory. The experimental accuracy of the third datum is also good, but theoretical calculation is made uncertain by relativistic effects; however, it provides an estimate of the proportion of D state to be expected in the deuteron ground state—usually taken as 4 per cent.

In neutron–proton scattering, states other than the ground state are involved, and this means that assumptions about exchange properties which are not involved for (1), (2) and (3) have to be made to interpret data (4). In the case of low-energy scattering, an explicit *exchange* assumption can be replaced by the assumption of the charge-independence hypothesis, viz. that the ^{1}S neutron–proton force is equal to the ^{1}S proton–proton force as derived from proton–proton scattering experiments. Data of type (5) of useful accuracy have only recently become available (Snell, Barker and Sternberg 1949, Wilson, Collie and Halban 1949, Barnes, Stafford and Wilkinson 1950). Datum (2) demands the inclusion of tensor forces in the interaction, but the quadrupole moment is not so large that the forces can be entirely tensor in character.

Therefore the simplest type of investigation pretending to some degree of completeness is an examination of the ground-state of the neutron–proton system, central and tensor forces being considered: the postulated forces must lead to the values of E, Q and μ given by experiment, and must be consistent with data of types (4) and (5).

It is well known that the exact law of radial dependence of the nuclear interaction has little effect on most of the measurable quantities, at least at low energies. This fact is implicit in the now well-established use of 'effective range'. It is, therefore, quite sensible to make calculations using potential wells of any convenient shape, say square wells, find the appropriate ranges and depths, and translate into 'effective ranges' or into the equivalent parameters for other well-shapes as required (cf. Blatt 1948).

For the ground state of the deuteron, using a chosen well-shape and central and tensor forces, the nuclear parameters may be taken as four in number—two ranges and two depths—i.e. one parameter more than can be determined by using data (1)–(3). Rarita and Schwinger (1941) found for a square-well potential and *equal* tensor and central ranges a unique solution satisfying (1)–(3). The value of the common range was $2{\cdot}8 \times 10^{-13}$ cm. This solution also gave extremely good agreement with the data of type (4), and, with some reservations, those of type (5) then available. More recent experiments, particularly those on the scattering of neutrons in ortho and para hydrogen, however, have indicated that this range of $2{\cdot}8 \times 10^{-13}$ cm is much too large to be compatible with data (4). Blatt and Jackson (1949) gave $1{\cdot}56 \times 10^{-13}$ cm (corresponding to a square well of roughly $1{\cdot}7 \times 10^{-13}$ cm) as the best value for the effective range in the triplet state. This figure has been revised to $1{\cdot}74 \times 10^{-13}$ cm by Hughes, Burgy and Ringo (1950).

The results also of Barnes, Stafford and Wilkinson (1950) have been shown by Schiff (1950) to be consistent with an effective range of about $1{\cdot}74 \times 10^{-13}$ cm for the central force.

Interesting figures have been given by Tsi-Ming Hu and Massey (1949) who derive optimum ranges to fit separately (*a*) the magnetic moment, (*b*) 1–6 Mev n–p scattering, (*c*) scattering of thermal neutrons by hydrogen molecules,

(*d*) diffraction of neutrons by hydrogen in crystals, (*e*) photodisintegration of the deuteron. For a square well only the Rarita–Schwinger figure (for (*a*)) lies outside the region 1·4 to 2×10^{-13} cm.

On the other hand, Bohm and Richman (1947) quote unpublished work by Sen (supported by later evidence) showing that $2{\cdot}4 \times 10^{-13}$ cm is the smallest range for which quadrupole moment and magnetic moment of the deuteron can be simultaneously satisfied. Both of these quantities are primarily dependent on the tensor force.

The above mutually exclusive estimates of range are based on the assumption of a *single* range common to all the types of force which may be acting. The discrepancy of the results may therefore be read to mean that two or more ranges must be used if the properties of the neutron–proton ground state are to be satisfactorily accounted for. In the present work this hypothesis is investigated. We shall discuss the possibility of describing the ground-state phenomena in terms of a square potential well for the central force and a square well, but of different depth *and* width, for the tensor force.

To conform to the indications of scattering and photodisintegration experiments we shall make the central force range of the order of magnitude 1·4 to 2×10^{-13} cm, while the tensor range and the two depths will be chosen to fit the data (1), (2) and (3). This is the main object of the following work. The general mode of interdependence of parameters and physical quantities will also be illustrated, and the usefulness and limitations of the differential analyser as a tool for this type of problem will be seen.

§ 2. THE DEUTERON EQUATIONS

The equations for the neutron–proton system can be written

$$\left.\begin{aligned} &\frac{d^2u}{dr^2} + (A_r - \alpha^2)u = -B_r w \\ &\frac{d^2w}{dr^2} - \frac{6w}{r^2} + \left(A_r - \alpha^2 - \frac{B_r}{\sqrt{2}}\right) w = -B_r u \end{aligned}\right\} \quad \ldots\ldots \text{I}$$

where A_r, α^2 and $B_r/2\sqrt{2}$ are proportional to the central force potential, binding energy and tensor force potential respectively.

We shall use the square-well potentials

$$A_r = A, \; r<a; \quad A_r = 0, \; r>a;$$
$$B_r = B, \; r<b; \quad B_r = 0, \; r>b.$$

In this paper the units of A, B, a, b are those which were found convenient in the course of calculation. These units are defined, and the notation put into conformity with previous work, by the relations

$a = 0{\cdot}115\, r_0$ where r_0 = range of ordinary forces in 10^{-13} cm
$b = 0{\cdot}115\epsilon\, r_0$ where ϵr_0 = range of tensor forces in 10^{-13} cm
$A = 1{\cdot}83J$ where J = depth of ordinary well in Mev
$B = 5{\cdot}17\gamma J$ where γJ = depth of tensor well in Mev.

The boundary conditions to be satisfied by equations I are: u, w both zero at $r=0$, u, w both $\to 0$ at $r \to \infty$, u, w, du/dr, dw/dr continuous at $r=a$, $r=b$.

Given a, b, A, B, the two simultaneous differential equations for u, w with two-point boundary conditions (0, ∞) for each of u, w would lead to an eigenvalue problem in α^2. Since α^2 is in fact known from experiment (binding energy)

we shall instead treat equations I as an eigenvalue problem in one of the other parameters a, b, A or B, choosing whichever is mathematically more convenient.

It is clear that the functions u, w, have different analytical forms in each of the three regions: (1) $0<r<a$, (2) $a<r<b$, (3) $b<r<\infty$, and that in region (1) a series solution will be tolerably convenient, while in region (3), where $A_r=B_r=0$, the equations separate and must have the solutions

$$u=U\exp(-\alpha r), \quad w=W\left(1+\frac{3}{\alpha r}+\frac{3}{\alpha^2 r^2}\right)\exp(-\alpha r),$$

where U, W are constants.

To use a series or other analytic form of solution in region (2) and to find the analytic conditions for simultaneous fitting at $r=a$, b looks unwieldy, although Demeur (1950) succeeded in doing some work along these lines, viz. for $r_0=2{\cdot}8$ and $\epsilon=0{\cdot}8$, $0{\cdot}9$ and 1. This work enabled him to show that for $r_0=2{\cdot}8$ the experimental values of binding energy, quadrupole moment and magnetic moment could be accounted for only if $\epsilon=1$.

In the present work fitting at $r=a$, b was obtained by linear combination of trial solutions. In region (2) numerical solutions were used, and, except for the final results, in which maximum accuracy was desired, the Cambridge differential analyser was used to perform this numerical integration.

To make good use of this mechanical aid it is necessary, first, to obtain a fairly good estimate of the eigenvalue before attempting the exact solution and to have a rough idea of the values of u, w and their derivatives in the numerical integration region, and secondly to treat A, B as given parameters (since they must be represented by gears on the machine) and either a or b as eigenvariable (preferably the greater, b), since a, b can easily be varied by running the machine for a longer or shorter time before altering the gears representing A_r, B_r.

The procedure used was as follows:

(i) Approximate eigenvalues were found by an ordinary variational method. To be more explicit, a, b, A were allowed to take values of the sort of magnitude to be expected, i.e. $8{\cdot}7a=r_0\sim 1{\cdot}2$ to 3 (10^{-13} cm), $8{\cdot}7b=\epsilon r_0\sim 2{\cdot}0$ to 7 (10^{-13} cm), $0{\cdot}548A=J\sim 0$ to 100 (MeV) and for each set of a, b, A the corresponding eigenvalue B was found. This approximate calculation also provided a rough guide to the behaviour of u, w, du/dr, dw/dr, and, consequently, an order of magnitude guide to the values of quadrupole moment and percentage D state resulting from each chosen set of a, b, A.

(ii) The exact solution could now be tackled. Sets of a, A, B were chosen on the guidance of the variational calculation; b was yet to be determined exactly. The differential analyser was set up for solving equations I with these values of A, B. It was also arranged that the value of A_r could quickly be altered from A to 0 at the appropriate point ($r=a$) of the run.

(iii) Since the differential analyser cannot be used at or too close to the singularity at the origin, a series solution was used for small values of r ($r\leqslant 0{\cdot}1$ was chosen for simplicity). The differential analyser started from the series solution values of u, w, du/dr, dw/dr at $r=0{\cdot}1$, and the mechanical solution was run out to $r=a$, where A_r was put equal to zero and the solution continued to the region $r\sim b$.

(iv) The exact value of b was determined as described below, the corresponding eigenvalues u, w, du/dr, dw/dr at $r\leqslant b$ deduced, and the asymptotic solutions fitted on to these differential analyser functions at $r=b$.

§ 3. DETERMINATION OF b

The general solution of the two coupled second-order differential equations I involves four arbitrary constants, but the boundary condition $u(0)=0$, $w(0)=0$ reduces this number to two, and the homogeneity of the equations means that a third is an irrelevant multiplicative factor. Hence if (u_1, w_1), (u_2, w_2) are two independent solutions non-singular at the origin, the eigensolution will be of the form $(u_1+\beta u_2, w_1+\beta w_2)$.

With β chosen so that there was rough agreement with the variational estimates of the functions and their derivatives, a solution was run out to the region $r\sim b$. The value of r at the point where the function u would fit on to the required asymptotic form $U\,\mathrm{e}^{-\alpha r}$ we call b_1, i.e. we define b_1 by

$$\left(\frac{1}{u}\frac{du}{dr}\right)_{b_1} = -\alpha.$$

Similarly we define b_2 from the differential analyser solution for w by the requirement

$$\left(\frac{1}{w}\frac{dw}{dr}\right)_{b_2} = -\alpha\left[\left(1+\frac{3}{\alpha r}+\frac{6}{\alpha^2 r^2}+\frac{6}{\alpha^3 r^3}\right)\Big/\left(1+\frac{3}{\alpha r}+\frac{3}{\alpha^2 r^2}\right)\right]_{b_2}.$$

For an eigensolution β must be adjusted until $b_1=b_2$ $(=b)$. At the expense of one or two extra runs on the machine (which were, however, very useful checks on mechanical and operational accuracy), solutions so close to the eigensolution were obtained that b could be determined as the point of intersection of graphs of b_1 against β and b_2 against β.

Some comments will now be made on the several parts of the procedure outlined above.

§ 4. THE VARIATIONAL CALCULATIONS

Since the object of the variational calculation was rather to obtain information over a wide field than to get accurate results in a limited one, the simple polynomial forms $u=r+\alpha' r^3+\beta' r^5$, $w=\gamma' r^3+\delta' r^5$ were taken, these promising a reasonable reward for the amount of labour involved. (The primes distinguish the coefficients from α's and β's used elsewhere.)

The above forms were fitted on to

$$u=U\,\mathrm{e}^{-\alpha r},\ w=W\,\mathrm{e}^{-\alpha r}\left(1+\frac{3}{\alpha r}+\frac{3}{\alpha^2 r^2}\right)$$

at $r=b(>a)$ (or in one case $r=a>b$).

This requirement completely determines the shape of the w function, only its size relative to u being adjustable. However, as experiment requires only about 4% D state, the above forms, giving the greater flexibility to the u function, seem reasonable.

The information about eigenvalue behaviour obtained from this approximation is shown in figs. 1 (*a*), (*b*).

The circled points are accurately known, those on the $B=0$ axis from simple calculation, others from data given by Rarita and Schwinger. The full curves are those deduced from the variational calculation; the dotted curves are estimated correction curves adjusted to pass through the accurately known points. It will be seen that the variational calculation looks tolerably good for b of the same order as a, but bad for b much greater than a.

Figure 2 shows the quadrupole moment behaviour indicated by the variational calculations. It is to be expected that these curves are much less reliable than those of fig. 1.

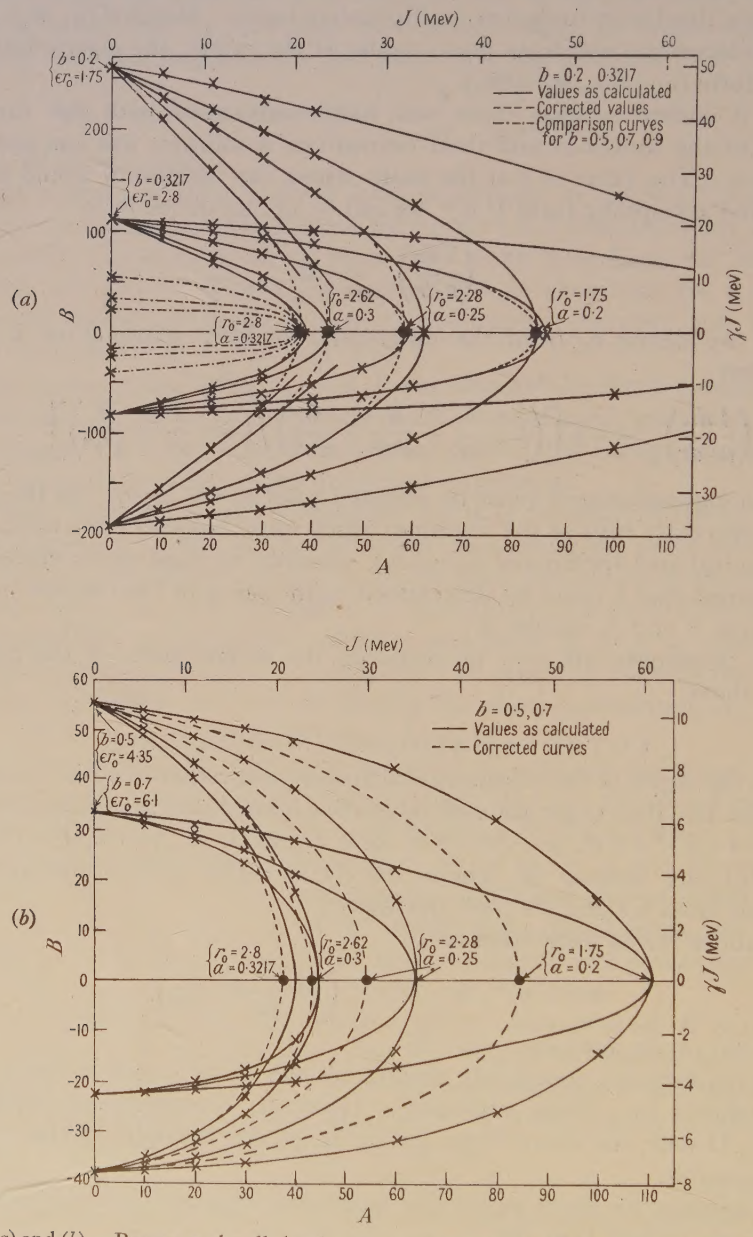
J (MeV)
b = 0·2 , 0·3217
Values as calculated
Corrected values
Comparison curves for b = 0·5, 0·7, 0·9
b = 0·2 εr0 = 1·75
b = 0·3217 εr0 = 2·8
r0 = 2·62 α = 0·3
r0 = 2·28 α = 0·25
r0 = 1·75 α = 0·2
r0 = 2·8 α = 0·3217
(a)
B
γJ (MeV)
A
b = 0·5, 0·7
Values as calculated
Corrected curves
b = 0·5 εr0 = 4·35
b = 0·7 εr0 = 6·1
(b)

Figs. 1 (*a*) and (*b*). Ranges and well depths giving correct energy (rough variational calculation).

In figs. 1–7:

$a = 0{\cdot}115\ r_0$ where r_0 = range of ordinary forces in 10^{-13} cm.
$b = 0{\cdot}115\ \epsilon r_0$ where ϵr_0 = range of tensor forces in 10^{-13} cm.
$A = 1{\cdot}826\ J$ where J = depth of ordinary well in Mev.
$B = 5{\cdot}17\ \gamma J$ where γJ = depth of tensor well in Mev.
Q = electric quadrupole moment in 10^{-27} cm^2.

§ 5. THE MECHANICAL SET-UP ON THE DIFFERENTIAL ANALYSER

In designing a set-up for the differential analyser the following considerations are important: (i) The functions on the displacement tables should be such that it is easy to satisfy the initial and boundary conditions. (ii) The generation of awkward multiples and awkward functions (e.g. $(A_r-\alpha^2-B_r/\sqrt{2})w$ and $6w/r^2$) must be allowed for. (iii) Each integrator should achieve its maximum displacement at some point of the run. (This requires a knowledge of the magnitudes

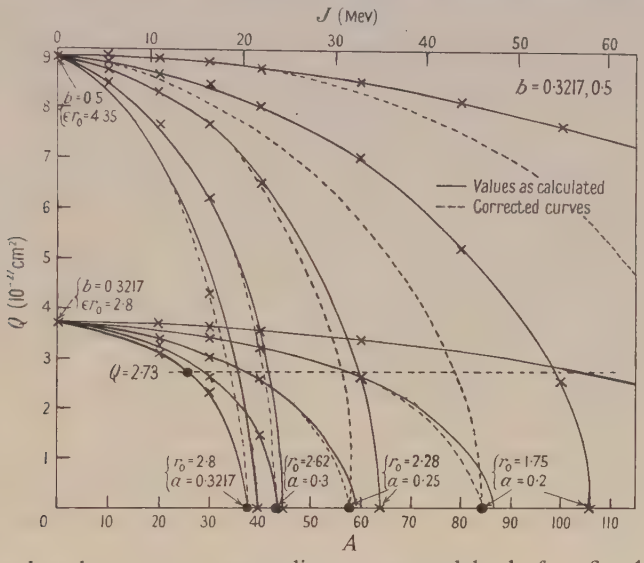

Fig. 2. Quadrupole moments corresponding to ranges and depths from figs. 1 (*a*) and (*b*).

of u, w, etc., conveniently provided by the variational calculation already carried out.) Also the multiples used on each shaft must be such that all rotate at similar speeds. These conditions are required for efficient running and best accuracy. The first of the above requirements was satisfied by using the integrated form of the equations

$$\frac{du}{dr}+(A_r-\alpha^2)\int^r u\,dr=-B_r\int^r w\,dr,$$

$$\frac{dw}{dr}-\int^r\frac{6w}{r^2}\,dr+\left(A_r-\alpha^2-\frac{B_r}{\sqrt{2}}\right)\int^r w\,dr=-B_r\int^r u\,dr.$$

The integrator displacements involved were then u, w, du/dr, dw/dr, initial conditions for which were easily available, and the continuity conditions for these functions at $r=a$, $r=b$ meant that no recalculation or resetting was necessary.

The integration, then, followed the scheme:

$$\frac{du}{dr}\longrightarrow u\longrightarrow\begin{cases}(A_r-\alpha^2)\int u\,dr & \longrightarrow \dfrac{du}{dr},\\ B_r\int u\,dr & \longrightarrow \dfrac{dw}{dr},\end{cases}$$

$$\frac{dw}{dr}\longrightarrow w\longrightarrow\begin{cases}\displaystyle\int\frac{6w}{r^2}\,dr & \longrightarrow \dfrac{dw}{dr},\\ \left(A_r-\alpha^2-\dfrac{B_r}{\sqrt{2}}\right)\displaystyle\int w\,dr & \longrightarrow \dfrac{dw}{dr},\\ B_r\displaystyle\int w\,dr & \longrightarrow \dfrac{du}{dr}.\end{cases}$$

The essential integrations $du/dr \to u \to \int u\,dr$, $dw/dr \to w \to \int w\,dr$ used four of the eight integrators of the Cambridge machine.

The term $\int (w/r^2)\,dr$ demanded the further use of *one* integrator if an input curve were used (say an input curve of $1/r$, so that $\int (w/r^2)\,dr = -\int w d(1/r)$), or of *two* if it were desired to avoid the use of an input table. The second of these alternatives was chosen, and was carried out by means of a feedback set-up based on the two relations

$$\int^r (r-K)\,d\left(\int^r \frac{w}{r}\,dr\right) = \int^r w\,dr - K\int^r \frac{w}{r}\,dr. \qquad \ldots\ldots(1)$$

$$\int^r (r-K)\,d\left(\int^r \frac{w}{r^2}\,dr\right) = \int^r \frac{w}{r}\,dr - K\int^r \frac{w}{r^2}\,dr. \qquad \ldots\ldots(2)$$

Thus, in step (1), given $\int w\,dr$ and a displacement $(r-K)$, we generated $\int (w/r)\,dr$, and, similarly, from (2), having $\int (w/r)\,dr$ and displacement $(r-K)$ we found $\int (w/r^2)\,dr$.

This left two integrators free out of the eight: these were conveniently used for the multiplications by $(A_r - \alpha^2)$ and $(A_r - \alpha^2 - B/\sqrt{2})$ which otherwise could only have been represented by the nearest fraction obtainable from a chain of gears of the ratios supplied for the differential analyser.

Since no integrator was left for the B multiplications, the values of B were chosen so as to be easily obtainable from a chain of gears.

The set-up, conforming to the requirements of (iii) above, and allowing for a running time of about half an hour per solution, was designed by Mr. B. Noble, to whom my thanks are due for much help and advice.

§ 6. RESULTS OBTAINED FROM THE DIFFERENTIAL ANALYSER SOLUTIONS

The results obtained from the differential analyser consist of the eigenvalue deduced for b given a, A, B, and tables of values of u, w, du/dr, dw/dr, for $0{\cdot}1 \leqslant r \leqslant b$, the interval of tabulation being 0·025. The initial and asymptotic forms of the functions can then be calculated, and the corresponding quadrupole moment Q and the percentage D state D can be found.

These, the most direct data obtainable, are shown (expressed in terms of r_0, J etc.) in table 1.

Our main interest, however, is not to find Q and D for arbitrary a, A, B, but to investigate the possibility of satisfying the simultaneous requirements $E \simeq 2{\cdot}23$ MeV, $Q \simeq 2{\cdot}76 \times 10^{-27}$ cm^2, $D \simeq 4\%$ for a chosen value of a, the values of A, B, b being deduced. (At the time when this work was done the value of E used was 2·18 MeV and that of Q $2{\cdot}73 \times 10^{-27}$ cm^2. The calculations have been revised to the Bell and Elliot value of $E = 2{\cdot}237$ MeV, but further revision to the latest values of E and Q seems unnecessary. The (small) corrections necessary for adjustment to any new E, Q values can easily be estimated from the graphs given in this paper.)

To obtain the sort of results mentioned above it was necessary to interpolate from a scattered lot of only about twenty eigenvalue sets, with three independent variables. However, the sets seemed capable of yielding very plausible results by means of the graph systems shown in figs. 3–7. These graphs probably become progressively less reliable as points on later graphs are deduced from the earlier ones.

The process works as follows:

(i) A 'preliminary eigenvalue plot' (fig. 3) is made of B against b. This consists of a number of approximately parallel curves on each of which a, A are constant. From these the values of A for constant b can be read off, and a 'full eigenvalue plot' (fig. 4) of exactly the same type as was made for the variational calculation can be produced. The advantage of this procedure is that it allows us in our later graphs to reduce the number of variables; but, in contrast to the situation which would have arisen had the actual runs been performed with more constancy in the choice of parameters, we retain highest accuracy in the regions in which we are most interested.

Table 1

$r_0(10^{-13}\text{cm})$	J (MeV)	γJ (MeV)	$\epsilon r_0(10^{-13}\,\text{cm})$	$Q(\times 10^{-27}\,\text{cm}^2)$	$D(\%)$
1·31	46·4	14·5	2·77	2·64	5·07
1·31	46·4	$15{\cdot}4_5$	2·64	2·53	4·76
1·74	27·3	13·5	2·75	—	—
1·74	27·3	14·5	2·62	—	—
1·74	28·4	$12{\cdot}5_5$	2·84	2·76	4·79
1·74	28·4	13·5	2·69	2·52	4·46
1·74	29·5	$12{\cdot}5_5$	2·77	2·54	4·14
1·74	29·5	13·5	2·63	2·36	4·19
1·74	26·2	13·5	2·81	2·85	5·16
2·18	20·5	11·6	2·77	2·62	4·29
2·18	20·5	13·5	2·50	2·18	3·69
2·61	15·8	10·6	2·79	2·63	3·84
2·61	15·8	11·6	2·64	2·41	3·55
2·8	14·0	10·8	2·79	2·70	3·89
1·74	42·6	$2{\cdot}8_5$	5·30	3·71	2·64
1·74	42·6	$3{\cdot}1_8$	4·70	3·18	2·38
2·18	26·2	$3{\cdot}1_8$	6·80	6·71	6·20
2·18	29·5	$3{\cdot}1_8$	3·92	2·92	2·04
2·8	$18{\cdot}8_5$	$2{\cdot}8_5$	4·88	10·91	2·87
2·8	$18{\cdot}8_5$	$3{\cdot}1_8$	4·37	8·04	2·03
2·8	$18{\cdot}8_5$	$3{\cdot}5_3$	3·87	9·63	2·52

(ii) For the quadrupole moment a 'preliminary Q plot' of Q against b analogous to the preliminary eigenvalue plot (i.e. A, a constant on each curve) was made. The parameter B is, of course, uniquely determined for each point on these Q curves by the full eigenvalue plot. Then a 'full Q plot' (fig. 5) of Q against A, each curve referring to constant a, b, is derived. From this a curve complying with $Q=2{\cdot}73$ can be drawn for each a. The 'Q compliance curve' (fig. 6) gives the relationship between b and A necessary for correct values of E and Q when B is taken at the value given by the eigenvalue plot. For each a also, a 'D compliance curve' for 4% D state can be drawn (fig. 6). Thus at the point of intersection of the two compliance curves for any particular a we can read off the b, A, and hence deduce the B which will simultaneously give correct E, Q and D for the deuteron.

It will be noted that the final value of B cannot be found directly from fig. 4, since b will not in general be one of the values chosen there. But an auxiliary curve of the same type and corresponding to the required value of b can readily be drawn for the purpose of this final determination.

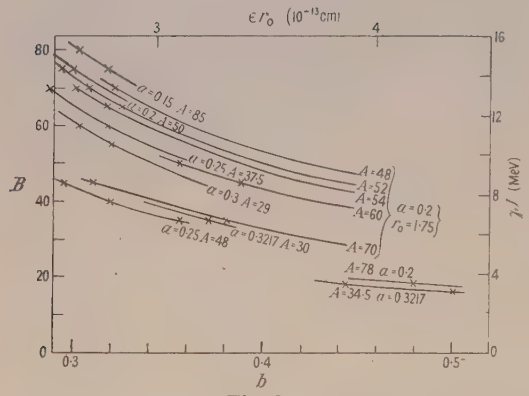

Fig. 3.

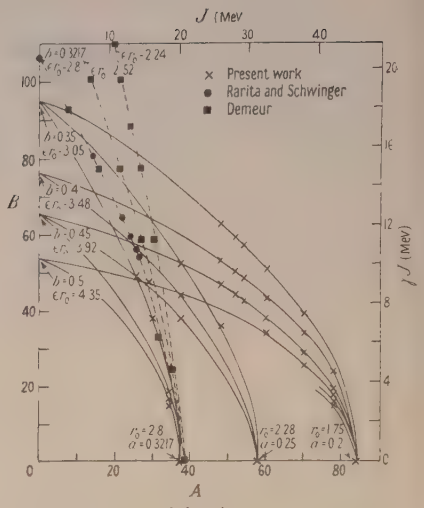

Fig. 4.

Figs. 3 and 4. Ranges and well depths giving correct energy (differential analyser calculation).

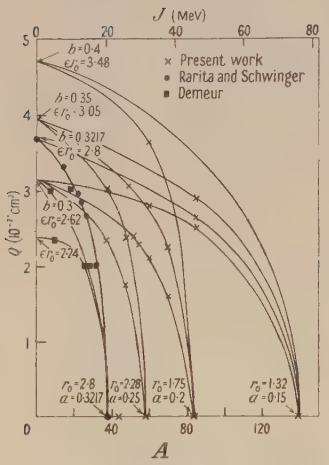

Fig. 5. Quadrupole moments corresponding to ranges and depths from fig. 4.

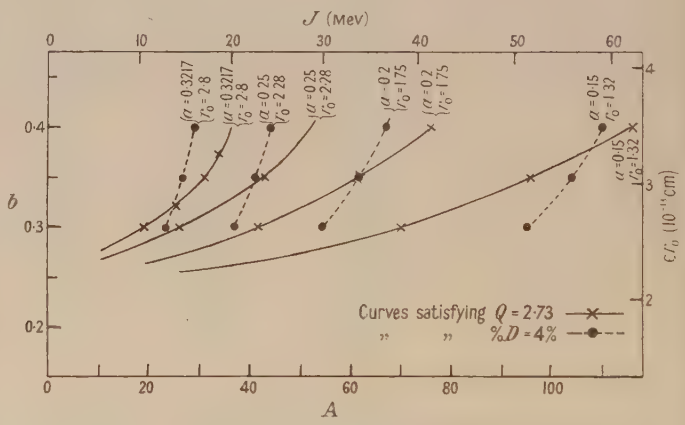

Fig. 6. Determination of parameter sets satisfying E, Q and D conditions simultaneously.

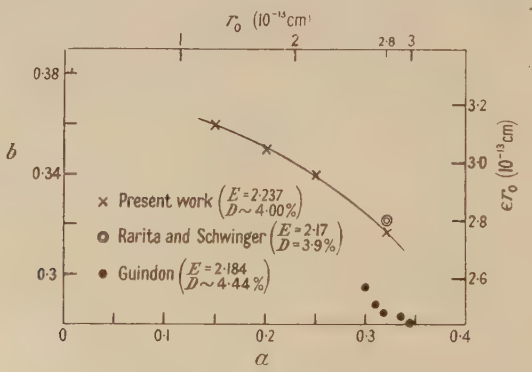

Fig. 7. Variation of tensor range with ordinary range, the E, Q, D conditions all being satisfied.

The variation of b with a when all the deuteron conditions are satisfied is perhaps of interest. This is shown in fig. 7. The Rarita–Schwinger point here corresponds to $D=3{\cdot}9$; the Guindon points to $D\sim4{\cdot}44$, while the full curve is for $D=4$. In figs. 3–7, values obtained by Rarita and Schwinger, by Guindon (1948) and by Demeur (1950) have been included wherever comparison is possible. The good agreement of these points gives grounds for a degree of confidence in the above method in spite of its dependence on extrapolation and graphical methods.

At this stage the error was assessed at about 5%. A second set of differential analyser runs was done with values of a, b, A, B concentrated in the regions of interest. Interpolation to $Q=2{\cdot}73\times10^{-27}$ cm^2 was performed with the aid of figs. 3–7, and table 2 obtained.

Table 2. Final Parameter Sets deduced from Differential Analyser Solutions

$r_0(10^{-13}\,\text{cm})$	1·4	1·6	1·8	2·0
$\epsilon r_0(10^{-13}\,\text{cm})$	2·94	3·04	3·06	3·04
J (Mev)	46·86	39·33	32·33	26·19
γJ (Mev)	11·57	10·04	9·52	9·52
D (%)	4·62	4·14	4·00	4·00

§7. ACCURACY AND FURTHER NUMERICAL WORK

Since the precise amount of the error of the figures quoted above was very much in doubt—many of the tests carried out during the running of the machine were far from reassuring—numerical integrations using a desk calculating machine were carried out for six cases, viz. for $r_0=1{\cdot}4\times10^{-13}$ (two values of γJ), $1{\cdot}6\times10^{-13}$ (two values of γJ), $1{\cdot}8\times10^{-13}$ and $2{\cdot}0\times10^{-13}$ cm.

The series solution was used to $r=r_0$; step by step integration was performed with intervals of $0{\cdot}1\times10^{-13}$ cm in r, and the usual checking of fourth differences applied. The eigenvalues were found from two independent solutions, and the quadrupole moment and % D state calculated using the optimum 5-, 6- and 8-point formulae given by Bickley (1939). The results were as shown in table 3.

Table 3. Direct Results of the Computed Solutions

$r_0(10^{-13}\,\text{cm})$	1·4	1·6	1·8	2·0	1·4	1·6
$\epsilon r_0(10^{-13}\,\text{cm})$	3·121	3·108	3·005	3·010	2·692	2·968
J (Mev)	51·78	39·60	32·23	26·19	51·78	39·60
γJ (Mev)	9·52	9·52	9·52	9·52	11·42	9·96
$Q(10^{-27}\,\text{cm}^2)$	2·728	2·781	2·605	2·687	2·095	2·567
D (%)	4·043	4·144	3·850	3·966	3·384	3·979

It is of interest to see what errors this implies in the differential analyser results. The largest errors indicated in the differential analyser solutions are of the order of $\frac{1}{2}$% for ϵr_0 and of the order of 1% for J, r_0, γJ being presumed given. An error of $\frac{1}{2}$% in γr_0 may give rise to errors of $1\frac{1}{2}$% in Q, D, while an error of 1% in J may make Q, D in error by nearly 4%. Naturally, a small error in J may correspond to a large error in the binding energy—for $r_0=0{\cdot}14$ an error of 1% in J is 0·5 Mev which is approximately 25% of the binding energy, and although this is not an indication of the probable error in E, it shows that an error of several per cent would not be surprising.

The above error estimates apply to the differential analyser solutions. The errors in the numerical solutions are very much less. Comparison with the

solution by the same method of the hydrogen atom ground-state equation $d^2y/dr^2 = z - 2y/r$, whose exact solution is $y = r\,e^{-r}$, shows that the rounding-off errors are not likely to start building up in the deuteron equations in the region $r < \gamma r_0$ with which we have been concerned. The results of table 3 may be reliable to 0·1%.

Once again using figs. 3–7 to correct values to $Q = 2{\cdot}73 \times 10^{-27}$ cm^2, we finally obtain table 4.

Table 4. Final Parameter Sets satisfying $E = 2{\cdot}237$ MeV and $Q = 2{\cdot}73 \times 10^{-27}$ cm^2

r_0 (10^{-13} cm)	1·4	1·6	1·8	2·0
ϵr_0 (10^{-13} cm)	3·12	3·08	3·06	3·04
J (MeV)	51·78	39·79	31·94	26·12
γJ (MeV)	9·520	9·520	9·520	9·520
D (%)	4·04	4·06	4·00	4·00

It would appear safe to say that for $E = 2{\cdot}237$ MeV, $Q = 2{\cdot}73 \times 10^{-27}$ cm^2 this set of values is reliable to $\frac{1}{2}$% in each of ϵr_0, J where r_0, γJ have been chosen exactly; and the corresponding values of D are not in error by as much as 4%.

As mentioned before, the more recent values of the binding energy and quadrupole moment (Newell 1950) do not necessitate material alteration of the results given above. It is found that for $E = 2{\cdot}22$ MeV the quantities ϵr_0, J, D in table 4 are all changed by less than 0·2%, i.e. by less than the suggested error magnitude. It therefore seems unnecessary, at least until values are well established, to give adjusted figures. Table 4 can therefore be taken as embodying the main results of this investigation.

ACKNOWLEDGMENTS

It is a pleasure to express my thanks to those who have helped me in this work, especially to Dr. N. Kemmer for his kind interest and supervision, to the University College of the South-West, Exeter, for early encouragement and generous financial aid, to Girton College, Cambridge, for a studentship, and to the director and staff of the Cambridge Mathematical Laboratory and to the Durham Colleges in the University of Durham for the provision of facilities.

REFERENCES

Barnes, C. A., Stafford, G. H., and Wilkinson, D. H., 1950, *Nature, Lond.*, **165**, 69.
Bickley, W. G., 1939, *Math. Gaz.*, XXIII, No. 256.
Blatt, J. M., 1948, *Phys. Rev.*, **74**, 92.
Blatt, J. M., and Jackson, J. D., 1949, *Phys. Rev.*, **76**, 18.
Bohm, D., and Richman, C., 1947, *Phys. Rev.*, **71**, 567.
Broyles, A. A., and Hull, M. H., 1950, *Phys. Rev.*, **79**, 247.
Demeur, M., 1950, *Physica*, **16**, 353.
Guindon, W. G., 1948, *Phys. Rev.*, **74**, 145.
Hu, Tsi-Ming, and Massey, H. S. W., 1949, *Proc. Roy. Soc.* A, **196**, 135.
Hughes, D. J., 1950, *Phys. Rev.*, **78**, 315.
Hughes, D. J., Burgy, M. T., and Ringo, G. R., 1950, *Phys. Rev.*, **77**, 291.
Newell, G. F., 1950, *Phys. Rev.*, **78**, 711.
Rarita, W., and Schwinger, J., 1941, *Phys. Rev.*, **59**, 436, 556.
Schiff, L. I., 1950, *Phys. Rev.*, **78**, 733.
Snell, A. H., Barker, E. C., and Sternberg, R. L., 1949, *Phys. Rev.*, **75**, 1290.
Wilson, R., Collie, C. H., and Halban, H., 1948, *Nature, Lond.*, **162**, 185 ; 1949, *Ibid.*, **163**, 245.

On Electrical Effects due to Sound Waves in Colloidal Suspensions

By F. BOOTH and J. A. ENDERBY
Wheatstone Physics Laboratory, King's College, London

MS. received 19*th July* 1951

ABSTRACT. An expression is given for the potential differences set up in colloidal suspensions of solid particles by the passage of sound waves which is correct to the first power of the zeta potential of the particles. The question was examined in detail by Enderby in 1951. For a certain range of values of relevant parameters it was found necessary to introduce the simplification that the mobilities of the various ionic species in the electrolyte surrounding the colloidal particles were identical. In the present paper it is shown how the potential may be calculated quite generally without this restriction by the use of vector methods.

§ 1. INTRODUCTION

In a recent paper (Enderby 1951, to be referred to as E) a theoretical analysis was given of the electrical effects accompanying the propagation of sound waves through suspensions of charged colloidal particles. It was shown in this paper that differences of electrical potential arise between different points in the wave train owing to the disturbance of the ionic double layers surrounding the particles; the spherical symmetry of the double layer field is modified by the flow of the liquid. Solutions for the potential distribution in the suspension, correct to the first power of the zeta potential of the particles, were obtained. These solutions are exact provided that the quantities $(\omega_i \boldsymbol{k} T/\sigma)^{1/2}$ are much greater or much less than the double layer thickness. The ω_i denote the ionic mobilities, $\sigma/2\pi$ is the frequency of the sound waves, and T the temperature. In the intermediate region of values it was found necessary to introduce the simplification that all the ionic mobilities were equal. The following note indicates how the general solution can be evaluated for this region even though the ionic mobilities are not necessarily all identical. Hence the problem may now be regarded as solved over the whole range of frequency and double layer thickness. The method uses the concept of the 'ion space' and algebraic methods similar to those employed by Onsager and Fuoss (1932) in their treatment of the conductivity, viscosity and diffusion of mixtures of strong electrolytes.

§ 2. GENERAL SOLUTION FOR THE POTENTIAL

The method described in E was to evaluate the alterations in the mean potential and mean ionic concentrations in the neighbourhood of a single particle due to the passage of the sound waves. From these quantities the average potential in the wave train can easily be found by integration. To solve the equations of motion and of continuity for the ions it is necessary to expand the changes in potential and concentration in powers of the total charge on each particle. Thus, if ϕ denotes the alteration in the mean potential and p_i the alteration in the concentration of the ion of type i, at a point distant r from the

centre of the particle, the radius vector making angle θ with the direction of propagation of the sound waves, we write

$$\phi = A \sum_{\nu=1}^{\infty} \sum_{n=0}^{\infty} Q^{\nu} \lambda_{\nu, n}(r) P_n(\cos\theta), \qquad \ldots\ldots(2.1)$$

$$p_i = A \sum_{\nu=1}^{\infty} \sum_{n=0}^{\infty} Q^{\nu} \pi_{i, \nu, n}(r) P_n(\cos\theta), \qquad \ldots\ldots(2.2)$$

where A is the amplitude of the sound waves, $Q\boldsymbol{e}$ the total charge on the particle, and $P_n(\cos\theta)$ is the usual Legendre polynomial. The $\lambda_{\nu, n}$ and $\pi_{i, \nu, n}$ are functions of r only. For a solution correct to the *first* power of Q or of the zeta potential we only need to consider those λ and π functions for which the suffix ν equals unity. All of these for which the second suffix n is not equal to unity vanish, for reasons given in E. Hence the basic equations to be solved for a result correct to the first power of the zeta potential are eqns. (3.9) and (3.11) of E. When the ionic mobilities are not all equal, it is not in general possible to combine the two equations into a single fourth-order differential equation for the potential coefficient $\lambda_{1,1}$ as in eqn. (3.12) of E. Suppose, however, we associate s potentials $\lambda_{i,1,1}$ with the charge densities $\pi_{i,1,1}$ by means of the relations

$$\Delta_1 \lambda_{i\,1,1} = -\frac{4\pi \boldsymbol{e}}{\epsilon} \pi_{i,1,1}, \quad i = 1, 2, \ldots . s. \qquad \ldots\ldots(2.3)$$

s denotes the number of ionic species present, ϵ the dielectric constant of the electrolyte and Δ_1 is the operator defined in eqn. (3.10) of E. We now find, instead of the single eqn. (3.12) of E, the set of s equations:

$$\Delta_1 \left[\left(\Delta_1 - \frac{i\sigma}{\boldsymbol{k}T\omega_i} \right) \lambda_{i,1,1} - \frac{4\pi \boldsymbol{e}^2 n_i z_i}{\epsilon \boldsymbol{k}T} \sum_{j=1}^{s} z_j \lambda_{j,i,1} \right]$$
$$= \frac{4\pi \boldsymbol{e}^2 n_i z_i}{\epsilon \omega_i (\boldsymbol{k}T)^2} \left[V_r \frac{d\Psi_1}{dr} + \Psi_1 \operatorname{div} \mathbf{V}' \right]. \qquad \ldots\ldots(2.4)$$

In these equations we have used the notation of paper E. n_i denotes the concentration of the ion of type i outside the double layer region of the particle, and z_i its valency. V_r, Ψ_1 and $\mathbf{V}'$ are defined in eqns. (2.2), (3.9) and (2.3) respectively of E. Equations (2.4) give, when integrated,

$$\left(\Delta_1 - \frac{i\sigma}{\boldsymbol{k}T\omega_i} \right) \lambda_{i,1,1} - \frac{4\pi \boldsymbol{e}^2 n_i z_i}{\epsilon \boldsymbol{k}T} \sum_{j=1}^{s} z_j \lambda_{j,1,1}$$
$$= \frac{4\pi \boldsymbol{e}^2 n_i z_i g}{(\epsilon \boldsymbol{k}T)^2 \omega_i (1+b)} \left[R(b, x) + \frac{1}{x^2} \left\{ G(b, \gamma) + \left(\frac{2\pi}{\kappa\lambda} \right)^2 H(b, \gamma) \right\} \right]. \qquad \ldots\ldots(2.5)$$

All the quantities $R(b, x)$, $G(b, \gamma)$, $H(b, \gamma)$ and g have been calculated in E. The boundary conditions used in eqn. (2.5) are, first, that $\lambda_{i,1,1}$ tends to zero at infinity, and secondly, that the field inside the particle is not affected by the conditions outside (eqn. (4.5) of E).

To solve eqn. (2.5) we now introduce a space of s dimensions. The s potentials $\lambda_{1,1,1}, \lambda_{2,1,1} \ldots . \lambda_{s,1,1}$ may now be regarded as defining a vector $\mathbf{l}$ in this space. Similiarly let $\mathbf{z}$ have components $z_1, z_2 \ldots . z_s$ and let $\mathbf{t}$ have components $n_1 z_1/\omega_1, n_2 z_2/\omega_2, \ldots .$ Equation (2.5) may now be written

$$(\Delta_1 - A)\mathbf{l} = \mathbf{t} \frac{4\pi \boldsymbol{e}^2 g}{(\epsilon \boldsymbol{k}T)^2 (1+b)} \left[R(b, x) + \frac{1}{x^2} \left\{ G(b, \gamma) + \left(\frac{2\pi}{\kappa\lambda} \right)^2 H(b, \gamma) \right\} \right], \ldots\ldots(2.6)$$

where A is the matrix operator with components

$$a_{ij} = \frac{i\sigma\delta_{ij}}{\boldsymbol{k}T\omega_i} + \frac{4\pi\boldsymbol{e}^2 n_i z_i z_j}{\epsilon \boldsymbol{k}T}. \qquad \ldots\ldots(2.7)$$

The real parts of the characteristic numbers of the matrix A are all positive. This can easily be shown by first symmetrizing the matrix and then examining the quadratic form corresponding to the new matrix. Let B denote the transform of A defined by

$$B = SAS^{-1}, \qquad \ldots\ldots(2.8)$$

where the components of the matrix S are given by

$$S_{ij} = \delta_{ij} n_i^{-1/2}. \qquad \ldots\ldots(2.9)$$

We now find that if b_{ij} is a component of B,

$$b_{ij} = \frac{i\sigma\delta_{ij}}{\boldsymbol{k}T\omega_i} + \frac{4\pi\boldsymbol{e}^2 (n_i n_j)^{1/2} z_i z_j}{\epsilon \boldsymbol{k}T}. \qquad \ldots\ldots(2.10)$$

Hence the matrix B is symmetric; it is easily verified that the quadratic form corresponding to the real part of B is positive definite.

Having obtained this result on the characteristic numbers, it is now possible to solve eqn. (2.6) for the potential vector by Onsager and Fuoss's method. The solution will consist of a part decaying exponentially with increase of r, and a contribution varying as r^{-2}. The second part only is of interest for our purpose, and its value is

$$\mathbf{l} = -\frac{4\pi\boldsymbol{e}^2 g[G(b,\gamma) + (2\pi/\kappa\lambda)^2 H(b,\gamma)]}{(\epsilon \boldsymbol{k}T\kappa)^2(1+b)r^2} A^{-1}\mathbf{t}. \qquad \ldots\ldots(2.11)$$

From the definition of the $\lambda_{i,1,1}$ it follows that the potential $\lambda_{1,1}$ is simply the scalar product of the two vectors $\mathbf{z}$ and $\mathbf{l}$. Hence, the effective dipole moment of the field round the particle is easily deduced from eqn. (2.11). The calculation of the potential difference Φ across the half wavelength in the sound wave now follows exactly as in the earlier paper. The final expression for Φ is

$$\Phi = \frac{8N\lambda AQ(1-\rho)}{\epsilon \boldsymbol{k}T(1+b)\sum_{i=1}^{s} n_i z_i^2} \left| \frac{(\mathbf{z}.A^{-1}\mathbf{t})(G + (2\pi/\kappa\lambda)^2 H)}{1 + 2\rho + 9\gamma^{-1} + 9\gamma^{-2}} \right|. \qquad \ldots\ldots(2.12)$$

It only remains to evaluate the scalar products $(\mathbf{z}.A^{-1}\mathbf{t})$; this can in principle be done directly, but the inversion of the matrix A is rather tedious. The procedure of Onsager and Fuoss could be applied, but the most convenient technique seems to be the application of the Lagrange–Sylvester expansion for A^{-1}. This method was used by Guryanova (1936) to simplify the computations of Onsager and Fuoss. We have

$$A^{-1} = \sum_{k=1}^{s} \frac{(A - x_1 1)\ldots(A - x_{k-1}1)(A - x_{k+1}1)\ldots(A - x_s 1)}{x_k(x_k - x_1)\ldots(x_k - x_{k-1})(x_k - x_{k+1})\ldots(x_k - x_s)}, \qquad \ldots\ldots(2.13)$$

where 1 denotes the unit matrix and $x_1, x_2, \ldots x_s$ are the characteristic numbers of the matrix A, that is, roots of the equation

$$\det(A - x1) = 0. \qquad \ldots\ldots(2.14)$$

Except for the case of a binary or ternary electrolyte, a numerical solution of eqn. (2.14) is necessary.

§ 3. POTENTIAL SOLUTION FOR A BINARY ELECTROLYTE

For a binary electrolyte s equals 2, and so an explicit expression for Φ may be given without much difficulty, since the roots of the characteristic equation are easily determined. The roots are

$$x_1, x_2 = \frac{1}{2}\left[\kappa^2 + \frac{i\sigma}{\boldsymbol{kT}}\left(\frac{1}{\omega_1}+\frac{1}{\omega_2}\right) \pm \left\{\kappa^4 + \frac{8\pi \boldsymbol{e}^2 i\sigma}{\epsilon(\boldsymbol{kT})^2}\left[\frac{1}{\omega_1}-\frac{1}{\omega_2}\right]\left[n_1 z_1^2 - n_2 z_2^2\right] - \frac{\sigma^2}{(\boldsymbol{kT})^2}\left(\frac{1}{\omega_1}-\frac{1}{\omega_2}\right)^2\right\}^{1/2}\right]. \quad \ldots\ldots(3.1)$$

Using eqn. (2.13), we find

$$A^{-1} = \{(x_1+x_2)1 - A\}/x_1 x_2, \quad \ldots\ldots(3.2)$$

and for $(\mathbf{z}, A^{-1}\mathbf{t})$

$$(\mathbf{z}, A^{-1}\mathbf{t}) = \frac{i\sigma(n_1 z_1^2 + n_2 z_2^2)}{\boldsymbol{kT} x_1 x_2 \omega_1 \omega_2}. \quad \ldots\ldots(3.3)$$

This reduces to the result already obtained when ω_2 is set equal to ω_1.

The real part of the scalar product is very complicated, but gives a simple formula if z_1 and z_2 are equal in magnitude. A straightforward calculation shows that for the case

$$z_1 = -z_2, \quad n_1 = n_2, \quad \ldots\ldots(3.4)$$

eqn. (2.12) may be written in the form of eqn. (3.27) of E multiplied by a factor β^*, where

$$\beta^* = \kappa^2 \Big/ \bar{\omega}\,\overline{\omega^{-1}}\left[\kappa^4 + \left(\frac{\sigma}{\bar{\omega}\boldsymbol{kT}}\right)^2\right]^{1/2} \quad \ldots\ldots(3.5)$$

and

$$\bar{\omega} = \tfrac{1}{2}(\omega_1+\omega_2), \qquad \overline{\omega^{-1}} = \frac{1}{2}\left(\frac{1}{\omega_1}+\frac{1}{\omega_2}\right). \quad \ldots\ldots(3.6)$$

Thus, in this simple case the more exact theory merely changes the β of E, defined in eqn. (4.7), to β^* of eqn. (3.5) above. Some idea of the extent of the modification can be obtained by comparing the two quantities β and β^*. If we attempt to use the approximate theory of E, § 4, for the case s equal to 2 but ω_1 and ω_2 unequal, by identifying the ω of eqn. (4.7) with the mean mobility $\bar{\omega}$, we find

$$\beta^*/\beta = 1/\bar{\omega}\,\overline{\omega^{-1}}. \quad \ldots\ldots(3.7)$$

This ratio is always less than unity; this means that the correct dotted curve of E, fig. 2, should lie below the one drawn there. For water the ratio β^*/β is 0·93. The *maximum* difference between β^* and β would be expected for an electrolyte in which one ion has a very high mobility and the other a very low one. An example of this type is acetic acid, which gives the value 0·36 for β^*/β at 25° C.

The general conclusion would seem to be, therefore, that the more exact theory gives potentials rather less than the approximate theory, but the effect is not important unless the mobilities differ considerably. In the latter case, however, it would be essential to use the more exact calculation in a careful comparison of experiment and theory. It is of interest to note that the previous calculations gave results rather greater than the experimental values, but for the reasons given in E it is not possible to conclude whether the present work agrees substantially better with the data.

REFERENCES

ENDERBY, J. A., 1951, *Proc. Roy. Soc.* A, **207,** 329.
GURYANOVA, E. N., 1936, *J. Chem. Phys.*, **4,** 741.
ONSAGER, L., and FUOSS, R. M., 1932, *J. Phys. Chem.*, **36,** 2689.

Discontinuities in the Variation of Magnetization with Temperature

By V. L. NEWHOUSE*
Physics Department, The University, Leeds

Communicated by E. C. Stoner; MS. received 27th December 1951

ABSTRACT. It is demonstrated that magnetic discontinuities accompany changes of temperature at constant field. The effect is investigated for hard-drawn iron and nickel and is accounted for in terms of two mechanisms, one associated with the decrease of coercivity with rise of temperature and the other associated with the disperse field due to the thermal oscillations of the carriers of magnetic moment.

§ 1. INTRODUCTION

It has recently been shown experimentally by Tebble and Wood (unpublished work) that changes of magnetization with temperature at constant field are reversible when the specimen is on a reversible portion of its hysteresis loop. When the constant field is in the region of the coercive force, however, irreversible changes of magnetization occur. It would be expected that the irreversible magnetization changes due to a change of temperature would take place in discontinuous jumps, as in the ordinary Barkhausen effect. Such discontinuities, which del Nunzio (1930) attempted but failed to detect, have now been demonstrated, and have been investigated in a qualitative manner for two materials.

§ 2. EXPERIMENTAL

The specimens, in the form of wires of 26 s.w.g. and of 17 cm length, were placed in a narrow glass tube, surrounded by a search coil. The temperature could be raised by the passage of hot air through the tube, and measured by means of a thermocouple placed in contact with the specimen. Any sharp discontinuous changes of magnetization were picked up by the search coil which was connected to a detecting system similar to that used by Tebble, Skidmore and Corner (1950). The search coil and specimen were surrounded by a polarizing coil, and the whole system was magnetically screened. The minimum discontinuities detectable by the apparatus are of the order of 10^{-6} e.m.u.

The first specimen, of hard drawn nickel, had a coercivity of about eight oersteds. No effect was detectable for this specimen in a saturating field of eighty oersteds, even with a temperature increase of as much as 100° c from room temperature. This was also the case at remanence. When the specimen, after having been brought into a cyclic condition, was subjected to a demagnetizing field of nine oersteds, however, a rise in temperature of anything over 0·2° c produced many thousands of magnetic discontinuities, in such a direction as to increase the magnetization. When the temperature after having been raised was allowed to fall a very few discontinuities, still in the direction of increasing magnetization, could be detected while the temperature was still near its maximum

* Now at Messrs. Ferranti Ltd., Moston, Manchester.

value. When the temperature was raised for a second time, only a few discontinuities occurred, in the same direction as before, as long as the temperature did not approach the previous maximum more closely than a few degrees centigrade. Eventually when the temperature had been raised and lowered several times over a given range, no further effect was observed in that range.

It has been known for some time (Bush and Tebble, unpublished work) that if in the course of a slow traversal of the hysteresis loop the magnetizing field is allowed to fall by an amount whose magnitude varies with different materials, no Barkhausen pulses can be detected. If the specimen investigated was brought into a 'reversible' region of this kind, by lowering the applied field, and the temperature was then raised, no discontinuities were detected for a rise of several degrees centigrade. A further analogy between the effect of small changes of temperature and small changes of field was shown by the fact that, if the specimen was first cycled and then brought to the coercive region at a raised temperature such as 40° C, a decrease of temperature of as much as 20° C gave rise to hardly any detectable discontinuities at all. Any discontinuities observed were again in a direction of increasing magnetization.

The second specimen investigated was of hard-drawn Swedish charcoal bright iron, with a somewhat lower coercivity than the nickel. Similar results were obtained, except that a rise of about 100° C at remanence produced a few small discontinuities so distributed in direction as to decrease the magnetization of the specimen. This effect was not repeated when the temperature was raised a second time.

§ 3. THEORETICAL DISCUSSION

These results can be explained on the basis of two rather different mechanisms, one involving the thermal fluctuation field discussed by Néel (1950) in a treatment of the after effect in the Rayleigh region of ferromagnetics, and the other (suggested to the writer by Dr. P. Rhodes) arising from the decrease of the obstacles to domain wall movement, which usually accompanies a rise in temperature.

The action of both these effects can be understood by considering the motion of a point representing the position of a domain boundary on an energy curve of the type described by Stoner (1950, p. 134). In a specimen subjected to a gradually increasing field, all the domain walls will occupy positions below points of inflection of the curve. As the position of each boundary is determined by an expression of the form $H = \text{const.}\ dE/dx$, where E is the energy of the system and x the position of the domain boundary, and as Barkhausen jumps take place only when a boundary passes a point of inflection, it is clear that with a small decrease of field the effects should be reversible. This general picture is consistent with the experimental results, though it should be stressed that these give evidence of the absence of discontinuities above a certain minimum size, over a field range of up to 3 or 4 oersteds, and not of complete reversibility over that range.

If the temperature of a specimen in a magnetic field is raised the thermal fluctuation field, which causes an oscillation of the domain boundaries, will be increased; in addition the slopes of the peaks of the energy curves for each boundary

will in general be decreased. For both of these reasons previously stable boundaries may execute irreversible jumps, though not necessarily instantaneously, in a direction of increasing magnetization. Neither of these mechanisms will of course operate for a fall of temperature, whether or not this was preceded by a rise in temperature at that particular field.

If the applied field is lowered slightly before the temperature is raised, it is clear that a temperature rise large enough to cause the formerly most critically placed domain boundaries to jump, should now no longer be sufficient, since through the action of both the mechanisms mentioned above, all domain walls will have been moved to a more 'reversible' region by the decrease of field. This again is in accordance with the experimental findings.

At remanence, all domain walls will be in the troughs of their energy curves, and a much larger rise in the fluctuation field, or decrease in slope of the energy curves will be required to cause a Barkhausen jump. The existence of a demagnetizing field will cause any jumps that do occur to be in a direction of demagnetization.

A rough estimate of the relative importance of the two mechanisms discussed can be obtained by comparing the decrease of the coercivity with the increase of the internal fluctuation field with increase of temperature. Differentiation of the expression given by Néel (1950) for the fluctuation field leads to $dH_f/dT=(\pi \boldsymbol{k}/vT)^{1/2}$ where T is the absolute temperature, $\boldsymbol{k}$ is Boltzmann's constant, and v will be taken as the volume of those Barkhausen discontinuities which make the largest contribution to the susceptibility. For both materials investigated v will certainly be less than $10^{-10}\,\mathrm{cm}^3$ (Bush and Tebble 1948), which at room temperatures gives $dH_f/dT \sim 10^{-4}$ oersteds/° C.

Corner (1949) found that for nickel which had been placed under a strain of $5\,\mathrm{kg/mm}^2$ for several hours and then released, the rate of change of the coercivity with temperature is given by $dH_c/dT \sim 2\times10^{-3}$ oersteds/° C at room temperature, and that for hard drawn iron $dH_c/dT \sim 2\times10^{-2}$ oersteds/° C also at room temperature.

These figures indicate that at least for the second material the boundary oscillation effect is probably of subsidiary importance. For other materials, however, such as permanent magnet materials with their necessarily smaller domain volumes, the thermal fluctuation effect may be of paramount importance.

§ 4. RELEVANCE OF THE EXPERIMENTAL RESULTS TO OTHER WORK

The experimental results described above, as well as the theoretical discussion, indicate that the changes of magnetization resulting from a *decrease* of temperature at any part of the hysteresis loop are likely to be almost entirely reversible, and that the irreversible component of the magnetization change will be a far smaller proportion of the total magnetization change than for a *rise* of temperature. This implies that the thermodynamic relations derived by Stoner and Rhodes (1949), between the magneto-caloric effect and the rate of change of magnetization with temperature at constant field, should be applicable over the whole region of the hysteresis loop instead of merely the saturation region, provided that the measurements of the magneto-caloric effect are carried out for small *decrements* of field, and provided that the measurements of $(dI/dT)_H$ are carried out for small *decrements* of temperature.

ACKNOWLEDGMENTS

I should like to thank Professor E. C. Stoner, who suggested this investigation, for the interest he has taken in it throughout, Dr. Philip Rhodes for a contribution already acknowledged in the text, and Dr. R. S. Tebble for much help and advice. I am deeply indebted to the University of Leeds for a scholarship, which made this work possible.

REFERENCES

Bush, H. D., and Tebble, R. S., 1948, *Proc. Phys. Soc.*, **60**, 370.
Corner, N. D., 1949, *Thesis*, University of Leeds.
Néel, L., 1950, *J. Phys. Radium*, **11**, 49.
del Nunzio, B., 1930, *Accad. Linceii, Atti.*, **12**, 125.
Stoner, E. C., 1950, *Rep. Prog. Phys.*, **13**, 134 (London : Physical Society).
Stoner, E. C., and Rhodes, P. C., 1949, *Phil. Mag.*, (7) **11**, 481.
Tebble, R. S., Skidmore, I. C., and Corner, W. D., 1950, *Proc. Phys. Soc.* A, **63**, 739.

The Construction and Testing of a Magnetic Prism β-Spectrograph of High Resolution, with a Note on the reported Fine-structure of certain Internal Conversion Lines of RaC.C′

By R. E. SIDAY* and D. A. SILVERSTON†

Communicated by N. Feather; *MS. received 27th September* 1951, *and in final form* 1*st January* 1952

ABSTRACT. The first set-up of a very simple high resolution β-spectrograph is described. The instrument employs the focusing action of a magnetic prism with circular plane poles of 20 cm diameter. For this area of pole surface the dispersion is large, giving advantage to the width of source that may be used; and the instrument can focus electrons with energies up to 4 mev. It has been used with resolving powers $H\rho/\Delta(H\rho)$ up to 1 300 as measured from microphotometer traces on the plates. It appears to be the only instrument that has been operated at these resolutions as a spectrograph.

As a β-spectrometer, the resolving power should be 15% higher, but this has not yet been tested. As far as can be seen it has a luminosity roughly comparable with that of the ketron, but unlike that instrument it has considerable flexibility of experimental arrangement promising improved performance.

It has been used to look for the fine structure of the K-conversion line corresponding to the 1414 kev γ-transition in the disintegration RaC.C′ reported by Latyshev and others. In agreement with the work of Bashilov and others who employed the ketron, and of Serebriskaya, Shpinel and Forafontov who used a spectrometer of completely novel design, this line was found to be highly monokinetic.

§ 1. THE ORIGIN AND RELATIONS OF THE METHOD

In the β-spectroscope described here a single magnetic prism with plane circular pole faces is used to focus monokinetic β-rays from a line source placed in a direction parallel to the axis of the poles.

Consideration of the field of two ideal circular poles separated by a distance equal to their radius (Siday 1947) showed that under appropriate conditions,

* I.C.I. Fellow, Department of Natural Philosophy, University of Edinburgh, now at Birkbeck College, London W.C.1
† Department of Natural Philosophy, University of Edinburgh.

and as far as rays in the median plane are concerned, the quadratic aberration in the image could be eliminated and the cubic aberration reduced by a suitable choice of image position corresponding to unit magnification. The appropriate conditions were:

(*a*) that the principal ray of the bundle focused should be initially directed towards the axis of symmetry of the field; (*b*) that a particular deviation of the principal ray of about 1·33 radians should be chosen. This means that with a given strength of magnetic field, the best focusing is obtained for a particular value of momentum, or $H\rho$.

These considerations formulate the essential requirements for the arrangement to function as a β-spectrometer of high resolution. A Geiger counter slit, or other line detector, is placed at the image position, and the instrument is operated as a spectrometer by varying the magnetic field.

Subsequent theoretical considerations (Jennings 1952) and experimental work with an electronic model apparatus (Ehrenberg and Jennings 1952) have demonstrated that 'cubic' focusing occurs under more general conditions. A new cubic focus can always be found by changing both the direction of the principal ray and its deviation. Thus a series of images corrected for quadratic aberration exists, and if a photographic plate is placed to receive these the instrument so constructed will behave as a β-spectrograph; with a fixed field the spectrum of β-particles over a significant range of $H\rho$ is dispersed along the plate with approximately constant resolution.

The elimination or reduction of an aberration in β-image formation appears to offer the β-spectroscopist the advantages of greater gathering power and greater resolution. Unfortunately, in spite of many important recent improvements in β-spectroscopy, modern instruments appear to fall into two categories offering one or the other advantage, but not both. The aim underlying the development of the instrument described here has been to obtain high resolution; the gathering power is limited by the poor focusing properties (z-focusing) of the field on the trajectories not lying in the median plane. As an introduction and summary the present instrument is compared first with other instruments serving a similar purpose.

(i) *The Semi-Circular Focusing Spectrograph*

This instrument of classic importance is attractive because of its great simplicity of design, and because it gives a constant resolution over a very wide range of $H\rho$. The essential disadvantage from which it suffers is the quadratic aberration of its image formation, making the line shapes unsuitable for the highest resolution.

In its present form the new instrument gives cubic focusing, but the range of constant resolution is reduced to a 5% variation of $H\rho$, although the degradation of the image for greater variations is slow. Also it is worse than the semi-circular focusing instrument with respect to its z-focusing properties.

On the credit side, the present arrangement of two cylindrical poles of 20 cm diameter, in which no special trouble has been taken to avoid the effect of the magnetizing coils and yoke on the axial symmetry of the field, is even simpler than that required for the semi-circular focusing spectrograph where attention has to be paid to uniformity of field.

Another attractive feature of the new instrument is the large separation of source and image which enables a modest magnet to focus high energy electrons

(4 Mev in the present case). This, of course, is one of the factors giving rise to the high dispersion of the instrument. If Δs is the change of image position along the photographic plate measured in centimetres for a change $\Delta(H\rho)$ in $H\rho$, it is convenient to define the dispersion as $[\Delta s/\Delta(H\rho)]H\rho$ cm. For an instrument of given type the dispersion is directly proportional to the size (linear dimension) of the instrument. The dispersion of the semi-circular focusing spectrograph is roughly equal to the distance between source and image. The new instrument with a 20 cm pole diameter has a dispersion of approximately 33 cm, so is equivalent in this respect to a very large semi-circular focusing spectrograph.

(ii) *High Resolution Spectrometers*

In the very considerable variety of recent development in instrumental design for β-spectroscopy the instrument described here appears to be unique in its function as a β-spectrograph. In its more limited use as a β-spectrometer it can be compared with other high resolution instruments. Resolution is conventionally defined as the fraction $\Delta(H\rho)/H\rho$ where $\Delta(H\rho)$ is the width of a monokinetic spectrum line at half its height above background, and resolving power as the reciprocal of this quantity. Recent writers have been using the term 'high resolution' or 'very good resolution' to cover widely different values, so for definiteness it is taken here that an instrument does not fall into this class unless it has actually been used to give a resolution (in the presence of all attendant effects which cooperate in spreading the image) that is better than 0·2%.

The principal instrument at present achieving this resolution is that developed by Korsunsky, Kelman and Petrov (1944) and later by Dzhelepov and Bashilov (1950), and is called by them a ketron. It is a modified semi-circular focusing spectrometer in which the field in the median plane is given a (one-dimensional) gradient in a direction perpendicular to the line joining source and image. A total angle of collection of 30° in this plane is used, and theoretically an aberration-free image should be obtained. The shaping of the pole surfaces to give the appropriate theoretical field distribution, a feature common to a great deal of modern β-spectroscopic design, of course introduces a considerable complexity into the experimental set-up.

It is interesting to note that, as in the instrument described here, the improved focusing in the median plane is achieved in the ketron only at the expense of a considerable deterioration of the z-focusing compared with that of the standard semi-circular focusing spectrometer. For this reason, both the ketron and the spectrometer described here are operated for high resolution with very small aperture angles in a plane perpendicular to the median plane (z-aperture).

With principal aperture angles of 2° and 30° respectively the ketron gives a resolving power of 660. It appears that the practice with this instrument is to change the resolving power by changing only the z-aperture.

With the new instrument using principal apertures of 1·5° and 6° respectively a best resolving power of 1 300 was obtained as measured by microphotometer traces from the photographic plates. Taking count of the intensity–density characteristic of the emulsion used, this should correspond to a resolving power of 1 500 in counter experiments. This last prediction has yet to be tested by detailed experiment. As regards dispersion, the ketron is essentially a semi-circular focusing instrument and will therefore have the small dispersion

associated with the latter. With poles 34 cm × 24 cm, the distance between source and image used by Dzhelepov and Bashilov was 16 cm, which we take as the dispersion of their instrument. For equal pole area the new instrument would have a dispersion of $(34 \times 24/\pi \times 100)^{1/2} \times 33 = 53$, more than three times as large. On the other hand, at the same resolving power the ketron appears to have a higher luminosity than our instrument.*

Quite recently some other experiments have been described in which a resolution of about 0·13% was obtained. In achieving this, Shpinel (1946, 1950) has developed a spectrometer of a novel design, but it is not yet possible to compare its performance with that of the ketron.

(iii) *The Logistics of the Experimental Arrangement Adopted*

It should be emphasized that the experimental arrangement described here must be regarded as a first set-up. It is explained below how the effective part of the field used can be regarded as agreeing with that given by two ideal plane poles separated by a distance equal to their radius. The choice of this field distribution depended on convenience rather than merit since, as was mentioned above, the behaviour of trajectories in it had been computed, and the knowledge so obtained facilitated the assembly of the instrument. A few preliminary experiments with very narrow angle bundles sufficed to show that the instrument behaved very closely in accordance with the calculations.

The calculations were made for bundles of β-rays with their principal rays directed initially towards the axis of symmetry of the field. The distances of closest real approach to the axis of rays inclined at different angles to the principal ray were computed, and by placing stops in positions thus calculated angular apertures could be defined accurately. So it was again for reasons of convenience rather than merit that this direction for the principal rays was chosen in practice.

It is not intended to discuss here how the performance of the instrument can be improved, except to point out that the cubic coefficient of aberration can be reduced and indeed eliminated for one particular $H\rho$ by bringing the poles closer together (Siday 1941, Jennings 1952), and that, by changing the direction of the principal ray in the sense that it would pass through more of the field, the z-focusing properties can be improved until for a *single* direction of a ray double focusing conditions can be attained (Ehrenberg and Jennings 1952)—although it may not be advisable to change the direction as much as this. There does appear to be considerable flexibility in arrangement in the new instrument and we shall merely say that improvement in some directions is to be expected.

§ 2. APPARATUS AND THE FIELD CALIBRATION

(i) *Description of the Magnet*

Figures 1 and 1 (*a*), show the magnet that was used as the magnetic prism. The pole pieces were of 10 cm radius, of 10 cm depth, and their separation was also 10 cm. The poles were connected via the rectangular portions A and B to the yoke Y of diameter 12 cm.

The magnet was mounted so that its median principal plane was at right angles to the direction of the earth's (total) field.

The magnetizing coils consisted of three coils of eight, six, and four layers, the three coils fitting coaxially one over the other, and the innermost, of eight

* These rather elaborate details of comparison are given as the Russian publications may not be readily available everywhere.

layers, fitting closely over the yoke of the magnet. The diameters of these coils were such that the resistance was about the same for each, of the order of 15 ohms. Each coil was wound over a tank through which cooling water was circulated.

(ii) *Magnetic Measurements and Adjustment of Field*

Standardization of search coils. An apparatus was devised whereby field measurements could be made in the median principal plane at 1 cm intervals along radial lines from the cylindrical axis of the magnet with sufficient accuracy for comparison with the computed field.

A small search coil was used and its area found electrically by comparing the mutual inductance between the coil and a pair of Helmholtz coils, with that of a larger standard coil whose area had been directly determined from its dimensions

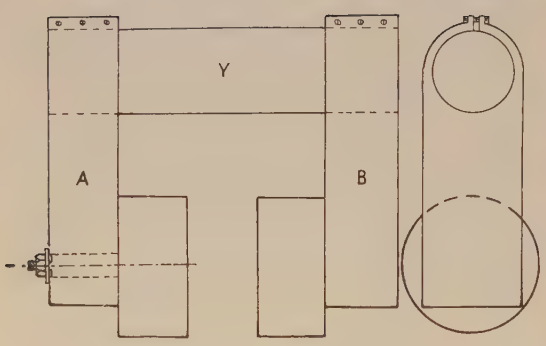

Fig. 1. Design of prism magnet.

Fig. 1 (*a*). The spectrograph assembly.

and number of turns. The Helmholtz coils and the standard coil were those used by Nettleton and Sugden (1939), and the method of calibrating the standard coil is described in detail by them.

The magnetic field was measured by balancing the flux due to the removal of the search coil against the flux in the secondary of a standard mutual inductance, when a known current in the primary was broken. Using highly stretched 'elastic', the search coil was catapulted from a fixed position in the field and at the same time the current was broken in the primary of the standard mutual inductance, the two charges resulting from these actions reaching their final values in less than $\frac{1}{40}$ second. Due to the inertia of the suspended system, the fluxmeter did not detect the differences in the rates of growth of the two charges, and provided the two charges were equal and opposite the fluxmeter recorded zero. No difference in result was obtained for large variations in the elastic tension employed, but a lower limit of tension was found, below which the two charges were seen to record independently. The tension employed in the elastic was always well above this limit.

The field in oersteds is given by the relation $H = 100\,Mi/A$, where A cm² is the effective area of the search coil, M is the mutual inductance in μH, and i is the current in amperes in the primary of the mutual inductance. An accuracy of field measurement of 1 part of 500 was satisfactory for our purposes and was achieved without particular difficulty.

As the search coil had to be removed from the field with considerable acceleration, its path had to be guided in some way. This was done by sinking the coil in a block of wood 3 inches long and 1 inch square in cross section, and shooting the block along a hollow brass tube of the same (internal) cross section. To one end of the block was attached the elastic and to the other end was screwed a brass cylinder with a central hole with $\frac{3}{8}$ in. Whitworth thread. Attached to the bottom of the brass guide tube and at right angles to it were three rectangular bars of $\frac{1}{2}$ inch cross section. These fitted into rails on a horizontal table, part of which extended between the poles of the magnet. The height of the table could be adjusted. With this arrangement the brass tube could be slid across the table in a direction parallel to the vertical* plane of symmetry of the magnet and at right angles to the length of the tube; the table height could be adjusted so that the central plane of the search coil lay in the median plane of the magnet.

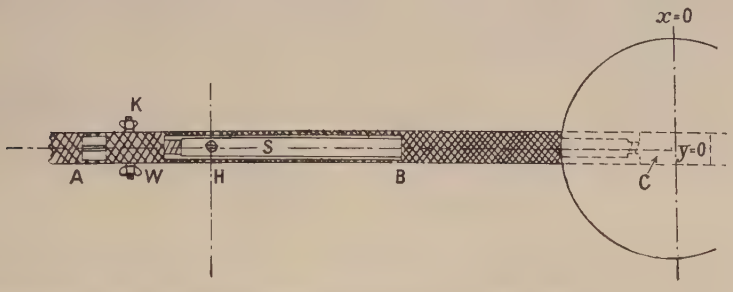

Fig. 2. Catapult for measuring the magnetic field. (Not to scale; the length of the tube is 6 feet.)

The position of the tube relative to the magnet is shown in fig. 2 when the axis of the tube passes through the central vertical axis of the magnet. The top of the tube was removed over the portion AB and the centre of the sides slotted over the same distance, while a slit 1 mm wide was milled in the centre of the bottom of the tube. A square piece of paper on which were ruled two lines at right angles—$x = 0$ in the direction of the plane of vertical symmetry, $y = 0$ in the direction at right angles to this—was placed under the tube so that the line $y = 0$ was visible through the 1 mm slit over its whole length. The lines were marked off in 1 cm intervals. K is a brass block similar to the block C containing the search coil, and it can be fixed rigidly in any position by means of the wing nuts W. A half-inch brass rod can be screwed into the block K at one end and the block C at its other end. Thus the block C can be held rigidly in any position by clamping block K.

The block K was moved until, on looking downwards through the $\frac{1}{4}$ inch hole H drilled in the $\frac{1}{2}$ inch brass rod S, the pair of cross wires above and below the hole were coincident with a desired mark on the paper. The distance from the centre of the search coil to the centre of the crosswires was made equal to the distance from the centre of the magnetic poles to the origin $x = 0$, $y = 0$ on the paper,

* The field plotting was done before the magnet was mounted with its axis in the direction of the earth's field.

then if the crosswires were set on a point $y=0$, $x=r$, it was known that the centre of the search coil was r cm from the centre of the pole. The brass rod was rotated by means of a special key, so that it unscrewed from the block C and screwed into block K. In this way the search coil was released.

At the same instant a switch was automatically broken in the circuit of the primary of the mutual inductance and the secondary flux balanced as previously explained. Values of the field H were obtained for corresponding values of the radial distance r along the line $y=0$ up to $r=32$ cm.

A small correction for the error in not placing the origin at exactly the correct distance from the centre of the magnet was found electrically by shooting the coil from a particular position $x=r'$, $y=0$, as read on the paper, and then from a position $x=-r'$, $y=0$. From the difference in the two readings of the magnetic field H, and a knowledge of the rate of change of H with r at this point r', the error x could be found from $x=\frac{1}{2}\Delta H/(dH/dr)_{r'}$.

A value $r'=9$ cm was chosen, for, in this region, $(dH/dr)_{r'}$ is nearly constant. This correction was additive to all values of x as read on the paper and amounted to 0·4 cm.

By moving the whole brass tube at right angles to itself and shooting the coil always from $x=0$ the variation of field in the y direction was explored.

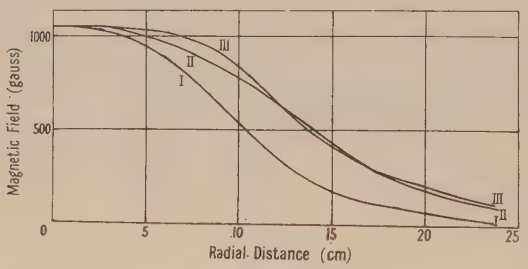

Fig. 3. Field distribution plotted radially. I theoretical. II experimental. III curve I with abscissae increased by factor 1·35.

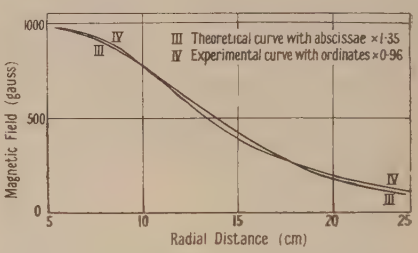

Fig. 4. Comparison of scaled computed theoretical (III) field strength with practical values.

As explained above it was decided to accept for preliminary work any field approximating reasonably well to the computed one. In fig. 3, curve I shows the field shape as computed, and curve II shows that determined experimentally along the $y=0$ axis. The field shape at right angles along the $x=0$ axis did not differ significantly from that of curve II, so that for the purpose of comparing the experimental and computed fields the asymmetry need not be further considered. It was noticed that, if the abscissae of curve I were multiplied by a constant factor 1·35, a fair fit with curve II was obtained (curve III). This means that the magnetic field shape in the plane of symmetry of the actual magnet is more nearly equivalent to the computed field shape for a magnet of pole radius 13·5 cm and separation 13·5 cm than of 10 cm. Therefore, the focusing properties of the actual magnet should be similar to those theoretically considered, provided all distances concerning electron trajectories are multiplied by a factor 1·35. It will be seen that the most significant disagreement between curves III and II occurs in the region between $r=0$ and $r=10$ cm. However, the focusing properties of the prism have been considered only for electrons leaving the source at an angle in the plane of symmetry $\sin^{-1}0{\cdot}3$. The nearest approach of these electrons to the vertical axis of the magnet, according to computation, is 4·27 cm for the optimum $H\rho$ value, and 3·75 cm for the greatest $H\rho$ value of

electrons to be received on the photographic plate. If these values of r are multiplied by 1·35 it will appear that the field of the actual magnet in the region $r < 5{\cdot}4$ cm has no bearing on the performance of the instrument. This being the case (so long as the angular spread of the accepted sheaf of electrons is limited as described above) comparison of 'scaled computed' and experimental fields is best made by adjusting these to equality at $r = 5{\cdot}4$ cm. This is done in fig. 4, where remaining discrepancies are very small indeed.

Subsidiary experiments showed that the maximum change in effective field for 1° C rise in yoke temperature was less than one part in 30 000. Therefore, a hypothetical resolution as good as 1 part in 10 000 should not be impaired by temperature effects if it is supposed that by water cooling the coils the temperature of the magnet can be kept constant to one degree centigrade for several hours.

In order to maintain a reproducible relationship between magnetizing current and field, the magnet was first saturated by passing a total current of about 45 amperes for a period of about half a minute through the three coils connected in parallel. This current, obtained from the 230 volt d.c. mains, was then rapidly

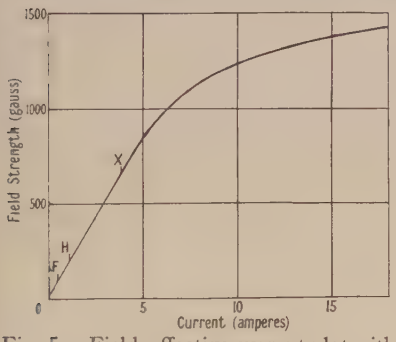

Fig. 5. Field–effective current plot with focusing field strength for some thorium active deposit line β-spectra.

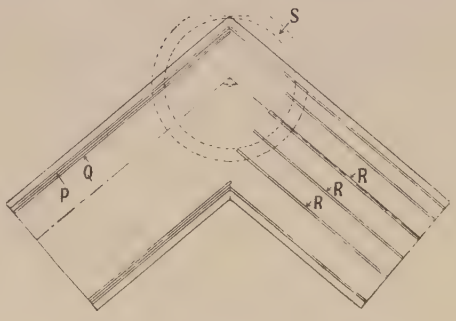

Fig. 6. Plan of vacuum chamber.

reduced to zero. It was found that a residual field of 14·7 oersteds was always obtained. Using the 'ascending' portion of the magnetization cycle it was then found that any required field could be set to at least 1 part in two or three hundred.

The inside magnetizing coil acting alone was capable of producing a field at the centre of 850 oersteds, but for fields above this value all three magnetizing coils were used in parallel. By means of simple experiments it was found possible to attribute relative magnetizing powers K and L to the middle and outer coils respectively. A current i_2 in the middle coil was thus equivalent to a current Ki_2 in the inner coil, and i_3 in the outer coil was equivalent to Li_3 in the inside coil. When all three coils were used the effective magnetizing current was taken as $i_1 + Ki_2 + Li_3$.

A graph showing the relationship between effective current and field is shown in fig. 5. The magnetizing current required to focus some of the well-known lines of Th(B + C) is indicated.

The field was stabilized by keeping the current through the magnetizing coils constant during the time electrons were being recorded. This current was supplied by a hundred-volt bank of accumulators. The current was measured by measuring the voltage drop across a standard resistance with a Tinsley vernier potentiometer used in conjunction with a low-resistance high-sensitivity galvanometer. A change in current of 1 part in 40 000 was readily detectable.

By connecting a high resistance in parallel with the control resistance and by using a gear reducing device for altering the former by small amounts, a magnetizing current of about half an ampere could be kept constant to considerably better than 1 part in 40 000 for several hours. The magnetizing current could easily be altered in measurable steps amounting to 1 part in 20 000 of its average value. The maximum energy of electrons that could be focused, using a magnetizing current supply from one hundred volts, was 4·2 MeV.

(iii) *Spectrograph Chamber*

The vacuum chamber was constructed of $\frac{3}{8}$ in. thick sheet brass, and parts were soft soldered. The external height of the chamber was 2·5 in. The top and bottom plates of the chamber were of identical construction, as shown in fig. 6. Slots $\frac{1}{8}$ in. deep and $\frac{3}{8}$ in. wide were milled in these plates and the source and detector of electrons could be placed in any required position, relative to the axis of the magnet, by sliding them along the slots. The chamber was lined with aluminium $\frac{1}{8}$ in. thick, which could be removed by sliding it along the outside slots P in fig. 6. The lining of the sides extended along their whole length, and

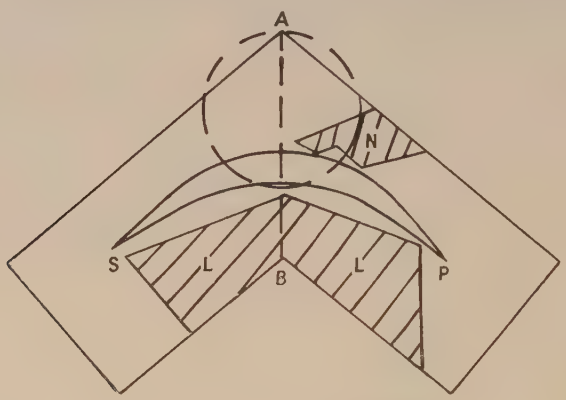

Fig. 7. Rays in vacuum chamber.

the lining of the top and bottom plates was attached to these sidepieces. To avoid covering up the slots Q and R (fig. 6) where they were required to hold the source and detector, the top and bottom plates were lined only in the region between the source and detector.

Two coaxial brass rings S were attached to the outside of the chamber, one to the bottom plate and one to the top plate. They were of 10 cm radius and 1·5 in. depth, and the pole pieces of the magnet fitted closely into them. Thus the position of the chamber was fixed relative to the axis of the magnet. The vertical plane of symmetry AB (fig. 7) of the chamber was then coincident with the vertical plane of symmetry of the magnet. Removable brass packing pieces were placed between the chamber and the magnetic poles so that the median principal plane of the magnet coincided exactly with that of the vacuum chamber.

Each end of the chamber terminated in a rectangular flange, and a rubber gasket of elliptical cross section fitted into a rectangular slot in each flange. An end plate could be clamped to each flange and the rubber gasket compressed to produce a vacuum seal.

The pumping system consisted of a two-stage Metropolitan-Vickers type O3B oil diffusion pump joined to the vacuum chamber by a pipeline less than two inches

long. The pump was of all brass construction and could be connected directly to the chamber without disturbing the distribution of the stray field of the magnet. The backing pump, however, was made of magnetic material and was placed at a distance of about six feet from the spectrometer. It was joined to the backing side of the diffusion pump by a long length of brass tubing. A pressure of less than 10^{-5} mm could be maintained in the spectrograph chamber.

In accordance with the plan of following the computations the angle of the chamber was made 100°.

For the optimum $H\rho$ value, the computations correlated the values of the initial inclination of a ray to the principal ray with the nearest real approach r_m of the electrons to the axis of the magnet. r_m lies in the vertical plane of symmetry AB (fig. 7) of the chamber. Within the range studied, any required angle of emergence could be selected by placing an aperture in the plane AB and choosing its limits r_m. The aperture was carried by an aluminium plate attached to the removable aluminium lining that fitted into the slots P (fig. 6) and was adjustable in the horizontal and vertical directions. Regarding the vertical direction, the computations show that most of the defocusing action of the prism takes place after the electrons have traversed the vertical plane of symmetry AB. Therefore the height of the aperture in the z direction was a good measure of the maximum angle of divergence of transmitted electrons, the angle being measured at right angles to the median principal plane. The edges of the aperture were bevelled to reduce scattering of electrons.

N was an aluminium block that prevented secondary electrons, produced by γ-rays striking the sides of the chamber, from reaching the detector P. Lead blocks L were placed between the source and detector.

The source of electrons. The performance of the instrument was investigated using the F line of thorium B. In a first series of experiments active deposit from radio-thorium was obtained on a platinum wire 2 cm long and 0·1 mm diameter. For more accurate work a second source holder was constructed so that a strip of platinum foil 0·1 mm thick, 2 cm long and 1 cm deep could be activated along the 2 cm edge. Only the edge of the foil was exposed to the radio-thorium, the contamination of the sides being prevented by compressing the foil between two thin pieces of rubber stuck to a brass plug. When the activity of the foil was very weak it was placed for a few seconds on a photographic emulsion. The blackening of the emulsion had a sharp edge corresponding to the edge of the foil and this showed that the side of the foil was not greatly activated.

After activation the foil was removed and mounted on a brass plug. It could always be replaced on this plug in an exact relative position by compressing it between two flat brass surfaces. In this way a non-contaminated source mounting could be placed in the spectrometer. The plug could be placed on a holder which slid into the spectrometer vacuum chamber along grooves Q (fig. 6). Its position relative to the axis of the magnet could be adjusted by a micrometer screw that could be attached to the end flange of the chamber before screwing on the end plate. A slot milled in the base of the micrometer plate allowed the plate to come into flat contact with the brass flange F without compressing the rubber gasket. The micrometer could be set to 0·01 mm.

By means of small adjusting screws the source could be made accurately parallel with the vertical component of the magnetic field.

§ 3. PERFORMANCE OF THE INSTRUMENT USED AS A SPECTROGRAPH

Photographic emulsions were used to record the focused electrons. Ilford X-ray plates and Ilford G-5 Nuclear Emulsion plates were used with the spectrometer. The former were very sensitive but had a large grain size. The nuclear emulsion plates were much slower, but had a very small grain size and an emulsion thickness of $50\,\mu$. For detection of weak lines against a continuous β-spectrum by eye, the X-ray plate was only slightly inferior, but the fluctuations due to grain size made photometric measurements of very weak lines difficult.

The plates were $3\frac{1}{4}$ in. long and 1 in. high. They fitted into a plateholder in a camera which was loaded in a darkroom. The camera was transferred to the vacuum chamber and its positions could be adjusted by a micrometer screw reading to 0·01 mm. Once a suitable vacuum had been obtained the front of the camera could be rapidly opened, by rotating a rod passing through a Wilson vacuum seal, and the plate exposed to the electrons. After exposure the camera could be closed and removed to the dark room for unloading. For a pole radius of 10 cm the focal length for best focusing for a principal ray was calculated to be 10·8 cm and therefore, taking account of the experimental field distribution, the source was placed at a distance $2\times10{\cdot}8\times1{\cdot}35=29$ cm from the axis of the magnet.

The investigation of the field shape enabled us to place the photographic plate in approximately the correct position, at the same distance from the axis of the magnet as the source. The angle of emission of electrons in the median principal plane was adjusted to 6° and several separate exposures were taken for different positions of the camera. The plates were microphotometered and it was found that the optimum position of focus differed from the theoretical by a few millimetres. The angle of emission was now increased to 18° and the focusing procedure repeated. The optimum focus for the larger aperture coincided with that for the smaller, but the image was wider.

The focusing field was increased by 10% and the camera refocused. The plate-holder was then placed so that the line joining the foci corresponding to H_0 and $1{\cdot}1\,H_0$ was coincident with the emulsion. With the plate at this angle, the same camera position gave the best focus for a magnetizing field 10% below the optimum. One photographic plate could thus record a spectrum range of 20% in momentum. The angle of incidence of the central ray at the plate in this arrangement was about 46°. The angle of deviation of the principal ray, characterized by $b=0$, for optimum focusing was in agreement with that computed.

The photographic plates were photometered with a Kipp automatic recording microphotometer. Two magnifications were possible, 50 times the distribution on the plate and 5 times the distribution on the plate. Horizontal and vertical scale lines were put on the recording film by two lamps; one of them flashed intermittently, the flashes being controlled by the motor. On the larger magnification the separation of the vertical distance lines was 5 mm corresponding to 0·1 mm of plate traversed. On the smaller magnification the separation was 2 mm corresponding to 0·4 mm of plate traversed.

Tests were made to ensure that the shape of the trace was not affected by small alterations in the width and length of the analysing slit of the microphotometer. Usually a slit width of about $10\,\mu$ and length 0·2 mm was employed. As was to be expected, the focused line varied in shape and intensity from point to point along its length (the z-direction). Two marked discontinuities in intensity were found at distances from the centre of the line or the median principal plane, which

depended upon the source-length and the angular aperture in the z-direction. The lines were not straight but slightly curved.

Reduced copies of microphotometer traces of the F line are shown in figs. 8 (*a*), (*b*) and (*c*). The source length was 2 cm and angle of emergence in the median principal plane was 6°. The total angle of emission in the z-direction was 1·5°. (*a*) is the trace across the centre of the line, (*b*) is 2 mm from the centre. (*b*) has the same intensity above background as (*a*), but the line shape of (*b*) is sharper, particularly on the low energy side. (*c*) is the trace measured at 4 mm from the centre.

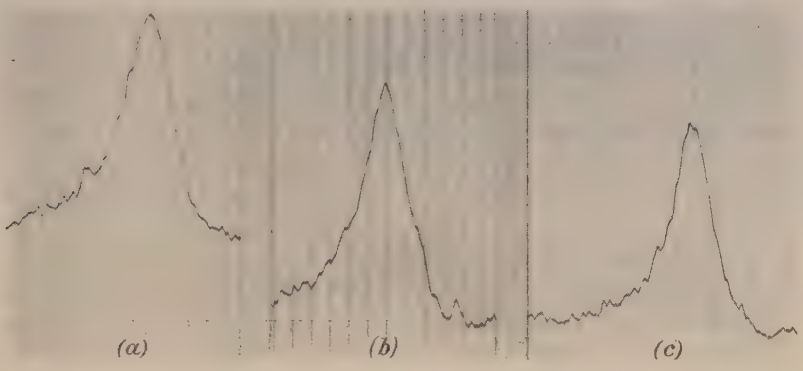

Fig. 8. Reduced microphotometer traces of F line.

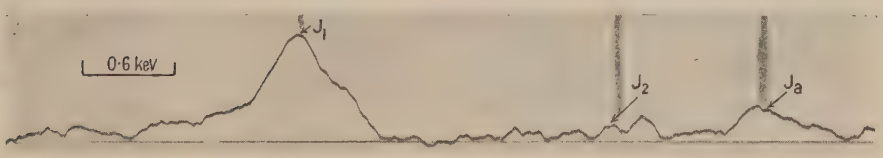

Fig. 9. Reduced traces of J_1, J_2 and J_a lines.

The width of the trace lines at half their height above background will be called the trace-breadth. This will be different from the true half width of the line and will vary with the exposure, even over the linear portion of the density–log (exposure) characteristic.

The dispersion factor was obtained by altering the magnetic field and measuring the line shift, and has also been obtained by recording two β-ray lines whose absolute energies are known and measuring their separation on the trace. The agreement between the two determinations was good. The J and Ja lines of thorium B had the most suitable energy difference, and the trace obtained is shown in fig. 9. The difference in energy (Ellis 1932) is 3 kev and the separation of their peaks is 2·5 mm on the photographic plate, giving a value $D = 330$ mm. Therefore each division on the trace (corresponding to 0·1 mm on the photographic plate) corresponds to $H\rho/\Delta(H\rho) = 3\,330$. Figure 8 (*b*) has a trace breadth corresponding to a resolving power, measured as $H\rho/\Delta(H\rho)$, of approximately 1 300.

A large number of exposures were taken for various source lengths and aperture sizes. The general results are summarized below.

Trace-breadths corresponding to better resolving power than about 1 300 could not be obtained by making the angle of emission in the median principal plane less than 6°.

The variation of angle of emission in the z direction did not change the intensity of the line in the median principal plane by a large amount until the angle of emission was greater than 2°, after which the resolving power decreased.

The decrease in resolving power with angle of emergence in the median principal plane was not very rapid up to an angle of 12°. Thus with an angle of emergence of 12° a resolving power of 800 was obtained. For an angle of emergence of 18° the resolving power, measured from the half-width, was 350, but the line had a long tail on both the high and low energy sides of the peak.

For changes in field of $\pm 3\%$ about the optimum H_0, there was no change in resolving power. For larger changes the resolving power decreased and the lines became asymmetric, having a tail on the high energy side. This tail could be considerably reduced by asymmetrical adjustment of the aperture in AB, that is by choosing a suitable direction of the principal ray, but this disturbed the focusing for fields of the order of H_0.

Figure 10 shows the trace obtained after a double exposure to the F line. The field was changed by 1 part in 1 200 and the lines are clearly resolved.

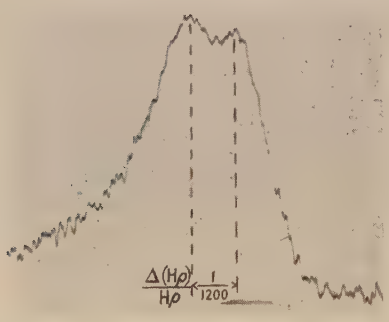

Fig. 10. Reduced microphotometer trace; resolution test on the F line.

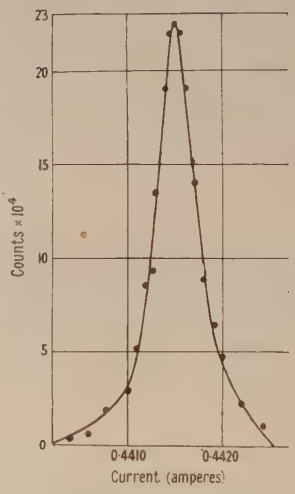

Fig. 11. Geiger counter determination of the thorium F line.

If a radioactive material has a short half-life it may be necessary to use several sources with the same photographic plate. It is then necessary to be able to replace the source exactly. To test the ability to do this, an exposure was taken using the Thorium F line. The camera was closed, the pumps were switched off and air admittted to the chamber. The source was completely dismantled and reassembled and a second exposure of the same length as the first one was taken. The microphotometer trace showed that the source was replaceable with such accuracy that no change in line shape could be detected.

§ 4. GEIGER COUNTER MEASUREMENTS

Geiger counters were also used for recording the focused electrons. Two counters were connected in coincidence so that only particles that passed through both counters were recorded.

The plate-holder in the camera could be removed and the two counters fixed in the camera. The counters were cylindrical in shape, the axis of each counter

being parallel to the axial component of the magnetic field. The counters were made of copper and were 1·25 in. long and $\frac{3}{8}$ in. in diameter, with $\frac{1}{16}$ in. wall thickness. The central wire was insulated from the walls by a small metal–glass seal and a small glass bead was attached to its other end.

Mica windows were fitted to the counters. The thinnest window that could be fitted to the first counter without breaking had an average thickness of 1·4 mg cm^{-2} and the thinnest fitted to the second counter an average thickness of 2·9 mg cm^{-2}. The counters were pumped out for long periods and filled with argon and about 10% of alcohol vapour. They were filled to a pressure of about 10 cm.

Two separate power units supplied the potentials for the central wires. They were standard A.E.R.E. power supply units type 1082 A. The scaler employed was also a standard A.E.R.E. scale of 100.

The scanning slit in front of the first counter was 40 μ wide in brass. It was placed at the focus of the electrons and was bevelled on the side furthest from the source. The permitted angle of acceptance of electrons by the slit was limited to about 6°. This was considered necessary because high energy electrons have a considerable range in brass. The slit was about 2 cm long and parabolic in shape. It was very difficult to be sure that the curvature of the slit was exactly the same as that of the natural line. The line curvature will be different from the photographed curvature for in the latter case the electrons are incident at an angle with the plate but strike the slit normally. The slit was adjustable in all directions.

The Geiger counters were not used to make a comprehensive study of the properties of the prism, but a line obtained with counters is shown in fig. 11. The magnetizing current was changed in steps of 5×10^{-5} amp near the peak and in steps of 2×10^{-4} amp at the base of the line.

The line has a half-width corresponding to $H\rho/\Delta(H\rho) = 900$. A piece of brass 2 mm wide was then placed across the centre of the slit, so that the rays focusing in the median principal plane were prevented from reaching the counters. The counting rate was decreased by about 20% but the resolving power was increased to 1100. Converting microphotometer traces to relative intensity units, using the measured characteristics of the blackening of the photographic plates, showed that under best conditions the true half-width as distinct from the trace-breadth corresponded to a resolving power of 1500. It seems likely that by more careful shaping of the scanning slit a resolving power nearer this figure could be obtained with counters.

With counters, for the F line of thorium B, the ratio of the height of the peak to the height of the continuous spectrum was found to be about 300.

§ 5. THE SEARCH FOR FINE STRUCTURE IN THE INTERNAL CONVERSION LINES OF RADIUM C

During 1948–49 Latyshev and his co-workers published a number of papers claiming that many of the well-known internal conversion lines of radium C.C′ exhibited a fine structure, the component lines being equally spaced. Latyshev has now (1950) withdrawn this claim and suggests that the multiple sharp peaks found experimentally were due to insufficient counting and to fluctuations in their magnetic field. Before this withdrawal preliminary investigations had already been made using the new prism spectrometer, and a brief report on our

definitive findings regarding the structure of the 1414 kev and 606 kev internal conversion lines is given below.

Because of its longer lifetime radon is more convenient to use as a source than is a deposit of radium C, though the straggling of the electrons in passing through the walls of the container of the radon gas will produce a broadening of the image. A thin-walled glass ampoule was therefore filled with 100 millicuries of radon. The wall thickness was 7×10^{-4} cm, or about 3 mg/cm². The tube was made by drawing out thin-walled soda glass tubing. Many tubes were drawn and examined under a microscope. A rough check of the wall thickness of the tube was obtained by measuring the maximum range in air of the α-particles emerging from the tube. The length of the ampoule was about 2 cm and its diameter 0·012 cm. The fine glass tube was mounted on the same source holder and in the same position as the platinum wire that was used in the focusing experiments. It was held in place by tap grease.

The K, L and M conversion lines of the 1414 kev γ-transition were recorded using Ilford G5 Nuclear plates. Several exposures were taken with this source and a microphotometer trace is shown in fig. 12. The trace breadth of the

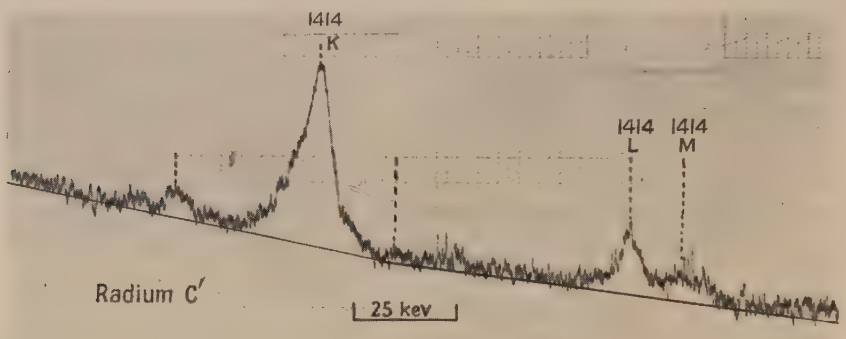

Fig. 12. Reduced microphotometer trace of the conversion lines of the 1414 kev γ-transition RaC.C′

K conversion line is about 10 kev. If, however, the trace is converted into relative intensity units, the line shape is considerably altered and the half-width is only 5 kev. From the results of White and Millington (1928), a line of zero width should be broadened to a half-width of about 4 kev for electrons of this energy passing through a 'light' material of thickness 3 mg/cm². The instrumental half-width corresponding to a resolving power of 1000 should be about 1·8 kev. Therefore the line had about the half-width to be expected from a single line for electrons passing through the walls of the glass ampoule.

To avoid the line broadening due to the straggling of the electrons in the glass, it was decided to activate the edge of a piece of platinum foil. The edge was exposed to radon gas and a negative potential of 1000 volts was applied to the foil; 200 millicuries of radon were used and the period of activation was one hour. The γ-ray activity of the active deposit on the foil was equivalent to that of about 25 mg radium in equilibrium with its products when first removed from the radon.

The Geiger counters were used in coincidence and the timing of the readings carefully noted in order to correct for source decay during counting.

With the K conversion line of the 1414 kev γ-transition the number of counts taken was such that the statistical mean error at the background level was

approximately 6%, and at the peak of the line 3%. Values between these were obtained at other points. The ratio of the height of the line to the height of the continuous spectrum was 6·9 : 1. This ratio is a measure of the resolving power of an instrument. The value obtained by Latyshev was 2 : 1. Figure 13 shows the line obtained (curve II); curve I represents Latyshev's line. The continuous spectrum has been deducted and the curves normalized to have the same peak intensity. The half-width of our line corresponds to a resolving power of approximately 800.

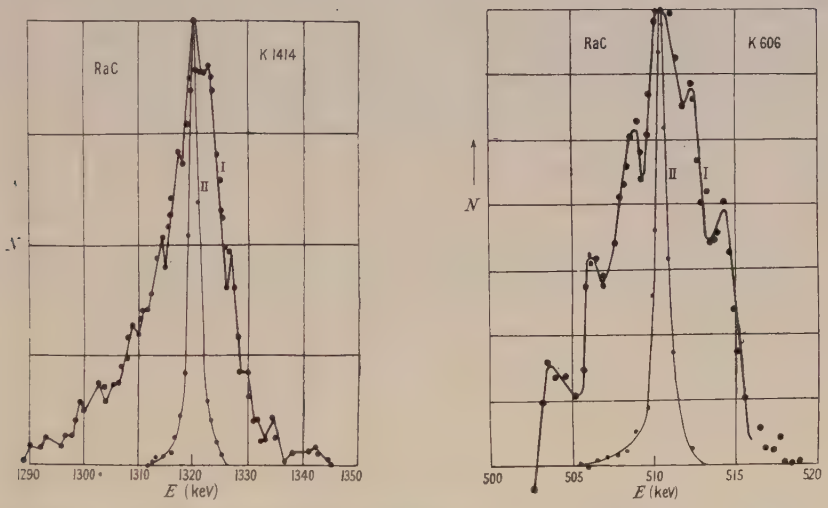

Figs. 13 and 14. Geiger counter determinations of the K conversion lines for the 1414 kev and 606 kev γ-transitions of RaC.C′. In each case the outer curve is that due to Latyshev.

The platinum foil was reactivated and the K conversion electrons from the 606 kev γ-ray were examined. Figure 14 shows the result in curve II, after subtraction of the continuous spectrum and normalizing the line, so that its peak coincides with the line obtained by Latyshev. The number of counts taken gave a statistical mean error at the background level of approximately 5% and at the peak 3%, and values between these at other points. The half-width of the line corresponds to a resolving power of approximately 1 000.

Bashilov, Antoneva and Zolotavin (1950) state that they have examined the 606, 1 120, 1 414 and 1 760 kev K conversion lines of radium C at a resolving power of about 400. They found no fine structure.

Serebriskaya, Forafontov and Shpinel (1950) also investigated the same lines but because they used radon gas in a glass ampoule their resolving power was inferior to that of Bashilov, Antoneva and Zolotavin.

ACKNOWLEDGMENTS

It is a pleasure to thank Professor Feather for his encouragement and generous support. We wish to thank Professor Greaves for permitting us to use the Royal Observatory Recording Microphotometer. We are indebted to the Department of Scientific and Industrial Research for a grant towards the cost of the apparatus, and one of us (D. A. S.) would like to thank this Department for a maintenance allowance.

REFERENCES

Bashilov, A. A., Antoneva, N. M., and Zolotavin, A. V., 1950, *Dokl. Akad. Nauk. S.S.S.R.*, **70**, 793.

Dzhelepov, B. S., and Bashilov, A. A., 1950, *Izv. Akad. Nauk, S.S.S.R.*, Ser. Fiz., **14**, 263.

Ehrenberg, W., and Jennings, J. C. E., 1952, *Proc. Phys. Soc.* B, **65**, 265.

Jennings, J. C. E., 1952, *Proc. Phys. Soc.* B, **65**, 256.

Korsunsky, M., Kelman, V., and Petrov, B., 1944, *J. Exp. Theor. Phys., U.S.S.R.*, **14**, 394, in Russian (1945, *J. Phys., U.S.S.R.*, **9**, 7, in English).

Latyshev, G. D., 1950, *J. Exp. Theor. Phys., U.S.S.R.*, **20**, 192.

Nettleton, H. R., and Sugden, S., 1939, *Proc. Roy. Soc.* A, **137**, 73.

Serebriskaya, V. M., Forafontov, N. V., and Shpinel, V. S., 1950, *J. Exp. Theor. Phys., U.S.S.R.*, **20**, 573.

Shpinel, V. S., 1946, *Dokl. Akad. Nauk., S.S.S.R.*, **53**, 801 (in Russian) ; *C. R. (Dokl.) Acad. Sci., U.R.S.S.*, **53**, 793 (in English) : 1950, *J. Tech. Phys., U.S.S.R.*, **20**, 834.

Siday, R. E., 1947, *Proc. Phys. Soc.*, **59**, 905.

White, P., and Millington, G., 1928, *Proc. Roy. Soc.* A, **120**, 701.

The Re-investigation of some Photoelectron Lines of Thorium (B+C)

By D. A. SILVERSTON

Department of Natural Philosophy, University of Edinburgh

Communicated by N. Feather; *MS. received 27th September* 1951, *and in final form* 1*st January* 1952

ABSTRACT. The β-ray spectrum of thorium (B+C) has been re-investigated using the β-ray spectrograph described by Siday and Silverston. The range 200 kev–300 kev was studied in detail using photographic recording and a previously unobserved γ-ray of energy 294·6 kev has been attributed to the transition thorium C.C″. The conversion lines of the γF ray of thorium B.C in the L_I, L_{II} electronic shells have been resolved and their relative intensities have been found using a Geiger counter. The conversion of the same γ-ray in the M_I, M_{II} electron shells has been measured and the lines have been partially resolved. The M photoelectron line associated with the transition thorium C″.D has been examined, and its suspected doublet structure confirmed.

The β-spectrograph described by Siday and Silverston (1952) has been used to record the lines in the region 200 to 300 kev. The thorium-active deposit was carried on a fine platinum wire of diameter 0·1 mm. The relative energies of the lines are given in the table and are compared with the values given by Ellis (1932 a) and Surugue (1937). Some microphotometer traces are shown in fig. 1. Not all the lines that are indicated could be identified from these traces alone, but a large number of traces at ten times this magnification were studied and the ordinates were averaged. The nomenclature is similar to that devised by Ellis (1932 b) and, except for the addition of a new line, is exactly the same as that adopted by Surugue (1937).

The difference in energy between the I and J lines, as given by Ellis (1932 a), was used to measure the dispersion of the spectrograph, and the energies of all the other lines were obtained on the assumption that the I and J lines differed in energy by 12·30 kev. This is the difference in energy between the L_I and M_I electron shell levels for element 83. The absolute energy of the I line was

Name	Energy (kev) Silverston	Ellis	Surugue
Ga	202·1	201·7	201·9
H	208·9	208·9	209·7
Ha	209·5	—	—
H_1	—	213·1	213·4
H_2	217·4	—	217·0
I	221·7	221·7	221·8
Ia	222·4	222·4	222·4
Ia_1	224·6	224·0	224·6
Ia_2	231·0	233·2	229·0
J	234·0	234·0	234·2
J_1	—	—	235·0
J_2	236·0	—	235·9
Ja	237·0	236·9	237·2
Ja_1	238·0	—	238·0

Name	Energy (kev) Silverston	Ellis	Surugue
Ja_2	241·4	241·5	241·9
Ja_3	255·4	255·5	256·0
Ja_4	257·7	257·7	258·4
Jb	260·9	260·9	261·0
Jb_1 (E)	263·9	263·6	—
Jb_1	271·7	—	271·9
Jb_2	272·6	272·4	272·7
Jb_3	275·7	—	275·8
Jb_4	279·9	—	278·4
Jc	283·7	282·8	283·8
Jc_1	284·3	—	284·6
Jc_2	295·5	295·7	296·1
Jc_3	300·3	—	299·3

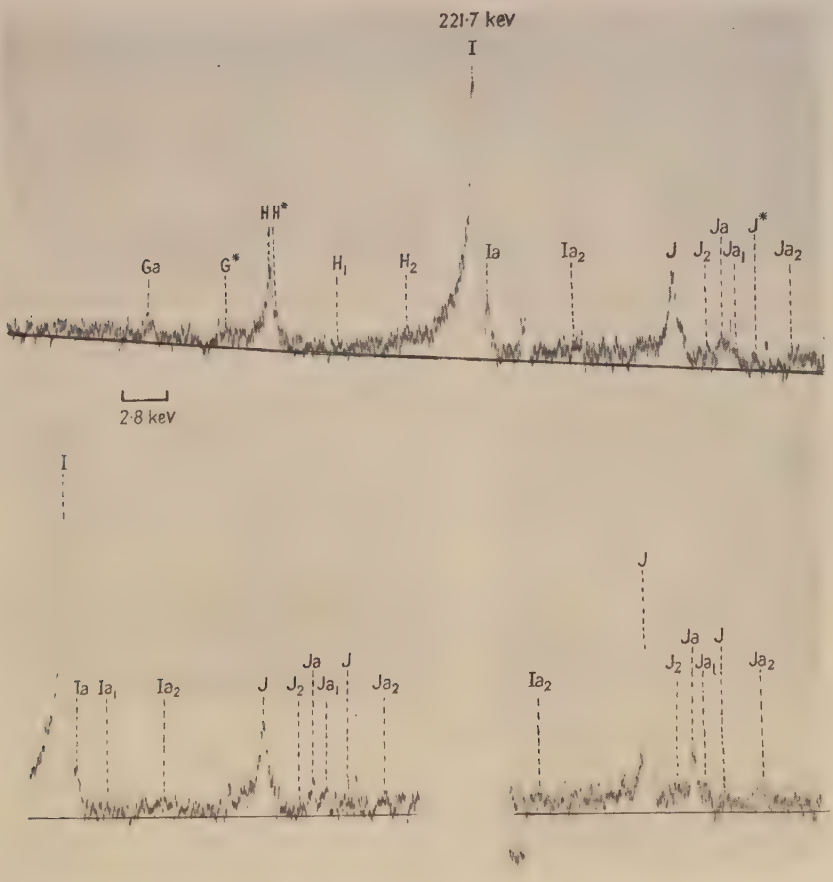

Fig. 1. Microphotometer traces of part of the β-spectrum of thorium (B+C). No line could be found in the position marked H_1 and the presence of a line in the position marked J* was not convincing.† ×3

† Note: In the lower two tracings the J on the right-hand side refers to J*.

assumed to be 221·7 kev, this being the figure given by Ellis (1932 a). Except in one or two instances the relative intensities of the lines have not been measured. The chief results of the new survey are as follows:

Ellis found the line Ia_2 to be of energy 233·2 kev and Surugue (1937) gave a value 229·0 kev. The energy discrepancy between these two lines is so large that, although both authors have given them the same name, Ia_2, it would appear likely that this refers to two different lines. Neither of these was found, however, but a line, which has also been referred to as Ia_2, was found at 231·0 kev. Its origin has not been explained.

The line listed by Ellis (1932 a) at 267·2 kev could not be found, nor could the H_1 line listed by Ellis and Surugue at about 213 kev.

Surugue interpreted the Ja and Ja_1 lines as being the N and O electron shell conversion lines of the γF ray of element 83. He gave the ratio of their intensities as greater than 18:1. The ratio has been found to be less than 4:1.

The Ha Line

There appears to be a weak line on the high energy side of the H line. Its energy is estimated to be 0·6 kev higher, that is 209·5 kev. If this line were due to the conversion in the K shell of the γ-ray from element 81 the energy of the γ-ray would be 294·6 kev. The L_I conversion of this γ-ray would give a line at 279·3 kev. The energy of the line Jb_4 was found to be 279·9 kev, in good agreement with this predicted value. The origin of the Jb_4 line has not been previously explained.

Measurement of the energies of the α-particles emitted in the transformation thorium C.C″ by several authors suggests that there should be a difference in the nuclear levels corresponding to 294 kev. Ellis (1932 a) suggested that the ray γH_1 of 298 kev could be associated with this energy difference of the α-particle groups. This is not very convincing for the following reason. He tabulated eight different γ-ray energies and compared them with the energy differences deduced from α-particle measurements. All the γ-rays with the exception of γH_1 had an energy a few kev less than the corresponding energies deduced from α-particle measurements. In the case of H_1 the energy was greater by about 4 kev. Furthermore, Surugue has attributed the H_1 β-ray to a thorium C″.D transition.

The H photoelectron line is due to the K conversion of the γH ray of element 83 and its L_1 conversion electrons account for most of the intensity of the Jc line. The ratio of the intensity of H:Jc is given as 10:1 by Surugue and about 8:1 by Ellis. These ratios are rather greater than the usual ratio of intensities for K:L conversion at this energy, but the fact that the Ha line was not previously resolved from H may account for the discrepancy.

The J Line

The microphotometer trace of this line is shown in fig. 2, and fig. 3 shows the form of this line after conversion to relative intensity units. The broken curves are the instrumental line shapes, and their intensities and separation have been adjusted so that the sum of their ordinates gives the experimental (full line) curve. The J line is due to the M_I and M_{II} conversion electrons of the γF ray of thorium C. The separation of the dotted curves in fig. 3 is 0·25 kev. From x-ray data the separation of the M_1 and M_{II} levels is 0·3 kev. The ratio of the intensities of the two components is 4·3:1.

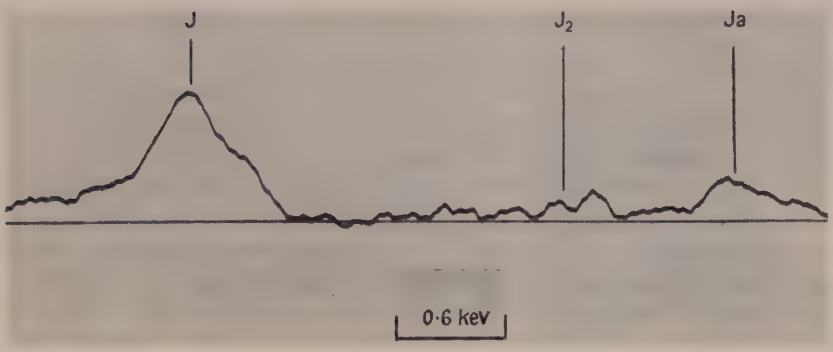

Fig. 2. Microphotometer traces of the J and Ja lines. ×30

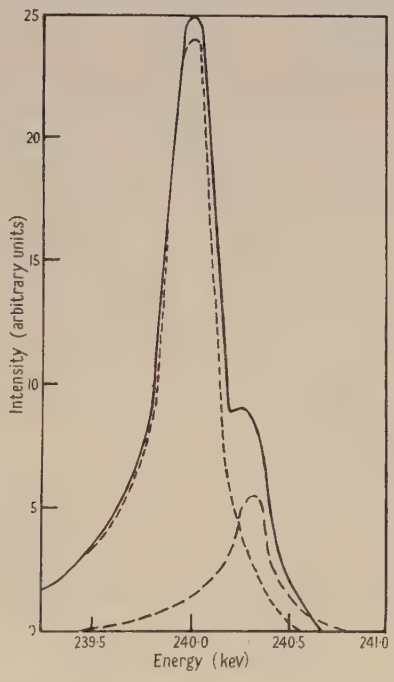

Fig. 3. The J line after conversion to relative intensity units.

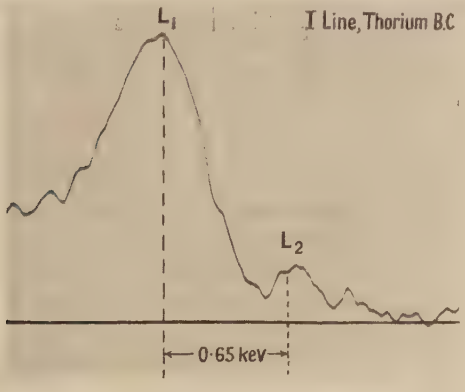

Fig. 4. Microphotometer trace of the I and Ia lines showing the L_I, L_{II} levels resolved. ×30
Note: L_2 refers to the L_{II} level.

The I Line

The I line is due to the L_I conversion of the γF ray from Thorium C. The L_{II} conversion level is at 0·6 kev higher energy, the separation of the levels requiring a resolving power of about 600 expressed as $H\rho/\Delta(H\rho)$.

The microphotometer trace is shown in fig. 4.

The lines were also measured with two Geiger counters in coincidence. The curve obtained after deduction of the continuous β-spectrum is shown in fig. 5. The number of counts taken on the high energy side gave a statistical mean error of less than 2% at the continuous background level.

The analysis of the line into the two components (broken curves), gives exactly the correct separation of the levels. The small dotted curve has been drawn to have the same shape as the larger curve but its area is one-eighteenth of the area of the larger curve.

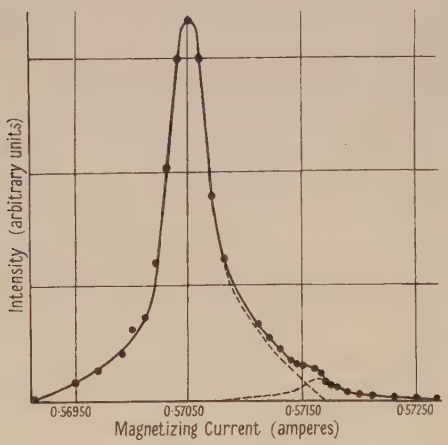

Fig. 5. Photoelectron spectrum of the I and Ia lines after deduction of the continuous β-spectrum. The statistical mean error is less than 2% at the background level. The analysis of the line into the two components (dotted curves) gives exactly the separation of the L_I, L_{II} levels. Their ratio of intensities is 18 : 1.

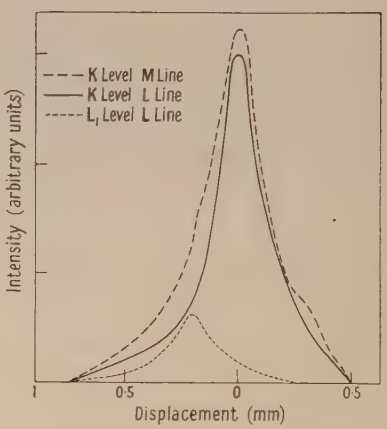

Fig. 6. The M and L lines. The weaker (dotted) curve on the low energy side has been drawn the same shape as the L line, but with one-fifth of its intensity. The addition of the ordinates approximates closely to the M line.

The ratio of the intensities of the L_I and L_{II} conversion lines was thus found to be 18 : 1. Forafontov and Shpinel (1950) have found this ratio to be approximately 20 : 1. The values obtained photographically by Ellis (1932 a), Surugue (1937) and Arnoult (1939) were 15·6, 16 and 11 respectively.

The M Line

In order to explain the fact that in the transition thorium C″.D the L, M and N photoelectron lines are equally spaced and appear to differ in energy by an amount equal to the difference in energy between the K and L_I electron shells of thorium D, it has been assumed that two γ-rays (γL and γM) differ in energy (fortuitously) by this amount. On this assumption the M line is of double origin, and its intensity relative to the L line (roughly equal according to Ellis and Surugue, 1 : 1·3 according to Flammersfeld (1939) and 1 : 0·83 according to Martin and Richardson (1948) is consonant with this view. Only about

one sixth of this intensity is likely to be due to the L_I photoelectrons from γL, the remainder arising from the K photoelectrons from γM.

In order to check this assumption directly, an attempt was made to resolve the M line photographically. Three exposures were taken and microphotometered at several points along each line. Three exposures were also taken of the L line. The traces have been averaged and converted to relative intensity units for each line, although the relative intensities of the L and M lines have not been compared.

Figure 6 shows the two curves. The weaker (dotted) line on the low-energy side has been drawn the same shape as the L line, but with one fifth of its intensity. If the ordinates of this line are added to those of the L line a line very similar to the experimental M line is obtained.

The bump at the base of the line on the high-energy side was not interpreted.

If fig. 6 represents the correct analysis, the separation of the L_I conversion line of the γL ray and the K conversion line of the γM ray is approximately 0·43 kev.

If the energy of the M photoelectron line is 494·17 kev (Ellis 1932 a), then the L_I conversion line of the γL ray will be 493·74 kev. Taking the K and L_I absorption energies as 87·50 kev and 15·82 kev, the energy of the L photoelectron line will be 422·06 kev. The value given by Ellis was 421·98 kev but the last figures cannot of course be considered as significant.

ACKNOWLEDGMENTS

It is a pleasure to thank Professor Feather for his encouragement and generous support. I am grateful to Professor Greaves for permitting me to use the Royal Observatory Recording Microphotometer and I am indebted to the Department of Scientific and Industrial Research for a maintenance allowance.

REFERENCES

Arnoult, R., 1939, *Ann. Phys. Paris*, **11–12**, 241.
Ellis, C. D., 1932 a, *Proc. Roy. Soc.* A, **138**, 330 ; 1932 b, *Nature, Lond.*, **129**, 276.
Flammersfeld, A., 1939, *Z. Phys.*, **114**, 227.
Forafontov, N. V., and Shpinel, V. S., 1950, *Dokl., Akad. Nauk, SSSR.*, **72** (No. 1), 49.
Martin, D. G. E., and Richardson, H. O. W., 1948, *Proc. Roy. Soc.* A, **195**, 287.
Siday, R. E., and Silverston, D. A., 1952, *Proc. Phys. Soc.*, A, **65**, 328.
Surugue, J., 1937, *Ann. Phys., Paris*, **8**, 484.

The Elastic Behaviour of a Crystalline Aggregate*

By R. HILL
H. H. Wills Physical Laboratory, University of Bristol

Communicated by N. F. Mott ; MS. received 17th December 1951

ABSTRACT. The connection between the elastic behaviour of an aggregate and a single crystal is considered, with special reference to the theories of Voigt, Reuss, and Huber and Schmid. The elastic limit under various stress systems is also considered ; in particular, it is shown that the tensile elastic limit of a face-centred aggregate cannot exceed two-thirds of the stress at which pronounced plastic distortion occurs.

* This paper is a slightly extended version of a lecture delivered on 14th September 1951 at the Bristol Summer School on the Physics of Solids.

§1. INTRODUCTION

As a method for calculating the elastic moduli of an aggregate of crystals, Voigt (1928) proposed the averaging, over all possible lattice orientations, of the relations expressing the stress in a single crystal in terms of the given strain. Reuss (1929) proposed, on the other hand, the averaging of the relations expressing the strain in terms of the given stress. Voigt's procedure contains the assumption that the strain is uniform throughout an aggregate, and Reuss's that the stress is uniform. In the first model, the forces between grains could not usually be in equilibrium, while in the second the distorted grains could not fit together. In general, then, both derivations are approximate. It is found, however, that the measured moduli for the aggregate invariably lie between the Reuss and Voigt values, the latter being greater (Boas and Schmid 1934). It is intended here to suggest an explanation, and to consider also other elastic properties of an aggregate.

§2. RELATION BETWEEN CRYSTALLINE AND POLYCRYSTALLINE ELASTICITY

Let the macroscopic stress and strain in the aggregate be denoted by $\mathbf{S}$ and $\mathbf{E}$; for convenience of notation, these are regarded as vectors in a nine-dimensional space. Let $\boldsymbol{\sigma}$ and $\boldsymbol{\epsilon}$ be the microscopic stress and strain at any point in any grain of the aggregate. Then, according to Bishop and Hill (1951 a), if the aggregate contains a sufficiently large number of grains and is macroscopically homogeneous

$$\mathbf{S} \cdot \mathbf{E} = \int \boldsymbol{\sigma} \cdot \boldsymbol{\epsilon} \, dV \qquad \ldots\ldots(1)$$

integrated through a (large) unit of volume.

In view of Maxwell's reciprocal relation, the following identities are true at each point of the aggregate

$$\boldsymbol{\sigma} \cdot \boldsymbol{\epsilon} + (\boldsymbol{\sigma} - \boldsymbol{\sigma}^*) \cdot (\boldsymbol{\epsilon} - \mathbf{E}) \equiv \boldsymbol{\sigma}^* \cdot \mathbf{E} + 2(\boldsymbol{\epsilon} - \mathbf{E}) \cdot \boldsymbol{\sigma},$$

$$\boldsymbol{\sigma} \cdot \boldsymbol{\epsilon} + (\boldsymbol{\sigma} - \mathbf{S}) \cdot (\boldsymbol{\epsilon} - \boldsymbol{\epsilon}^*) \equiv \mathbf{S} \cdot \boldsymbol{\epsilon}^* + 2(\boldsymbol{\sigma} - \mathbf{S}) \cdot \boldsymbol{\epsilon}.$$

$\boldsymbol{\sigma}^*$ is the stress that would exist in a crystal with the local orientation and having the strain $\mathbf{E}$; $\boldsymbol{\epsilon}^*$ is the strain that would be produced in such a crystal by the stress $\mathbf{S}$. Since the scalar product of any related stress and strain is essentially positive (being equal to twice the energy density)

$$\boldsymbol{\sigma} \cdot \boldsymbol{\epsilon} \leqslant \boldsymbol{\sigma}^* \cdot \mathbf{E} + 2(\boldsymbol{\epsilon} - \mathbf{E}) \cdot \boldsymbol{\sigma}$$

and

$$\boldsymbol{\sigma} \cdot \boldsymbol{\epsilon} \leqslant \mathbf{S} \cdot \boldsymbol{\epsilon}^* + 2(\boldsymbol{\sigma} - \mathbf{S}) \cdot \boldsymbol{\epsilon}.$$

It was shown by Bishop and Hill (1951 a, b) that the volume integral of the last term in each inequality vanishes. Hence, from (1)

$$\mathbf{S} \cdot \mathbf{E} \leqslant \begin{cases} \mathbf{E} \cdot \int \boldsymbol{\sigma}^* \, dV, \\ \mathbf{S} \cdot \int \boldsymbol{\epsilon}^* \, dV. \end{cases} \qquad \ldots\ldots(2)$$

The left-hand side of this equation is twice the actual energy density (as conventionally defined in terms of macroscopic quantities); the right-hand sides are twice the energy densities that would be calculated by the Voigt and Reuss theories respectively.

For an aggregate which is macroscopically isotropic, (2) must reduce to the following symmetric (and automatically quadratic) expressions in the principal components of stress and strain

$$\left.\begin{aligned} &K(E_1+E_2+E_3)^2+\tfrac{2}{3}G\Sigma(E_1-E_2)^2 \leqslant K_V(E_1+E_2+E_3)^2+\tfrac{2}{3}G_V\Sigma(E_1-E_2)^2, \\ &\frac{1}{K}(S_1+S_2+S_3)^2+\frac{3}{2G}\Sigma(S_1-S_2)^2 \leqslant \frac{1}{K_R}(S_1+S_2+S_3)^2+\frac{3}{2G_R}\Sigma(S_1-S_2)^2. \end{aligned}\right\} \quad \ldots\ldots(3)$$

K and G are the actual bulk and rigidity moduli, and suffixes V and R denote values calculated in the Voigt and Reuss theories from an evaluation of the integrals in (2). (Averaging the energy density, provided it is expressed in these respective forms, is equivalent to averaging the stress–strain relations for given stress or strain.) Since eqns. (3) are true for any stress and strain, it follows that

$$K_R \leqslant K \leqslant K_V; \quad G_R \leqslant G \leqslant G_V. \qquad \ldots\ldots(4)$$

The corresponding estimates of Poisson's ratio ν and Young's modulus E are obtained by substituting the appropriate values of K and G in

$$\nu=\frac{1}{2}\left[1-\frac{3G}{3K+G}\right], \quad \frac{1}{E}=\frac{1}{3G}+\frac{1}{9K}. \qquad \ldots\ldots(5)$$

From (4) it is evident that $E_R \leqslant E \leqslant E_V$.

It has thereby been proved that the Voigt moduli exceed the Reuss moduli, while the true values should lie between them. The former conclusion is purely mathematical, but the latter is dependent on the truth of the statistical hypothesis embodied in (1).

It was shown by Voigt that

$$\left.\begin{aligned} 9K_V&=(c_{11}+c_{22}+c_{33})+2(c_{12}+c_{23}+c_{31}), \\ 15G_V&=(c_{11}+c_{22}+c_{33})-(c_{12}+c_{23}+c_{31})+3(c_{44}+c_{55}+c_{66}); \end{aligned}\right\} \quad \ldots\ldots(6)$$

and by Reuss that

$$\left.\begin{aligned} 1/K_R&=(s_{11}+s_{22}+s_{33})+2(s_{12}+s_{23}+s_{31}), \\ 15/G_R&=4(s_{11}+s_{22}+s_{33})-4(s_{12}+s_{23}+s_{31})+3(s_{44}+s_{55}+s_{66}). \end{aligned}\right\} \quad \ldots\ldots(7)$$

It may be remarked that only nine of the 21 independent elastic constants for the single crystal occur in these formulae for the macroscopic moduli.

In particular, for a body or face-centred cubic crystal

$$c_{11}=c_{22}=c_{33}, \quad c_{12}=c_{23}=c_{31}, \quad c_{44}=c_{55}=c_{66},$$

with similar relations for the s coefficients, when the components of stress and strain are referred to the cubic axes. Also,

$$c_{11}-c_{12}=1/(s_{11}-s_{12}), \quad c_{11}+2c_{12}=1/(s_{11}+2s_{12}), \quad c_{44}=1/s_{44}. \qquad \ldots\ldots(8)$$

Equations (6) and (7) thus reduce to

$$\left.\begin{aligned} K_R&=K_V=\tfrac{1}{3}(c_{11}+2c_{12}), \\ 5G_V&=(c_{11}-c_{12})+3c_{44}, \quad 5/G_R=4(s_{11}-s_{12})+3s_{44}. \end{aligned}\right\} \quad \ldots\ldots(9)$$

That $K_R=K_V$ is otherwise obvious since a hydrostatic stress produces only an isotropic volume change in face- or body-centred cubic crystals, and so uniform distributions of hydrostatic stress and strain in the aggregate are compatible.*

* This would not be true of an aggregate of hexagonal crystals, for instance.

We may notice, in passing, that the Cauchy relation $c_{12}=c_{44}$ would make $G_V=3K/5$ and $\nu_V=\frac{1}{4}$. Again, the condition for isotropy, $c_{11}-c_{12}=2c_{44}$, makes $G_R=G_V(=c_{44})$; this is naturally to be expected since the aggregate is then microscopically homogeneous. Finally, for small amounts of anisotropy the difference between G_R and G_V is only a second-order quantity, since

$$G_V-G_R=\frac{3}{5}\frac{[2c_{44}-(c_{11}-c_{12})]^2}{[4c_{44}+3(c_{11}-c_{12})]}. \qquad \ldots\ldots(10)$$

§ 3. NUMERICAL ILLUSTRATIONS

Complete and reasonably accurate data are available for aluminium, copper, gold and α-iron. The c's in table 1 are taken from Boas and Mackenzie (1950). Figures given by other authorities (e.g. Hearmon 1946) occasionally differ by about 1%. The tabulated values are for atmospheric pressure; according to Lazarus (1949) a superposed hydrostatic pressure of order 10^{10} dyn cm^2 increases the moduli by several per cent.

Table 1

	c_{11}	c_{12}	c_{44}	G_R	G_V	$K_R=K_V$	E_R	E_V	ν_R	ν_V
Al	1·08	0·622	0·284	0·26	0·26	0·78	0·71	0·71	0·349	0·348
Cu	1·70	1·23	0·75	0·40	0·54	1·39	1·09	1·44	0·369	0·328
Au	1·86	1·57	0·42	0·24	0·31	1·67	0·69	0·87	0·431	0·413
α-Fe	2·37	1·41	1·16	0·74	0·89	1·73	1·93	2·29	0·313	0·280

Unit=10^{12} dyn/cm^2.

It will be observed that an aluminium crystal is much more nearly isotropic than the others.

Table 2 shows the measured constants for the aggregates. Authorities differ appreciably, owing possibly to the presence of slight preferred orientations in the specimens, and to the inherent difficulty of determining ν or K. The values adopted here have been chosen to conform to $1+\nu=E/2G$. The agreement with (4) and (9) appears satisfactory, in view of the uncertainty in the data. The measured values of G fall almost midway between those of Reuss and Voigt. (We may contrast this with the conjecture by Bishop and Hill that the work done in *plastic* distortion may be calculated, to a good approximation, as if the microscopic strain were uniform.) Empirically, $\frac{1}{2}(G_R+G_V)$ or $\sqrt{(G_RG_V)}$ suggest themselves as good approximations.

Table 2

	G	K	E	ν
Al	0·265	0·74	0·71	0·34
Cu	0·436	1·33	1·18	0·35
Au	0·278	1·66	0·79	0·42
α-Fe	0·808	1·59	2·07	0·285

Unit=10^{12} dyn/cm^2.

Mention may be made of a theory proposed by Huber and Schmid (1934) and elaborated by Boas (1934, 1935). Their procedure for calculating Young's modulus is tantamount to assuming that in any grain the stress is a pure tension parallel to some fixed direction, and of amount sufficient to produce a unit component extension in that direction. Effectively, a Young's modulus is defined for each direction in the crystal and is averaged over all possible

directions. In the Reuss theory, on the other hand, it is the inverse of the modulus that is averaged. Evidently, therefore, the Huber–Schmid modulus must exceed the Reuss modulus. Calculations by Boas and Schmid (1934) for the four metals considered above show that the Huber–Schmid modulus exceeds E_R by less than $0{\cdot}3(E_V - E_R)$. However, it has not yet been proved theoretically that the Huber–Schmid modulus is necessarily and invariably less than the true E or even less than E_V.

§ 4. THE ELASTIC LIMIT

The elastic limit of an aggregate under a given kind of macroscopic stress (tension, shear, etc.) is taken here to refer to the stress at which local plastic deformation is initiated. The elastic limit is necessarily dependent on any locked-up stresses existing before the external load is applied. It seems probable that such initial stresses must tend to lower the elastic limit. Conversely, the reduction of such stresses by a mild annealing often serves to raise the elastic limit.

In an aggregate of anisotropic crystals the elastic limit must also depend on the shapes of the grain boundaries, since these influence the local concentrations of stress. For this reason, we should expect a scatter in the measured elastic limits for macroscopically identical aggregates; other things being equal, the scatter should increase with the degree of elastic anisotropy in the constituent grains.

It is possible to estimate an upper bound to the elastic limit, corresponding to what are presumably the most favourable conditions. Suppose that the Schmid law for plastic yielding applies; that is, yielding in a crystal begins when the component shear stress, acting over any slip plane and in any slip direction, reaches a critical value τ (depending on the state of hardening). Suppose, further, that all grains are initially stress-free, equally hardened, elastically isotropic, and perfectly elastic until slip begins under the Schmid law. A uniform microscopic distribution of strain would then be produced by a uniformly applied external load not exceeding the elastic limit. Since all orientations are supposed to be present, local yielding begins in the grain(s) of 'weakest' orientation when the macroscopic maximum shear stress attains the value τ.

Bishop and Hill (1951 b) have calculated that pronounced plastic distortion should first become possible in a face-centred aggregate under tension at the stress $3{\cdot}06\tau$*; the writer has suggested the term 'yield point' for this stress. The tensile elastic limit, on the other hand, should be not greater than 2τ, that is, about two-thirds of the yield point. At loads between these two, the macroscopic strain (though partly plastic) is of elastic order (i.e. stress/E). Hence, until the yield point is reached, the load–extension curve deviates only slightly from the prolongation of the elastic line. The corresponding ratio for pure shear is 3/5, very nearly.

Extremely sensitive measurements are required for a reasonably close determination of the elastic limit, if the departure from the elastic line is due to slip in a few grains at most. Roberts, Carruthers and Averbach (1951) have been able to measure strains down to 2×10^{-6}, and have reported elastic limits and yield points in several steels. For an annealed 0·17% carbon steel with only a slight drop in load following the upper yield point, they observed an elastic limit of $1{\cdot}7 \times 10^9$ dyn/cm^2 and a lower yield point of $2{\cdot}4 \times 10^9$ dyn/cm^2. The

* Strictly, this value is for an aggregate whose elastic moduli are indefinitely large ; it should be a very good approximation for face-centred metals.

observed ratio was therefore a little over 2/3. This is in accord with the previous remarks, since it appears justifiable to suppose that the ratio calculated for a face-centred aggregate is approximately true for mild steel. It was further observed that the elastic limit had decreased to $1{\cdot}5 \times 10^9$ dyn/cm^2 after 9% strain, while the yield point had increased to $3{\cdot}5 \times 10^9$ dyn/cm^2. The ratio had thus fallen to 3/7, a circumstance which could be attributed to internal stresses introduced by cold-working. In the other steels, with various yield point drops, the ratio of elastic limit to lower yield point was between 2/3 and 4/5.

Consider, now, the elastic limit under a pure hydrostatic stress. In an aggregate of face- or body-centred cubic crystals we have seen that the microscopic stress distribution is uniform in this case. Hence, if initially there are no locked-up stresses, the elastic limit under hydrostatic stress is indefinitely great, provided the Schmid law is valid (or, more generally, provided hydrostatic stress does not cause plastic distortion). On the other hand, in an aggregate of non-cubic crystals an external hydrostatic stress produces non-uniform microscopic stresses and strains, and so local yielding must eventually occur. Thus, there is an elastic limit in a non-cubic aggregate under hydrostatic stress, but, as Bishop and Hill have shown, no yield point within the range of validity of the Schmid law. Hence, both plastic and elastic components of the strain increase indefinitely as the hydrostatic stress is increased, while the rate of increase of strain remains of order E and decreases only gradually.

§ 5. ELASTIC BEHAVIOUR DURING UNLOADING

Finally, we may enquire for what range of stress an aggregate might be expected to unload elastically immediately after a permanent distortion. According to the theory proposed by Bishop and Hill (1951 b), the microscopic stresses in a face-centred aggregate during plastic distortion differ considerably from the macroscopic stress, so much so, that, on starting to unload, local slip on certain previously active slip directions would occur at once.* According to this model, then, no elastic range is to be expected in the first part of the hysteresis loop. In practice, an elastic range is usually observed, but the extent to which this is a reflection of the sensitivity of the apparatus seems not to have been investigated.

REFERENCES

Bishop, J. F. W., and Hill, R., 1951 a, *Phil. Mag.*, **42**, 414 ; 1951 b, *Ibid.*, **42**, 1298.
Boas, W., 1934, *Helv. Phys. Acta*, **7**, 878 ; 1935, *Ibid.*, **8**, 674.
Boas, W., and Mackenzie, J. K., 1950, *Progress in Metal Physics*, 2 (London : Butterworths Scientific Publications).
Boas, W., and Schmid, E., 1934, *Helv. Phys. Acta*, **7**, 628.
Hearmon, R. F. S., 1946, *Rev. Mod. Phys.*, **18**, 409.
Huber, A., and Schmid, E., 1934, *Helv. Phys. Acta*, **7**, 620.
Lazarus, D., 1949, *Phys. Rev.*, **76**, 545.
Reuss, A., 1929, *Z. angew. Math. Mech.*, **9**, 55.
Roberts, C. S., Carruthers, R. C., and Averbach, B. L., 1951, *M.I.T. Department of Metallurgy Quarterly Report*, **2** (2).
Voigt, W., 1928, *Lehrbuch der Kristallphysik*, 962 (Leipzig : Teubner).

* I am indebted to my colleague, Dr. J. F. W. Bishop, for making the calculations on which the conclusion is based.

The Cellular Method of Determining Electronic Wave Functions and Eigenvalues in Crystals, with Applications to Sodium

By D. J. HOWARTH and H. JONES
Department of Mathematics, Imperial College, London

MS. received 1*st January* 1952

ABSTRACT. The eigenvalues and wave functions for the conduction electrons in metallic sodium are calculated for various points of high symmetry in the Brillouin zone. The method adopted is an extension of that used by von der Lage and Bethe in which boundary conditions are applied at a large number of points on the surface of the atomic polyhedron. Eigenvalues are obtained for states whose wave vectors lie at the ends of the 2-fold, 3-fold and 4-fold axes. The energy gap at the centre of a face of the zone is found to be 0·65 ev. A method of testing the results, of a more general nature than the empty lattice test of Shockley, is outlined and applied to certain cases.

§1. INTRODUCTION

The cellular method of determining wave functions and eigenvalues of electrons in crystals originated in the theory of Wigner and Seitz (1933) for the state of lowest energy of the conduction electrons in metallic sodium. Soon afterwards Slater (1934) developed the method to apply to states of higher energy, and he and his collaborators have made many calculations of the energy, as a function of the wave vector, for several metals. Unfortunately, the accuracy of these calculations is far less than that of the original Wigner–Seitz calculation. The reason is that the boundary conditions, which should be applied over the surface of the unit polyhedron, are much more complicated for states of higher energy than for the ground state, and consequently only approximate, and very inadequate, boundary conditions were, in fact, applied.

A great improvement in the method was made by von der Lage and Bethe (1947, hereinafter referred to as LB), who showed that for certain special points in the Brillouin zone results of significant accuracy could be obtained. This improvement was achieved by making use of the known symmetry properties of the wave functions at the particular points in the Brillouin zone considered. The theory of the determination of the symmetry properties of the wave functions was given in a fundamental paper by Bouchaert, Smoluchowski and Wigner (1936, hereinafter referred to as BSW).

The notations used hitherto to specify an electronic state at a particular point in the Brillouin zone are not really satisfactory. LB deal only with the centre and six equivalent corner points of the body-centred cubic Brillouin zone and use Greek letters to denote states of specified symmetry. This is unsatisfactory because it would require a new set of letters for each point considered in the Brillouin zone. BSW use a capital letter to indicate the point in the zone and numerical subscripts to distinguish between the different states associated with that point. This is also unsatisfactory, because the symbol denoting a state gives no direct information about the symmetry of the wave function, and this is of interest in many physical applications, e.g. soft x-ray emission. We have therefore modified the BSW notation to remedy this defect; the modification is described in §2.

One purpose of the present paper is to extend the calculations of LB to other points in the sodium Brillouin zone, in particular to obtain the energy gap at the centre of a zone face. We find this energy discontinuity to be 0·65 ev. In § 5 we obtain a correction to the eigenvalues, in the form of a surface integral; apart from increasing the accuracy of the calculation of an eigenvalue, this correction can be used as a criterion of the success of any chosen set of approximate boundary conditions. Hitherto the only check on the accuracy of a calculation by the cellular method has been the empty lattice test introduced by Shockley (1937). This clearly is limited, in its application, to electronic states in real metals whose wave functions approximate, at least roughly, to free electron waves. The test described in § 5, on the other hand, applies to any state however strongly the self-consistent field within the metal modulates the wave function.

§ 2. THE SYMMETRY PROPERTIES OF THE WAVE FUNCTIONS

The first step in the cellular method is to expand the wave function in a series of spherical harmonics, as follows:

$$\psi = \sum_{l,m} (A_{lm} \cos m\phi + B_{lm} \sin m\phi) P_l^m (\cos\theta) R_l(\epsilon, r). \qquad \ldots\ldots (1)$$

The radial wave functions R_l are determined by the equation

$$\frac{d^2R_l}{dr^2} + \frac{2}{r}\frac{dR_l}{dr} + \left\{\epsilon - V(r) - \frac{l(l+1)}{r^2}\right\} R_l = 0, \qquad \ldots\ldots (2)$$

in which energies are measured in Rydberg units and lengths in units of the radius of the first Bohr hydrogen orbit. It is assumed in all this work that the potential energy V is spherically symmetrical within the unit polyhedron of the lattice.

The wave functions associated with a particular point in the Brillouin zone fall into orthogonal sets, each set with a particular type of symmetry. If we select, therefore, a particular type, the number of coefficients in (1), up to some specified value of l, is in general reduced. The higher the symmetry of the type considered the smaller will be the number of coefficients remaining in (1) to be determined by the boundary conditions.

The symmetry of a wave function, with specified wave vector **k**, must be stated with respect to the operations which transform the Brillouin zone into itself without changing **k**, or by transforming **k** into an equivalent vector. These operations form a group called by BSW the group of the wave vector **k**. Thus, to take an example, let **k** correspond to the point N in fig. (1), i.e. a mid-point of a face of the Brillouin zone. The only equivalent **k** is that at the mid-point of the opposite face. The symmetry operations of this group of the wave vector **k** are therefore as follows: $C_2(\pi, \parallel)$ which denotes a rotation through π about the two-fold axis which is parallel to **k**; $C_2(\pi, \perp)$ which is a rotation through π about the two-fold axis at right angles to **k** (this transforms N into its equivalent point); $C_4(\pi)$, which is a rotation through π about the four-fold axis ΓH which is at right angles to **k**; J the inversion operator which reflects every point in the origin; and J times each of the above rotations. Including the identity operator E there are, therefore, eight symmetry operations which will transform a Bloch wave function at the point N into another Bloch wave function belonging to the same **k**.

Since the Schrödinger equation is invariant with respect to these operations, it can be shown that the wave functions associated with the point N fall into eight types, each with a distinctive symmetry. In this paper we shall use a notation to indicate a particular symmetry type which is different from that used by BSW and which shows at once the number of true nodal *planes* through the centre of each atom by means of the well-known spectroscopic letters s, p, d, f, etc. We use the same capital letter as do BSW to indicate the point under consideration in the Brillouin zone (see fig. 1), but instead of a numerical subscript we use use the letters s, p, d, etc., as subscripts to denote the symmetry. Since in the crystal wave functions with the same number of nodal planes do not,

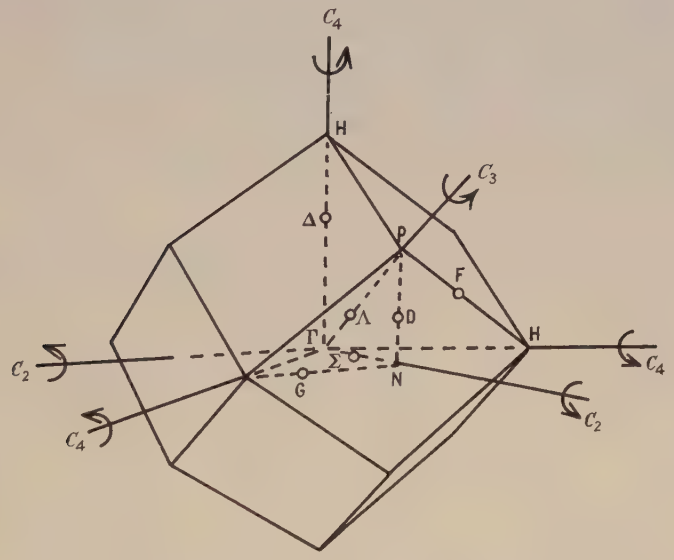

Fig. 1. Brillouin zone for sodium; letters indicate points at which the wave functions have special symmetries.

Table 1

	E	$C_4(\pi)$	$C_2(\pi, \parallel)$	$C_2(\pi, \perp)$	J	$JC_4(\pi)$	$JC_2(\pi, \parallel)$	$JC_2(\pi, \perp)$
N_s	1	1	1	1	1	1	1	1
N_p^1	1	−1	1	−1	−1	1	−1	1
N_p^2	1	1	−1	−1	−1	−1	1	1
N_p^3	1	−1	−1	1	−1	1	1	−1
N_d^1	1	−1	1	−1	1	−1	1	−1
N_d^2	1	−1	−1	1	1	−1	−1	1
N_d^3	1	1	−1	−1	1	1	−1	−1
N_f	1	1	1	1	−1	−1	−1	−1

in general, belong to the same type we have added a superscript (a number) to distinguish the wave functions with the same number of nodal planes. Table 1, which is taken from the character table XII of BSW, shows the eight symmetry types belonging to the point N in the present notation.

The number 1 in the table means that the wave function is symmetrical with respect to the operation shown, and −1 means that it is antisymmetrical. Thus the wave function $\psi(N_s)$ has no nodal planes; the wave function $\psi(N_p^1)$ a single plane node in the plane containing the axes $C_2(\perp)$ and C_4 (see fig. 2 (*b*)). These

are the functions with the two lowest energies at N for sodium; they correspond in the 'extended k-space' of elementary theory to the states on either side of the point N on the first Brillouin zone. It should be noted that the state N_p^2, which has a single nodal plane in the plane containing $C_2(\perp)$ and $C_2(\parallel)$, is *not* degenerate with N_p^1. It is, in fact, a state of much higher energy which in the approximation of 'nearly free electrons' would have many additional nodal planes. However, in a real metal these additional planes are distorted, and only the node in the $C_2(\perp)$, $C_2(\parallel)$ plane remains a true plane of antisymmetry, and this, therefore, defines the type.

Table 2 gives the relation between the notations of BSW, LB and the one adopted in the present paper (HJ). This table, besides correlating the different notations, gives information which can only be obtained, after some calculation, from the character tables of BSW; for example, we see that the state denoted by BSW as Γ_{12}, and by LB as γ, is in the present notation Γ_d^1, i.e. a state whose wave function has two nodal planes through the atom. This state, therefore, would behave rather like an atomic d state with regard, for instance, to the emission of x-rays.

Table 2. Classification of Wave Functions in a Body-centred Cubic Crystal

Equivalent points H, Γ

HJ	BSW	LB
Γ_s	Γ_1	α
Γ_p	Γ_{15}	δ
Γ_d^1	Γ_{12}	γ
Γ_d^2	Γ_{25}'	ϵ
Γ_f^1	Γ_2'	β
Γ_f^2	Γ_{25}	ϵ'
Γ_g	Γ_{15}'	δ'
Γ_h	Γ_{12}'	γ'
Γ_i	Γ_2	β'
Γ_k	Γ_1'	α'

Mid-points of faces N

HJ	BSW
N_s	N_1
N_p^1	N_1'
N_p^2	N_3'
N_p^3	N_4'
N_d^1	N_2
N_d^2	N_3
N_d^3	N_4
N_f	N_2'

Corner points P

HJ	BSW
P_s	P_1
P_p	P_4
P_d	P_3
P_f	P_5
P_i	P_2

On trigonal axis Λ and equivalent type F

Λ_s	Λ_1
Λ_p	Λ_3
Λ_f	Λ_2

Points on 4-fold axis Δ

HJ	BSW
Δ_s	Δ_1
Δ_p	Δ_5
Δ_d^1	Δ_2
Δ_d^2	Δ_2'
Δ_g	Δ_1'

Points on 2-fold axis Σ

HJ	BSW
Σ_s	Σ_1
Σ_p^1	Σ_3
Σ_p^2	Σ_4
Σ_d	Σ_2

Points on BZ face D, G

HJ	BSW
G_s	G_1
G_p^1	G_3
G_p^2	G_4
G_d	G_2
D_s	D_1
D_p^1	D_3
D_p^2	D_4
D_d	D_2

In this paper we shall only be concerned with the states of relatively low energy. These are: N_s, N_p^1; H_s, H_p, H_d^1; P_s, P_p. Taking the known symmetry of the wave functions into account, as given by the character tables of BSW, the expansions for N_s and N_p^1 in spherical harmonics, up to $l<8$, can be written

$$\psi(N_s) = R_0 + AR_2P_2(\cos\theta) + BR_4P_4(\cos\theta) + CR_6P_6(\cos\theta), \quad \ldots\ldots(3)$$

$$\psi(N_p^1) = R_1P_1(\cos\theta) + AR_3P_3(\cos\theta) + BR_5P_5(\cos\theta) + CR_7P_7(\cos\theta), \quad \ldots\ldots(4)$$

where A, B and C are, in each case, unspecified constants.

For any particular type of wave function we are at liberty to choose the polar axis, with respect to which θ is defined, in the most convenient way in order to make the expansion as simple as possible. For the two states N_s and $N_p{}^1$ we take as the polar axis $C_2(\text{II})$ (cf. fig. 2 (*b*)), and the dihedral angle ϕ is measured with respect to the plane $C_4C_2(\text{II})$.

The expansion (3) was obtained as follows: From table 1 we deduce that the wave function $\psi(N_s)$ is symmetrical with respect to reflection in each of the coordinate planes $C_2(\perp)$ $C_2(\text{II})$, $C_4C_2(\text{II})$ and $C_4C_2(\perp)$. Thus, with the polar axis as chosen, we see that there can be no term in the expansion in sin $m\phi$. Similarly

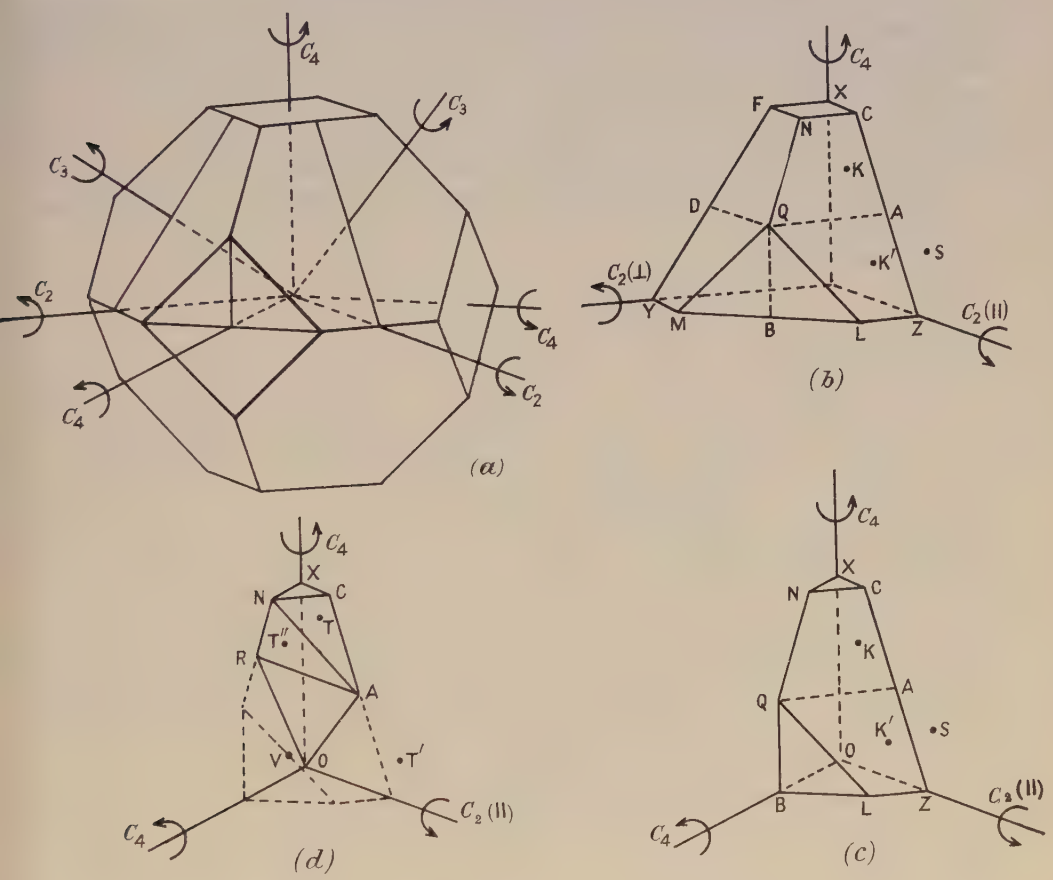

Fig. 2. The atomic polyhedron for sodium (see text).

there can be no odd spherical harmonic, i.e. $P_l^m(\cos\theta)\cos m\phi$ in which either m or l is odd. However, besides the terms shown in (3), others, of the above form with even m, could occur, e.g. $P_4{}^2(\cos\theta)\cos 2\phi$. These terms are not excluded by the known symmetry properties but have been omitted, in our approximate expansion up to $l<8$, because we use the empty lattice test to estimate the accuracy of our energies, and the terms in question do not occur in the expansion of the corresponding free electron wave function. This emphasizes the weakness of the empty lattice test and shows the need of a criterion such as that given in § 5.

For the wave functions associated with the point H (fig. 1) we take C_4 as the polar axis and measure ϕ relative to one of the planes containing two fourfold

axes (see fig. 2(*c*)). From the character table I of BSW, or from the data in LB, we deduce the following forms for the functions belonging to the states H_s, H_p, $H_d{}^1$.

$$\psi(H_s) = R_0 + AR_4\{P_4(\cos\theta) + \tfrac{1}{168}P_4{}^4(\cos\theta)\cos 4\phi\} + BR_6\{P_6(\cos\theta) - \tfrac{1}{360}P_6{}^4(\cos\theta)\cos 4\phi\}, \quad \ldots\ldots(5)$$

$$\psi(H_p) = R_1P_1(\cos\theta) + AR_3P_3(\cos\theta) + BR_5P_5(\cos\theta) + CR_7P_7(\cos\theta), \quad \ldots\ldots(6)$$

$$\psi(H_d{}^1) = R_2P_2{}^2(\cos\theta)\cos 2\phi + AR_4P_4{}^2(\cos\theta)\cos 2\phi + BR_6\{P_6{}^2(\cos\theta)\cos 2\phi + \tfrac{1}{360}P_6{}^6(\cos\theta)\cos 6\phi\}. \quad \ldots\ldots(7)$$

In the expansion for the wave function $\psi(H_p)$ we have omitted the harmonics $P_5{}^4(\cos\theta)\cos 4\phi$ and $P_7{}^4(\cos\theta)\cos 4\phi$ for the same reason that similar terms were omitted from $\psi(N_s)$ and $\psi(N_p{}^1)$. The state H_p is triply degenerate; the particular wave function given by (6) is the one in which the nodal planes are parallel to the plane containing $C_2(\perp)$ and $C_2(\parallel)$.

The group of operators belonging to the point P differs from those already considered (the groups of N and H) in that it does not contain the inversion operator J. Hence the wave functions associated with P do not fall into sets of odd or even parity. We shall write

$$\psi(P_s) = u_s + v_s \quad \text{and} \quad \psi(P_p) = u_p + v_p, \quad \ldots\ldots(8)$$

where in both cases u and v are complex functions which have even and odd parity respectively.

The group of P contains 24 operators, and if we add the products of the inversion J and the operators of P we obtain the full cubic group of 48 operators. u_s is invariant with respect to each of these 48 operators and has therefore the symmetry of Γ_s. From table XI of BSW we can read off the characters of P_s (i.e. BSW, P_1), and if J is represented by -1 for the term of odd parity v, the characters of the remaining 24 operations will be just those of this table (line 1) multiplied by -1. By comparing this set of characters for 48 operators with table I of BSW we see that v_s has the symmetry of type $\Gamma_f{}^1$ (LB, β). In a similar way we can show that u_p has the symmetry of $\Gamma_d{}^2$ and v_p the symmetry of Γ_p. From this knowledge of the symmetries of the wave functions we can determine the expansions in spherical harmonics, and we find

$$u_s = R_0 + AR_4\{P_4(\cos\theta) + \tfrac{1}{168}P_4{}^4(\cos\theta)\cos 4\phi\} + BR_6\{P_6(\cos\theta) - \tfrac{1}{360}P_6{}^4(\cos\theta)\cos 6\phi\}, \quad \ldots\ldots(9)$$

$$v_s = CR_3P_3{}^2(\cos\theta)\sin 2\phi + DR_7\{P_7{}^2(\cos\theta)\sin 2\phi + \tfrac{1}{1560}P_7{}^6(\cos\theta)\sin 6\phi\}, \quad \ldots\ldots(10)$$

and for the P_p type

$$u_p = CR_2P_2{}^2(\cos\theta)\sin 2\phi + DR_4P_4{}^2(\cos\theta)\sin 2\phi + FR_6P_6{}^2(\cos\theta)\sin 2\phi + GP_6{}^6(\cos\theta)\sin 6\phi, \quad \ldots\ldots(11)$$

$$v_p = R_1P_1(\cos\theta) + AR_3P_3(\cos\theta) + BR_5P_5(\cos\theta) + KP_5{}^4(\cos\theta)\cos 4\phi. \quad \ldots\ldots(12)$$

In the expansions (9), (10), (11) and (12) the angles θ and ϕ are measured with respect to the same axes as were used for the H types.

From considerations of symmetry alone no further information about the wave functions can be obtained than is given in the expansions of this section. The unknown constants along with the eigenvalues must now be determined by the boundary conditions.

§ 3. THE EXACT BOUNDARY CONDITIONS

Let $\mathbf{n}$ denote one of the fourteen vectors which may be written $\{1, 1, 1\}$ and $\{2, 0, 0\}$ with respect to the fourfold axes C_4. A face of the atomic polyhedron may then be denoted by the vector $\frac{1}{4}a\mathbf{n}$ which is the displacement from the origin to the centre of the face. If $\mathbf{R}_n$ denotes the displacement along the normal from any point on the face $-\frac{1}{4}a\mathbf{n}$ to the face $\frac{1}{4}a\mathbf{n}$, then clearly $\mathbf{R}_n = \frac{1}{2}a\mathbf{n}$. In accordance with Bloch's theorem we have, therefore,

$$\psi(\mathbf{r}+\mathbf{R}_n) = \exp(i\mathbf{k}\,.\,\mathbf{R}_n)\psi(\mathbf{r}), \qquad \ldots\ldots(13)$$

$$\mathbf{n}\,.\,\nabla\psi(\mathbf{r}+\mathbf{R}_n) = -\exp(i\mathbf{k}\,.\,\mathbf{R}_n)\,\mathbf{n}\,.\,\nabla\psi(\mathbf{r}). \qquad \ldots\ldots(14)$$

Let X_n denote a rotation through π about the normal to the face $\mathbf{n}$ through the centre, then

$$JX_n\psi(\mathbf{r}) = \psi(\mathbf{r}+\mathbf{R}_n) \qquad \ldots\ldots(15)$$

where J is the inversion operator. For the points N and H in the Brillouin zone the operator J is contained in the group of the wave vector and, therefore, every wave function associated with these points has either odd or even parity, i.e. $J\psi = \pm\psi$. For such points in the Brillouin zone the boundary conditions may, therefore, be written

$$X_n\psi(\mathbf{r}) = \pm\exp(i\mathbf{k}\,.\,\mathbf{R}_n)\psi(\mathbf{r}), \qquad \ldots\ldots(16)$$

$$\mathbf{n}\,.\,\nabla X_n\psi(\mathbf{r}) = \mp\exp(i\mathbf{k}\,.\,\mathbf{R}_n)\,\mathbf{n}\,.\,\nabla\psi(\mathbf{r}), \qquad \ldots\ldots(17)$$

where the upper sign is taken in both equations when ψ is of even parity and the lower sign when ψ is of odd parity.

The boundary conditions (16) and (17) are easier, both to visualize and to apply, than (13) and (14) because they now relate to points on the *same* face of the atomic polyhedron. We calculate, as an example, the boundary conditions over the faces shown in fig. 2(*b*) for the function $\psi(\mathrm{N}_s)$. The coordinates of the point N in the wave vector space, with respect to the axes C_4 shown in fig. 1, are $(\pi/a,\ \pi/a,\ 0)$ and, for the hexagonal face with centre A (fig. 2(*b*)), $\mathbf{R}_n = (\frac{1}{2}a,\ \frac{1}{2}a,\ \frac{1}{2}a)$ referred to the axes C_4. Thus $\mathbf{k}\,.\,\mathbf{R}_n = \pi$ and, since $\psi(\mathrm{N}_s)$ has even parity, we find $X_n\psi = -\psi$. Thus, referring to fig. 2(*b*), we have $\psi_K = -\psi_S$, where the subscript letters denote the points at which the function is evaluated, and since the function is symmetrical with respect to a reflection in the line CZ we have $\psi_K = -\psi_{K'}$. Hence the wave function must be antisymmetrical with respect to AQ and, therefore, vanishes along this line. Evidently the normal derivative is symmetrical with respect to AQ.

The hexagonal face with centre D corresponds to $\mathbf{n} = (1, -1, 1)$, with respect to the C_4 axes, therefore $\mathbf{k}\,.\,\mathbf{R}_n = 0$. Hence the wave function is symmetrical with respect to DQ and the normal derivative antisymmetrical. The face MQL is given by $\mathbf{n} = (2, 0, 0)$, therefore $\mathbf{k}\,.\,\mathbf{R}_n = \pi$ and thus $X_n\psi = -\psi$ so that the function is antisymmetrical with respect to BQ, which is a nodal line. The normal derivative is symmetrical with respect to BQ.

For the face FNC we have $\mathbf{R}_n = (0, 0, a)$ and, therefore, $\mathbf{k}\,.\,\mathbf{R}_n = 0$. Thus $X_n\psi = \psi$ and $X_n\psi' = -\psi'$, where the dash denotes differentiation with respect to the normal to the plane. In this case X_n, the rotation through π about C_4, is a member of the group of the point N, and we know that for the N_s type the wave function is symmetrical with respect to this rotation. Thus the first condition is automatically satisfied and the second necessitates $\psi' = 0$ over the whole face.

In this way the exact boundary conditions, for the types considered at N and H, have been obtained and are shown in table 3. ψ' denotes the normal derivative of ψ to the face which contains the line specified.

Table 3

Fig. 2 (*b*)	Line AQ		Line DQ		Line BQ		Face FNC	
	ψ	ψ'	ψ	ψ'	ψ	ψ'	ψ	ψ'
N_s	a	s	s	a	a	s		0
$N_p{}^1$	s	a	s	a	s	a		0

Fig. 2 (*c*)	Line AQ		Face QBL		Face NCX	
	ψ	ψ'	ψ	ψ'	ψ	ψ'
H_p	s	a		0	0	
$H_d{}^1$	s	a		0		0

Fig. 2 (*d*)	Line AN		Face NCX	
	ψ	ψ'	ψ	ψ'
H_s	a	s		0

s and a denote symmetry and antisymmetry with respect to the line indicated; 0 implies the vanishing of ψ or ψ' over the whole face.

The boundary conditions for the types P_s and P_p require more detailed consideration. Consider P_s first. For the hexagonal face $\mathbf{n}=(1,1,1)$ we find $\mathbf{k}\,.\,\mathbf{R}_n = 3\pi/2$ and thus $JX_n\psi = -i\psi$. Now let $u_s = \alpha_s + i\beta_s$ and $v_s = \lambda_s + i\mu_s$, where α_s, β_s, λ_s and μ_s are all *real* functions. Thus, since $Ju_s = u_s$ and $Jv_s = -v_s$, we find easily

$$X_n\alpha_s = \mu_s \quad \text{and} \quad X_n\lambda_s = -\beta_s. \qquad \ldots\ldots(18)$$

Now α_s stands for the expansion (9) in which the unknown constants are the real parts of A and B and $i\mu_s$ for the expansion (10), in which the constants are the imaginary parts of C, D. It will now be seen that the two equations (18) give exactly the same equation to determine the eigenvalue, by elimination of the unknown constants, and we need, therefore, only consider one of them. Thus, without loss of generality, we put $\beta_s = \lambda_s = 0$ and write $\psi(P_s) = u_s + iv_s$ where u_s and v_s are now real functions and may be taken to be the expansions (9) and (10), in which all the constants are real numbers.

Since u_s has the symmetry of Γ_s, for which the wave function transforms into itself under each of the 48 operations of the full group, it is only necessary to consider the region OARNCX of fig. 2(*d*), which is one forty-eighth of the whole polyhedron. The boundary condition (18) now implies that $u_s(T) = v_s(T')$ where, as shown in fig. 2(*d*), T and T′ are diametrically opposite points on the hexagonal face. Since the plane OVA is a symmetry plane for v_s (which is the LB β type) we can write $u_s(T) = v_s(T'')$, which we may express by saying that $u_s - v_s$ is antisymmetrical with respect to the line AN. The full boundary conditions are summarized as follows:

Table 4

Fig. 2 (*d*)	Line AN		Face NXC	
	$(u_s - v_s)$	$(u_s' - v_s')$	u_s	v_s'
ψ (P_s)	a	s	0	0

The symmetry of the P_p function may be defined with respect to fig. 2(*c*). For u_p the plane NQB is a nodal plane, i.e. a plane of reflection antisymmetry, whilst the planes XCAZ and OBLZ are planes of reflection symmetry. For v_p the planes XCAZ and XNQB are planes of reflection symmetry whilst the plane OBLZ is a nodal plane. The boundary conditions determined in the same way as for P_s are given in table 5.

Table 5

Fig. 2 (*c*)	Line AQ		Face NXC		Face QBL	
	(u_p-v_p)	$(u_p'-v_p')$	u_p	v_p'	v_p	u_p'
$\psi(P_p)$	a	s	0	0	0	0

As in table 3, primes indicate differentiation along the normals to the planes indicated.

§ 4. APPROXIMATE BOUNDARY CONDITIONS AND NUMERICAL RESULTS

From the exact boundary conditions, given in the previous section, we can obtain a set of particular relations which may be used to determine the constants, in the expansions of the wave functions, and the eigenvalues. Since we take only a finite number of terms in each expansion, there is inevitably an arbitrariness in the choice of the particular boundary conditions to be applied. For each type we have tested many sets of different boundary conditions. Those which give the best results in the empty lattice test are considered to be most suitable for the determination of the energies in the real metal, at least in the case of metallic sodium.

For the wave function $\psi(N_s)$ table 3 shows that the following equations must hold (subscript letters refer to fig. 2(*b*)):

(i) $\psi_C+\psi_Z=0$, (ii) $\psi_C'=\psi_Z'$, (iii) $\psi_A=0$, (iv) $\psi_L+\psi_M=0$,
(v) $\psi_L'=\psi_M'$, (vi) $\psi_B=0$, (vii) $\psi_X'=0$, (viii) $\psi_N'=0$,
(ix) $\psi_Q=0$, (x) $\psi_Q'=0$, (xi) $\psi_D'=0$.

Where the letter refers to a corner point of the polyhedron the particular plane to which the normal derivative applies can be seen at once by reference to table 3 and fig. 2(*b*); for example the derivative in $\psi_N'=0$ must be with respect to the normal to the plane NXC, whilst (x) must refer to the plane YDFQ.

The procedure followed in applying these boundary conditions was as follows: A value of the energy was chosen and the radial wave functions determined. In the empty lattice test the radial wave functions are Bessel functions and their values can be taken from existing tables. Any one of the above eleven conditions leads to a linear equation in the three unknown constants A, B and C of expansion (3). If we select three of the conditions, e.g. (ix), (i), (v), we can determine A, B and C for a given value of the eigenvalue ϵ. Hence we can calculate, for example, the numerical value of ψ_D' of condition (xi). This calculation is repeated for a few values of ϵ from which, either numerically or graphically, the value of ϵ can be found which makes ψ_D' vanish. We have therefore obtained the wave function, i.e. the constants of (3), and its eigenvalue by satisfying four of the boundary conditions.

Table 6 gives the eigenvalue of the N_s state as determined by different sets of boundary conditions, and also the percentage error in the empty lattice test. In the 'empty lattice' the eigenvalue is exactly $2\pi^2/a^2$. A percentage error of 0·036, for example, means that the eigenvalue, calculated by the expansion (3) with approximate boundary conditions, is $19{\cdot}732/a^2$ in place of $19{\cdot}739/a^2$.

Table 6

Conditions used	Error in E.L.T. (%)	Eigenvalue for Na (Ryd.)
(ix), (x), (xi), (i)	0·036	−0·319
(ix), (x), (xi), (iii)	0·036	−0·318
(ix), (x), (xi), (iv)	0·046	−0·318
(ix), (x), (xi), (vi)	0·046	−0·315
(ix), (i), (viii), (xi)	0·030	−0·315
(xi), (iii), (vi), (i)	0·091	−0·299
(xi), (iii), (vi), (ix)	0·036	−0·310
(xi), (iii), (vi), (x)	0·032	−0·299

Adopted mean value for the eigenvalue of $N_s = -0{\cdot}315$ Ryd.

In a similar manner a set of conditions, satisfied by the wave function $\psi(N_p{}^1)$ at various points on the octant of the polyhedron shown in fig. 2 (*b*), can be deduced from table 3. The conditions we have selected as most suitable are given below:

(i) $\psi_C = \psi_Z$, (ii) $\psi_C{}' + \psi_Z{}' = 0$, (iii) $\psi_A{}' = 0$, (iv) $\psi_C = \psi_M$,
(v) $\psi_L{}' + \psi_M{}' = 0$, (vi) $\psi_B{}' = 0$, (vii) $(\partial\psi/\partial r)_Q = 0$, (viii) $(\partial\psi/\partial\theta)_Q = 0$,
(ix) $\psi_N{}' = 0$.

Choosing sets of four of these conditions, the results given in table 7 were obtained for the eigenvalues of the $N_p{}^1$ state.

Table 7

Conditions used	Error in E.L.T. (%)	Eigenvalue for Na (Ryd.)
(ii), (vii), (viii), (vi)	0·286	−0·327
(ii), (vii), (viii), (ix)	0·0456	−0·270
(vii), (ix), (iv), (ii)	0·0456	−0·269
(vii), (ix), (iv), (v)	0·0912	−0·267
(ii), (ix), (v), (viii)	0·0760	−0·268
(ii), (ix), (v), (i)	0·1267	−0·267
(ii), (ix), (v), (iv)	0·0862	−0·267

Adopted mean value for the eigenvalue of $N_p{}^1 = -0{\cdot}268$ Ryd.

The first line of table 7 shows that a poor empty lattice test leads to an eigenvalue appreciably different from the rest. It has been included in order to serve as an example for the correction procedure which is developed in the next section.

The eigenvalues of five other states: H_s, H_p, $H_d{}^1$, P_s and P_p have been calculated in the same way. In each case several sets of boundary conditions were applied, those leading to small errors in the empty lattice test being considered most reliable. It is unnecessary to repeat the details of these calculations, and we give only our results in table 8.

The eigenvalue for Γ_5 has been taken from LB and was included in table 8 to complete the list of accurately known eigenvalues for sodium.

For any particular state the differences of the eigenvalues in the empty lattice test, resulting from the application of different combinations of boundary conditions, are very rarely above 1%, and in the majority of cases less than 0·1%, as exemplified by the two tables 6 and 7. Plots of the approximate wave

Table 8

State	Eigenvalue for Na (Ryd.)	Free electron value relative to Γ_s (Ryd.)
Γ_s	−0·608	
N_s	−0·315	−0·303
N_p^1	−0·268	
H_p	−0·0135	−0·012
Hd^1	+0·0172	
H_s	+0·0997	
P_s	−0·110	−0·152
P_d	+0·020	

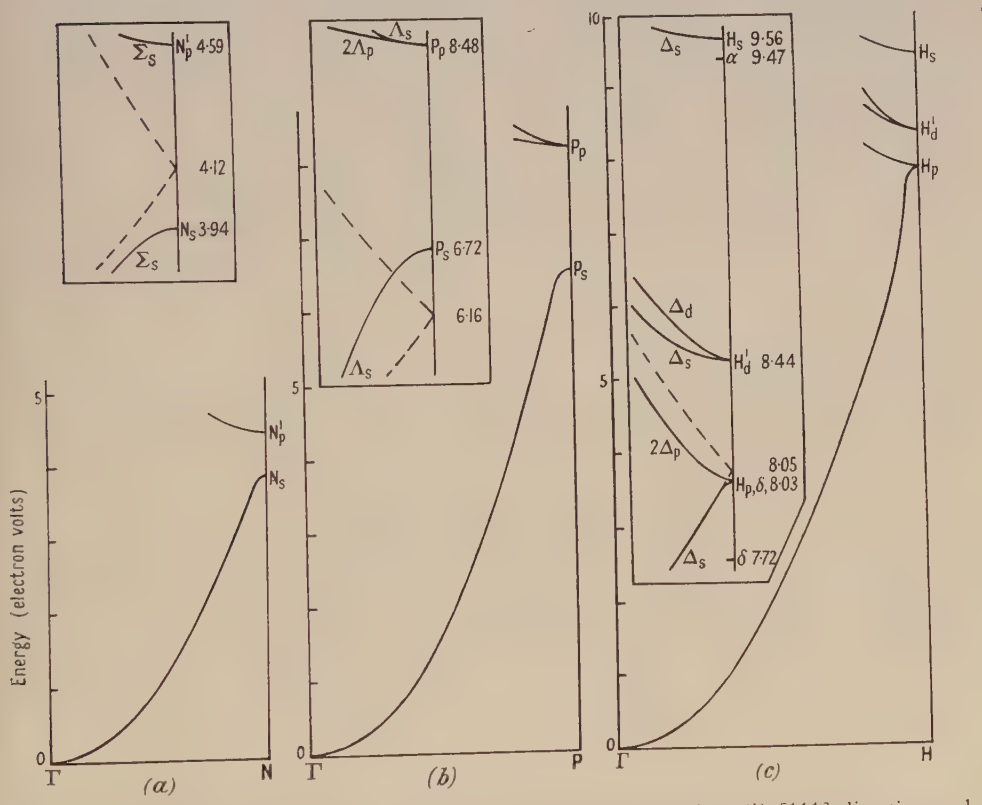

Fig. 3. Energies as functions of the wave vector: (*a*) [110] direction, (*b*) [111] direction and (*c*) [002] direction. Detailed figures show the deviations from the free electron energies (broken lines). (*c*) also shows a comparison with the energies at *H* as determined by LB. Energies are measured in electron volts relative to the energy of the Γ_s state.

functions in the empty lattice test along various selected directions showed very close agreement with the known true standing waves of a free electron. It may be noticed, for comparison, that in the original work of Slater and his collaborators errors in the empty lattice test of up to 20% occurred frequently, as was shown by Shockley.

It is clear that the accuracy of the results obtained for any real metal must depend upon the accuracy with which the radial wave functions $R_l(\epsilon, r)$ can be obtained by numerical integration. Since our result for H_d^1 does not agree with that obtained by LB, who give $-0{\cdot}036$ Ryd., a check was made in our radial wave functions by using them together with the boundary conditions employed by LB. Exact agreement was obtained with LB's numerical result. The difference, therefore, arises from the different boundary conditions which were applied. A plot of the function, along the line NL (fig. 2(*c*)), obtained by the LB boundary conditions, showed much less symmetry about the line AQ than the function obtained by our point boundary conditions. Strong evidence will be given in the next section for believing that our value is the correct one.

The quantities which are of most interest physically are usually differences between the eigenvalues, e.g. the energy gap across a face of the Brillouin zone. It is for this reason that high accuracy in the eigenvalues is essential if the results are to have a practical significance. Consider, for example, the two states N_s and N_p^1. The adopted means for the eigenvalues are $-0{\cdot}315$ and $-0{\cdot}268$ Ryd. respectively, with the greatest error in either case about $\pm 0{\cdot}002$, i.e. less than 1%. The energy gap, however, is only 0·047 Ryd. and, in the least favourable case, the error might be $\pm 0{\cdot}004$, which is 8%. Expressed in electron volts the energy gap at the centre of a face of the Brillouin zone is 0·65 ev. It is, perhaps, noteworthy that Butcher (1951), by comparing the absorption power of sodium with the calculated inner photoelectric absorption, obtained a value of 0·323 ev for the Fourier coefficient of the potential. In the approximation of 'nearly free electrons' it is well known that this Fourier coefficient is equal to one half of the energy gap.

Figure 3 shows graphically the results of the present calculations, and also the way the various states link together within the Brillouin zone. In the present example, sodium, the way the states join together is fairly obvious; in general it must be deduced from the compatibility relations given by BSW.

§ 5. CORRECTION TO THE ENERGY BY MEANS OF A SURFACE INTEGRAL

In the present application of the cellular method to the case of metallic sodium we have used the criterion of the empty lattice test to estimate the accuracy of the true eigenvalues in the metal. In this section we show how a correction to the energy may be obtained, and how this may be used to provide a test of the accuracy of any energy determined by approximate boundary conditions quite independently of the empty lattice test.

Let $\psi_0(\mathbf{r})$ be the approximate wave function which satisfies the equation

$$\nabla^2\psi_0 + (\epsilon_0 - V)\psi_0 = 0 \qquad \ldots\ldots(19)$$

exactly, but fits the boundary conditions only approximately; and let $\psi(x)$ be the function which satisfies the boundary conditions exactly and the equation

$$\nabla^2\psi + (\epsilon - V)\psi = 0. \qquad \ldots\ldots(20)$$

We now calculate the difference $(\epsilon - \epsilon_0)$. Multiply (19) by ψ and (20) by ψ_0; subtract and integrate over the cell. Then

$$(\epsilon - \epsilon_0)\int\psi_0\psi\, d\tau = \int(\psi\nabla^2\psi_0 - \psi_0\nabla^2\psi)\, d\tau = \int(\psi\nabla_n\psi_0 - \psi_0\nabla_n\psi)\, dS \qquad \ldots\ldots(21)$$

by Green's theorem, where ∇_n denotes differentiation along the normal to dS. The surface integral of (21) can be reduced further when we know the exact boundary conditions which ψ satisfies. We consider the case of H_d^1 in detail; others can be treated similarly. In this case the surface integral of (21) is 16 times the value taken over the three planes shown in fig. 2(*c*). Consider the surface NCZLQ. From table 3 we see that $\psi(H_d^1)$ is symmetrical and $\nabla_n\psi(H_d^1)$ antisymmetrical about the line AQ. Let any point K on the upper half NCAQ be denoted by $\mathbf{r}$ and let $\mathbf{r}'$ be the reflection of K in AQ, i.e. K′. We now define two functions of position on NCAQ as follows:

$$f(\mathbf{r}) = \psi(\mathbf{r}) - \psi(\mathbf{r}'), \qquad \ldots\ldots(22)$$

$$g(\mathbf{r}) = \nabla_n\psi(\mathbf{r}) + \nabla_n\psi(\mathbf{r}'). \qquad \ldots\ldots(23)$$

Thus the boundary conditions can now be expressed as $f(\mathbf{r}) = g(\mathbf{r}) = 0$ at every point of the surface NCAQ. Let $f_0(\mathbf{r})$ and $g_0(\mathbf{r})$ be defined in the same way as f and g except that the approximate wave function ψ_0 is used in place of ψ. If, now, S_1 denotes the area NCAQ and S_2 the area AZLQ, then, by using (22) and (23), we may write

$$\begin{aligned}\int_{S_1+S_2}(\psi\nabla_n\psi_0 - \psi_0\nabla_n\psi)\,dS &= \int_{S_1}(\psi\nabla_n\psi_0 - \psi_0\nabla_n\psi)\,dS \\ &\quad + \int_{S_1}\{\psi(g_0 - \nabla_n\psi_0) + (\psi_0 - f_0)\nabla_n\psi\}\,dS \qquad \ldots\ldots(24) \\ &= \int_{S_1}(\psi g_0 - f_0\nabla_n\psi)\,dS,\end{aligned}$$

where we have made use of the fact that ψ is exactly symmetrical and $\nabla_n\psi$ exactly antisymmetrical with respect to AQ.

Over the surface QBL, which we denote by S_3, we find $\nabla_n\psi = 0$, from table 3. Hence

$$\int_{S_2}(\psi\nabla_n\psi_0 - \psi_0\nabla_n\psi)\,dS = \int_{S_2}\psi\nabla_n\psi_0\,dS, \qquad \ldots\ldots(25)$$

and similarly the contribution from the surface NCX, which we denote by S_4, may be seen to be $\int_{S_4}\psi\nabla_n\psi_0\,dS$. Adding the contributions from the three surfaces together we obtain from (21)

$$\tfrac{1}{16}(\epsilon - \epsilon_0)\int\psi_0\psi\,d\tau = \int_{S_1}(\psi g_0 - f_0\nabla_n\psi)\,dS + \int_{S_3}\psi\nabla_n\psi_0\,dS + \int_{S_4}\psi\nabla_n\psi_0\,dS. \qquad \ldots\ldots(26)$$

This equation is exact; but we now approximate by replacing ψ by ψ_0 throughout (26). This amounts to neglecting products such as $(\psi - \psi_0)g_0$ over S_1, and $(\psi - \psi_0)\nabla_n\psi$ over S_3 and S_4. These are all quantities of the second order, since g_0 on S_1 and $\nabla_n\psi_0$ on S_3 and S_4 tend to zero as ψ_0 tends to ψ. Thus, if ψ_0 is normalized to unity, we have as a first order approximation

$$\tfrac{1}{16}(\epsilon - \epsilon_0) = \int_{S_1}(\psi_0 g_0 - f_0\nabla_n\psi_0)\,dS + \int_{S_3+S_4}\psi_0\nabla_n\psi_0\,dS, \qquad \ldots\ldots(27)$$

where the integrands are now known functions.

Equation (27) may be used as a test of the accuracy of any eigenvalue ϵ_0, or wave function ψ_0, obtained by approximate boundary conditions, and is quite independent of the use of the empty lattice test. We give below two numerical examples of the use of this equation.

The first entry in table 7 gives $-0{\cdot}327$ Ryd. for the eigenvalue of N_p^1, which is quite exceptionally far from the mean value. It can be shown that the correction for the state N_p^1 is given by

$$\tfrac{1}{8}(\epsilon - \epsilon_0) = \int_{\sigma_1}(\psi_0 g_0 - f_0\nabla_n\psi_0)\,dS + \int_{\sigma_2}\psi_0\nabla_n\psi_0\,dS, \qquad \ldots\ldots(28)$$

where σ_1 denotes the surfaces NCAQ+FNQD+QBL (fig. 2(*b*)) and σ_2 the surface FXCN.

We have, therefore, calculated the integrals of (28) using the corresponding wave function and found that $\epsilon-\epsilon_0=0{\cdot}043$, giving a corrected eigenvalue of $-0{\cdot}284$, which is much nearer to the mean value. The difference between this corrected value and the mean is probably due to computational errors in the evaluations of the integrals; no attempt was made to obtain these with great precision.

As a second example we consider the difference between the eigenvalue of H_{01} as calculated by LB and by ourselves. Using the wave function obtained by applying the 'average' boundary conditions of LB which, it was verified, correspond exactly to the eigenvalue given ($-0{\cdot}036$), the integrals of (27) were evaluated. It was found that $\epsilon-\epsilon_0=0{\cdot}060$, from which we deduce $\epsilon=+0{\cdot}024$ Ryd. The value obtained by our boundary conditions was 0·017 (cf. table 8). The difference between the corrected LB value and ours, viz. 0·007 Ryd., is again probably due, in the main, to lack of precision in the estimation of the surface integrals.

ACKNOWLEDGMENT

One of the authors (D. J. H.) is indebted to the Senate of the University of London for a Postgraduate Studentship.

REFERENCES

Bouchaert, L., Smoluchowski, R., and Wigner, E., 1936, *Phys. Rev.* **50,** 58.
Butcher, P. N., 1951, *Proc. Phys. Soc.* A, **64,** 765.
von der Lage, F. C., and Bethe, H. A., 1947, *Phys. Rev.*, **71,** 612.
Shockley, W., 1937, *Phys. Rev.*, **52,** 866.
Slater, J. C., 1934, *Phys. Rev.*, **45,** 794.
Wigner, E., and Seitz, F., 1933, *Phys. Rev.*, **43,** 804.

LETTERS TO THE EDITOR

Nuclear Spins of Samarium 147 and 149

Recently Murakawa and Ross (1951) reported the nuclear spins of samarium 147 and 149 as being 5/2 in each case. They based this on their observation of a maximum of six hyperfine structure components in the optical spectra of the separated isotopes. By means of paramagnetic resonance measurements on the ethyl sulphate of naturally occurring samarium we find instead that the spins are 7/2. The experimental evidence is presented below.

Bleaney, Elliott and Scovil (1951) showed that the spin–lattice relaxation time of samarium ethyl sulphate was too short at 14° K for the resonance spectrum to be observed. We have extended these resonance experiments to 4° K, where one electronic transition is found.

The spectrum is completely resolved in the concentrated ethyl sulphate and is essentially the same in a crystal diluted with lanthanum ethyl sulphate in the ratio Sm : La $\simeq$ 1 : 100. It consists of a single strong line flanked by sixteen satellites. The strong line is due to the even isotopes 144, 148, 150, 152 and 154 which have spin zero. The sixteen satellites fall into two groups of eight as shown in the figure. The two groups are identified as belonging to the isotopes 147 and 149, whose relative abundances are $15{\cdot}07\pm0{\cdot}15\%$ and $13{\cdot}84\pm0{\cdot}14\%$ respectively (Inghram, Hayden and Hess 1948). Since the hyperfine structure should consist of $(2I+1)$ lines from each isotope, the spin is shown to be 7/2 in each case. The intensity of the 147 lines relative to the strong line is $2{\cdot}69\pm0{\cdot}1\%$, which agrees favourably

with a relative intensity of 2·65% predicted by the known abundance and a spin of 7/2. The relative intensity of the hyperfine structure of isotopes 147 to 149 is $1{\cdot}10 \pm 0{\cdot}02$, which also agrees with the abundance ratio. Thus both spins are undoubtedly 7/2. Since this is in disagreement with the conclusions of Murakawa and Ross, we suggest that they did not observe transitions between levels with sufficiently high J to show the full multiplicity of the hyperfine structure.

Our measurements show that the ground electronic state of the samarium trivalent ion in this salt is a Kramers' doublet whose spectroscopic splitting factor g (in the dilute salt) is $0{\cdot}596 \pm 0{\cdot}002$ parallel to the hexagonal axis and $0{\cdot}604 \pm 0{\cdot}002$ perpendicular to the axis.

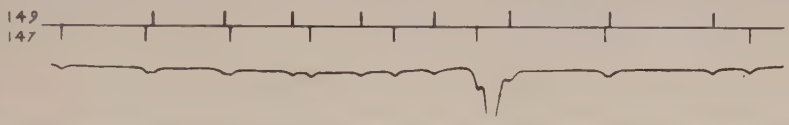

The hyperfine structure of Sm 147 and 149 arising from the $M = +\frac{1}{2} \rightarrow M = -\frac{1}{2}$ electronic transition in samarium ethyl sulphate. In this oscillogram, which was taken at an angle of 12·6° to the axis, the marked asymmetry of the spectrum results mainly from the large second-order effect near the axis and partly from the non-linearity of the sweep.

The hyperfine structure is described by the usual spin Hamiltonian :

$$g_{\parallel}\beta H_z S_z + g_{\perp}\beta(H_x S_x + H_y S_y) + A S_z I_z + B(S_x I_x + S_y I_y) + P\{I_z^2 - \tfrac{1}{3}I(I+1)\}\,.$$

The values of the constants are (dilute salt)

Sm 147	$A = 0{\cdot}0060 \pm 0{\cdot}0001$ cm^{-1}	$B = 0{\cdot}0251 \pm 0{\cdot}0001$ cm^{-1}
Sm 149	$A = 0{\cdot}0049 \pm 0{\cdot}0001$ cm^{-1}	$B = 0{\cdot}0205 \pm 0{\cdot}0001$ cm^{-1}

An upper limit of 4×10^{-4} cm^{-1} can be assigned to the P of either isotope. The precision of the measurements is shown by the following comparison of the observed and calculated positions (in gauss) of the eight hyperfine lines of isotope 147 in the perpendicular direction at a wavelength of 3·279 cm.

Observed	13833	12819	11856	10930	10054	9228	8368	7598
Calculated	13835	12830	11865	10933	10043	9190	8379	7607

This agreement could only be obtained with $I = 7/2$. The same holds true in the parallel direction and for the other isotope.

The ratio of the nuclear magnetic moments, given by the ratio of the widths of the hyperfine groups, is $\mu 147/\mu 149 = 1{\cdot}222 \pm 0{\cdot}008$, in fair agreement with the value of $1{\cdot}177 \pm 0{\cdot}015$ given by Murakawa and Ross. If this discrepancy is genuine it may be due to the fact that we are dealing exclusively with a 4f electron configuration, whereas they were observing transitions between levels involving s electrons. A nuclear size effect may be expected in the latter but not in the former case. It is interesting that the addition of two neutrons ($N = 85$ and 87) produces a considerable decrease in the magnetic moments of the nuclei, as in the case of Nd 143 and 145 ($N = 83$ and 85) (Bleaney and Scovil 1950), where it was even more marked.

The actual values of the nuclear magnetic moments and upper limits for the nuclear electric quadrupole moments have been calculated by Elliott and Stevens (1952), and are given by them in an accompanying letter.

The Clarendon Laboratory,
Oxford.
15th February 1952.

G. S. Bogle.
H. E. D. Scovil.

Bleaney, B., Elliott, R. J., and Scovil, H. E. D., 1951, *Proc. Phys. Soc.* A, **64**, 933.
Bleaney, B., and Scovil, H. E. D., 1950, *Proc. Phys. Soc.* A, **63**, 1369.
Elliott, R. J., and Stevens, K. W. H., 1952, *Proc. Phys. Soc.* A, **65**, 370
Inghram, M. G., Hayden, R. J., and Hess, D. C., Jr., 1948, *Phys. Rev.*, **73**, 180.
Murakawa, K., and Ross, J. S., 1951, *Phys. Rev.*, **82**, 967.

The Paramagnetism of Samarium Ethyl Sulphate: Theory

In an earlier letter (Elliott and Stevens 1951) we reviewed the paramagnetic resonance observations made on the rare earth ethyl sulphates. A resonance had not then been found in the samarium salt because of its low g-values and short relaxation time. In the accompanying letter Bogle and Scovil (1952) report new observations on this salt and it appears that the lowest doublet is, as predicted, approximately $|^6H_{5/2}\,;\, J_z=\pm 1/2\rangle$. The next multiplet is near 1000 cm^{-1} and small admixtures from this considerably affect the g-values. In fields of D_{3h} symmetry the lowest Kramers' doublet will be approximately

$$\cos\theta\ |J=5/2, J_z=\pm 1/2\rangle \pm \sin\theta\ |J=7/2, J_z=\pm 1/2\rangle$$

where θ is related to the crystal fields. Then

$$g_{\|}=\frac{2}{7}\left\{\cos^2\theta+\frac{26}{9}\sin^2\theta+3\sqrt{10}\sin 2\theta\right\}$$

$$g_{\perp}=\frac{2}{7}\left\{3\cos^2\theta-\frac{104}{9}\sin^2\theta-\frac{3}{2}\sqrt{10}\sin 2\theta\right\}$$

and the ratio of the hyperfine structure constants is

$$\frac{A}{B}=\frac{\left\{6\cos^2\theta+\frac{37}{9}\sin^2\theta-3\sqrt{10}\sin 2\theta\right\}-\delta\left\{2\cos^2\theta+\frac{19}{15}\sin^2\theta-\frac{3}{\sqrt{10}}\sin 2\theta\right\}}{\left\{18\cos^2\theta-\frac{148}{9}\sin^2\theta+\frac{3\sqrt{10}}{2}\sin 2\theta\right\}-\delta\left\{6\cos^2\theta+\frac{76}{15}\sin^2\theta+\frac{3}{2\sqrt{10}}\sin 2\theta\right\}},$$

where $\delta=13/45$. The hyperfine structure arises from the interaction of the nuclear magnetic moment with the orbital and spin magnetic fields of the electrons. A characteristic feature of the rare earths is that the spin contributions (here given by the terms in δ) are small. With $\theta=4°$ the comparative values of the experimental and theoretical values of $g_{\|}$, $g_{\perp}$ and A/B are

	$g_{\|}$	$g_{\perp}$	A/B
Theory	0·66	0·66	0·24
Experiment	0·595	0·605	0·24

The agreement is fairly good and can be improved by including the smaller admixtures from other J levels. Even when this is done there remains a discrepancy for what seem the most reasonable crystal fields. The details of this theory will be reported in forthcoming papers on the whole group of salts.

The theory gives $\mu\,(\overline{1/r^3})=+1{\cdot}52\times 10^3 B$, where $1/r^3$ is averaged over 4f electron wave functions and expressed in A^{-3}. $(\overline{1/r^3})$ is difficult to estimate, but from the spin–orbit coupling constant and the value for Eu given by Sternheimer (1950), a reasonable value would be 40 to 50. With the values of B given by Bogle and Scovil, we find for ^{147}Sm, $|\mu|=0{\cdot}68\pm 0{\cdot}1$, and for ^{149}Sm, $|\mu|=0{\cdot}55\pm 0{\cdot}1$ nuclear magnetons. The nuclear quadrupole moment Q as defined by Mack (1950) is given by $Q(\overline{1/r^3})=+7{\cdot}2\times 10^4\,P$, with P in cm^{-1}. The upper limits of $|P|=4\times 10^{-4}$ set by Bogle and Scovil give upper values for $|Q|$ of 0·72 in ^{147}Sm and ^{149}Sm.

The values of the magnetic moments are about 50% larger than those obtained by Murakawa and Ross (1951), even when 7/2 is substituted for the value of 5/2 which they give for the nuclear spin.

Spins of 7/2 are more consistent than 5/2 with the nuclear shell model (Mayer 1950). ^{143}Nd has 83 neutrons—one more than a magic number—and since it has spin 7/2 (Bleaney and Scovil 1950) it is apparently the nuclear $2f_{7/2}$ state, not the $1h_{9/2}$, which is preferred at the beginning of this shell. The corresponding proton case, ^{209}Bi, has spin 9/2. So far other isotopes (^{145}Nd, ^{147}Sm, ^{149}Sm) with three and five neutrons outside a closed shell have spin 7/2. Moreover ^{167}Er which has the 7/2 and 9/2 shells full except for one neutron, also has spin 7/2 (Bleaney and Scovil 1951). The addition of more neutrons fills these shells and

^{171}Yb and ^{173}Yb have spins of 1/2 and 5/2 (Mack 1950). Thus one might tentatively predict that all isotopes with an odd number of neutrons between 83 and 99 will have spins of 7/2, or just possibly 9/2.

The Clarendon Laboratory,
Oxford.
15th February 1952.

R. J. Elliott.
K. W. H. Stevens.

Bleaney, B., and Scovil, H. E. D., 1950, *Proc. Phys. Soc.* A, **63**, 1369 ; 1951, *Ibid.*, **64**, 204.
Bogle, G. S., and Scovil, H. E. D., 1952, *Proc. Phys. Soc.* A, **65**, 368.
Elliott, R. J., and Stevens, K. W. H., 1951, *Proc. Phys. Soc.* A, **64**, 205.
Mack, J. E., 1950, *Rev. Mod. Phys.*, **22**, 64.
Mayer, M. G., 1950, *Phys. Rev.*, **78**, 22.
Murakawa, K., and Ross, J. S., 1951, *Phys. Rev.*, **82**, 967.
Sternheimer, R., 1950, *Phys. Rev.*, **80**, 102.

Proton Magnetic Resonance in Solid Cyclohexane

The nuclear magnetic resonance absorption spectrum and the spin–lattice relaxation time T_1 have been measured for the protons in polycrystalline cyclohexane between 100° K and its freezing point (279·6° K). The second moment (mean square line width) of the measured spectrum is shown as a function of temperature in fig. 1. Measured values of T_1 are shown in fig. 2.

Below 150° K the spectrum does not change, indicating that the molecular lattice is effectively rigid. The mean experimental value of the second moment between 100° K and 150° K is $26{\cdot}0 \pm 0{\cdot}5$ gauss^2. A theoretical value of $27{\cdot}3 \pm 1{\cdot}5$ gauss^2 has been obtained using the formula of Van Vleck (1948). The agreement between measured and calculated values

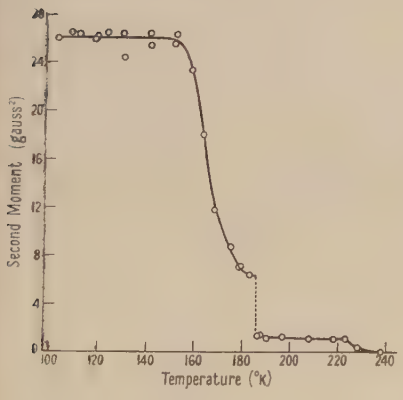

Fig. 1.

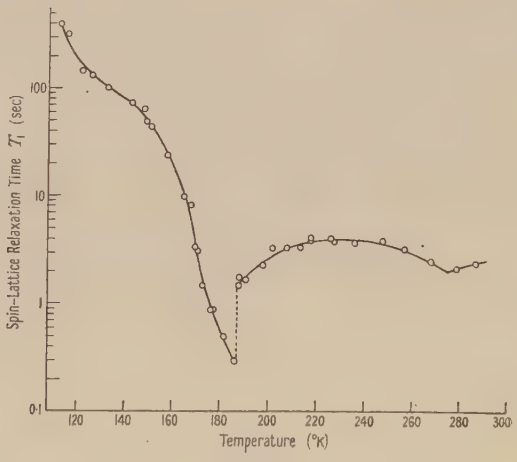

Fig. 2.

provides general confirmation of the molecular configuration assumed in the calculation, namely D_{3d} symmetry with tetrahedral bond angles of 109° 28′, C–C bond lengths of 1·54 Å and C–H bond lengths of 1·10 Å. The main uncertainty in the calculation arises from the lack of exact knowledge of the crystal structure below 186° K, at which temperature there is a first order phase transition.

Between 155° K and 180° K the absorption line narrows, the second moment falling to 6·4 gauss^2. The molecular motion most likely to cause this narrowing is the re-orientation of each molecule about its triad axis. Calculation of the effect of such motion on both the intramolecular and the intermolecular contributions to the second moment lead to a theoretical value of $6{\cdot}1 \pm 1{\cdot}0$ gauss^2 in satisfactory agreement with the experimental value.

If the re-orientation process can be described by a single correlation time τ_c, the relation between T_1 and τ_c should be of the form derived by Bloembergen, Purcell and Pound (1948):

$$1/T_1 = C_1[\tau_c/(1+\omega^2\tau_c^2) + 2\tau_c/(1+4\omega^2\tau_c^2)], \quad \ldots\ldots (1)$$

where $\omega/2\pi$ is the radio frequency in use (23·4 Mc/s). Below 186° K $\omega^2\tau_c^2 \gg 1$ since T_1 increases rapidly with decrease of temperature; relation (1) thus approximates to $T_1 = 2\omega^2\tau_c/3C_1$. Taking $\tau_c = \tau_0 \exp(E/RT)$, a plot of log T_1 against $1/T$ yields for E, the height of the barrier restricting re-orientation about the triad axis, the value 11 ± 1 kcal/mole.

The line width–temperature curve has been reconstructed in the manner described by Gutowsky and Pake (1950), and can be fitted using the same value of E. This enables the value of C_1 to be found, namely 3×10^9 sec^{-2}. An approximate value of C_1 may be calculated by assuming that the relaxation of each proton is predominantly caused by re-orientation relative to the other proton in the same methylene group. The relation $C_1 = 3\gamma^4\hbar^2/10b^6$ due to Bloembergen *et al.* (1948), which strictly applies to isotropic re-orientation as in liquids, may then be used. (γ is the nuclear gyromagnetic ratio of the proton and b is the interproton distance.) A value of 5×10^9 sec^{-2} is obtained in satisfactory agreement with the experimental value.

Below 160° K T_1 is shorter than is to be expected from this re-orientation mechanism alone. Thus, below 160° K, this relaxation process ceases to be dominant, other processes having comparable or greater efficacy.

The solid–solid phase transition at 186° K is accompanied by discontinuous changes in both second moment and relaxation time. The reduction of second moment to 1·4 gauss^2 implies that the molecules are now able to re-orient about other axes besides the triad, and since T_1 is increasing with temperature the frequency of re-orientation $1/2\pi\tau_c$ must now exceed the radio frequency 23·4 Mc/s. Thermal data indicate that there must be a relatively large increase in molar volume at the transition; this in turn must reduce the barriers hindering molecular re-orientation, and thus accounts for the greater molecular freedom observed.

The decrease of T_1 above 240° K is presumably associated with the further increase in molecular freedom which causes the final reduction of second moment between 220° K and 240° K to less than 0·01 gauss^2. The absence of a measurable discontinuity in either the second moment or in T_1 at the melting point emphasizes the considerable molecular freedom of the molecules just below the melting point.

Department of Natural Philosophy,
The University,
St. Andrews, Scotland.
18th February 1952.

E. R. Andrew.
R. G. Eades.

Bloembergen, N., Purcell, E. M., and Pound, R. V., 1948, *Phys. Rev.*, **73**, 679.
Gutowsky, H. S., and Pake, G. E., 1950, *J. Chem. Phys.*, **18**, 162.
Van Vleck, J. H., 1948, *Phys. Rev.*, **74**, 1168.

Wavelength Resolution of X-Ray Proportional Counters

In a recent letter on a "Comparison of Geiger and Proportional Counters for Intensity Measurements in X-ray Diffraction", Arndt and Riley (1952) state that the proportional counter's "response to any particular characteristic wavelength employed can be made as sharp as required". It should be pointed out, however, that the wavelength resolution of proportional counters is fundamentally limited by statistical fluctuations in the number of primary ion pairs formed and in the amount of gas amplification. On the other hand, Arndt and Riley were unable to discriminate completely against harmonic radiation according to the account given of their experiments, whereas the writer has previously shown (Lang 1951) that separation of CuKα radiation from its first harmonic can be complete.

The purpose of this note is to deal quantitatively with the case, important in practice, of detecting CuKα radiation in the presence of slightly softer fluorescent radiations which can be excited by the CuKα rays.

The variation of pulse height from CuKα radiation was found to follow closely a gamma distribution function. The experimental points and the fitted curve are shown in fig. 1. Distribution curves for the other radiations can be computed from the CuKα distribution since the variance of the distribution is proportional to the energy of the radiation. The ratio of variance to the square of the mean pulse height obeys the relation $\sigma^2/\bar{p}^2 = C/\bar{N}$ where $\bar{N}$ is the mean number of ion pairs formed before gas multiplication and C is a constant. For CuKα radiation $\bar{N} = 298$, taking the value of the energy required per ion pair formation in argon to be 27 ev (Valentine 1952). With this value of $\bar{N}$ the constant C is found to equal 1·1. The distribution curves shown for CrKα, MnKα, FeKα and CoKα radiations are all normalized. The FeKβ curve has an area 0·13 of the Kα curves. The experimentally observed subsidiary peaks centred 3 kev below the main peaks, which are due to loss of

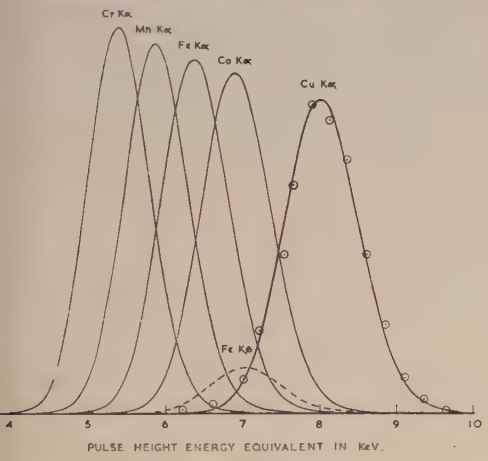

1. Pulse height distribution curves for argon proportional counter.

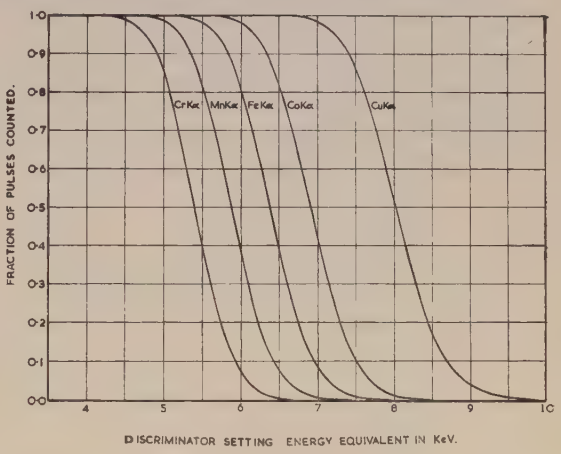

Fig. 2. Computed bias curves for argon proportional counter.

argon K fluorescent radiation in the absorption process, are not shown here since they contain only about 4% of the number of pulses in the main peak (Lang 1951). This fraction will perforce be lost when discrimination against slightly softer radiation is attempted.

From measurements on these curves, or on bias curves computed from them (fig. 2), the degree of discrimination obtainable is readily calculated. It will be seen that CrKα, MnKα and FeKα can be almost completely separated from CuKα radiation. Discrimination at 7·5 kev will pass 85% of the CuKα radiation main peak and only 10% of the CoKα radiation. FeKβ radiation can be largely excluded but not so CoKβ radiation (only the FeKβ pulse distribution is shown in the figure).

The help of Mr. D. R. Cox and Mr. D. A. East of the Cambridge University Statistical Laboratory in computing the distributions is gratefully acknowledged.

Crystallographic Laboratory, A. R. Lang.
Cavendish Laboratory, Cambridge.
20th February 1952.

Arndt, U. W., and Riley, D. P., 1952, *Proc. Phys. Soc.* A, **65**, 74.
Lang, A. R., 1951, *Nature, Lond.*, **168**, 907.
Valentine, J. M., 1952, *Proc. Roy. Soc.* A, **211**, 75.

The Ultra-Violet Spectrum of a Diatomic Hydride

In the course of a search for the emission spectrum of KF, which should consist of fluctuation bands in the ultra-violet region, we have recently examined the emission from a Schüler discharge-tube, running in hydrogen, in which the heated hollow cathode contained KF. No KF bands were observed, but a many-line spectrum in the region 2150–2650 Å was sometimes developed with some intensity. The spectrum appeared to be the same as that

obtained under similar conditions by Woods (1943), who suggested that it might be the $^2\Sigma-{}^2\Pi$ system of HF^+. No analysis of this system seems yet to have been published. On the assumption that the emitter was HF^+, we photographed the spectrum when KHF_2 was used in place of KF in the cathode. The same many-line spectrum appears strongly in this source, but it is somewhat capricious of excitation, and a good deal of difficulty was experienced in getting plates adequate for a preliminary rotational analysis. However, satisfactory spectrograms on a Hilger large quartz instrument have now been taken. The results of the analysis are unexpected.

Most of the strong lines, about 230 in all, have been assigned as P or R branch lines to one of five bands constituting a $v'=$constant progression. The bands are degraded strongly to longer wavelengths, and no heads are apparent. The values of the constants derived in the preliminary analysis are given below.

v', v''	ν_0	B''	D''
0, 0	46380	11·920	$1{\cdot}47\times10^{-3}$
0, 1	44345·5	11·261	1·59
0, 2	42471·2	10·524	1·79
0, 3	40779·5	9·665	1·92
0, 4	39291·3	8·718	2·23

$$F'(J)=4{\cdot}016_6\,J(J+1)-1{\cdot}89_6\times10^{-4}\,J^2(J+1)^2+4{\cdot}_2\times10^{-9}\,J^3J(+1)^3.$$

$$\omega'\simeq(4B'^3/D')^{1/2}-1170\ \text{cm}^{-1}.$$

$$B_v''=12{\cdot}215-0{\cdot}56_1(v+\tfrac{1}{2})-0{\cdot}047_9(v+\tfrac{1}{2})^2.$$

$$G_v''=2174{\cdot}_3(v''+\tfrac{1}{2})-64{\cdot}0_5(v''+\tfrac{1}{2})^2-3{\cdot}6_0(v''+\tfrac{1}{2})^3.$$

In the lower rotational states the terms in $HJ^3(J+1)^3$ become of increasing importance as v'' increases: because of the magnitude of these terms the values of D'' given above are only approximate. The vibrational quantum numbers are assigned on the assumption that the band at shortest wavelength is the 0, 0 band: it may prove later that these values of v', v'' should be increased.

Further work designed to identify the emitting molecule is in progress. The constants do not fit with those of any known state of a diatomic hydride, but the number of possibilities is not large. The value of B_0'' is such that the emitter must almost certainly be the hydride of a first-row element (see, for example, Douglas and Herzberg 1942). Although other possibilities cannot yet be eliminated, it is probable that the transition is $^1\Sigma-{}^1\Sigma$, for no Q branches have been found, which indicates that $\Delta\Lambda=0$, and no spin or Λ-doubling effects have been observed up to $J=30$, although lines about 1 cm^{-1} apart are clearly resolved. If the transition is $^1\Sigma-{}^1\Sigma$, HF^+ is ruled out, and of the possible emitters remaining, CH^+ or OH^+ are the most likely.

Physical Chemical Laboratory,
University of Oxford.
28th February 1952.

A. D. Caunt.
R. F. Barrow.

Douglas, A. E., and Herzberg, G., 1942, *Canad. J. Res.* A, **20**, 71.
Woods, L. H., 1943, *Phys. Rev.*, **64**, 259.

Derivation of the Velocity of Second Sound from Maxwell's Equation of Transfer

Starting from the Boltzmann equation for the distribution function, Ward and Wilks (1952) have recently derived the relation $c_2=c/\sqrt{3}$ for the velocity of second sound in a gas of phonons moving with velocity c. In this note we use an argument of a similar type to calculate c_2 for a general energy spectrum $E=E(p)$ (where p is the momentum of an excitation), and compare the resultant theory with that of Landau (1941).

The most convenient starting point is Maxwell's general equation for the transfer of any quantity Q per unit volume. This reads (cf. Jeans 1940, § 191)

$$\frac{\partial}{\partial t}\overline{Q}+\text{div}\,(\overline{\mathbf{v}Q})+\dot{\mathbf{v}}\,.\,\overline{\text{grad}\,Q}=\Delta_{\text{collisions}}\,Q\,, \qquad \ldots\ldots(1)$$

where $\mathbf{v}$ is the velocity of a particle or excitation carrying Q, $\dot{\mathbf{v}}$ its acceleration, and the bars denote values integrated over the distribution function f. For instance,

$$\bar{Q}=\frac{1}{h^3}\int\int\int Qf\,p^2\sin\theta\,dp\,d\theta\,d\phi=\frac{1}{h^3}\int Qf\,d^3p\,. \qquad \ldots\ldots(2)$$

We restrict our attention to the case of plane waves propagated along the x direction. Assuming that the only forces acting on the excitations are those exerted during collisions, $\dot{\mathbf{v}}=0$. If Q refers to either energy or momentum, $\Delta_{\text{collisions}}Q=0$, so that

$$\frac{\partial}{\partial t}\int Ef d^3p=-\frac{\partial}{\partial x}\int Ev_x f d^3p \quad \ldots\ldots(3) \qquad -\frac{\partial}{\partial x}\int p_x v_x f d^3p=\frac{\partial}{\partial t}\int p_x f d^3p\,. \quad \ldots\ldots(4)$$

We cannot assume that the distribution function f is equal to its undisturbed symmetrical value $f_0=1/\{\xi\exp(E/kT)\mp1\}$, because the right-hand sides of (3) and (4) would then vanish while the left-hand sides would not. Instead, we assume that there is a small distortion of the distribution function, and therefore put $f=f_0+f_1$, where f_1 is the unsymmetrical part. Since $\mathbf{v}$ and $\mathbf{p}$ are parallel vectors, averaging over angles gives $p_x v_x f\to\frac{1}{3}pvf_0$, while $v_x f\to v_x f_1\to vf'$ and $p_x f\to p_x f_1\to pf'$, f' being a measure of the distortion of the distribution function. Thus (3) and (4) become

$$\frac{\partial}{\partial t}\int Ef_0\,p^2\,dp=-\frac{\partial}{\partial x}\int Evf'\,p^2\,dp \quad \ldots\ldots(5) \qquad -\frac{1}{3}\frac{\partial}{\partial x}\int vf_0\,p^3\,dp=\frac{\partial}{\partial t}\int f'p^3\,dp\,. \quad \ldots\ldots(6)$$

The elimination of the unknown quantity f' is particularly simple for a phonon gas, for then $E=pc$ and $v=c$, and the integrals on the left-hand sides of (5) and (6) are identical, while the integral on the right-hand side of (5) is just c^2 times that on the right-hand side of (6). Thus $\partial^2/\partial t^2=\frac{1}{3}c^2\,\partial^2/\partial x^2$, leading to a velocity $c_2=c/\sqrt{3}$.

For a general energy spectrum, however, it is both simpler and more instructive to compare the equations with those of Landau's theory, rather than attempt to eliminate f' directly. The integrals on the left-hand sides of (5) and (6) are ordinary thermodynamic functions, for

$$\frac{4\pi}{h^3}\int Ef_0\,p^2\,dp=U\,, \qquad \ldots\ldots(7)$$

the internal energy per unit volume, while putting $v=\partial E/\partial p$ (cf. Dingle 1951, § 4, 1952, § 5), it is easily shown that, provided $E(p)\to\infty$ as $p\to\infty$,

$$-\frac{4\pi}{3h^3}\int vf_0\,p^3\,dp=F\,, \qquad \ldots\ldots(8)$$

the free energy per unit volume.* For small temperature fluctuations, and neglecting thermal expansion,

$$\partial U/\partial t=T\,\partial S/\partial t\;;\quad \partial F/\partial x=-S\,\partial T/\partial x\,,$$

so that (5) and (6) become

$$\frac{\partial S}{\partial t}=-\frac{\partial}{\partial x}\frac{4\pi}{Th^3}\int Evf'\,p^2\,dp \quad \ldots\ldots(9) \qquad -S\frac{\partial T}{\partial x}=\frac{\partial}{\partial t}\frac{4\pi}{h^3}\int f'p^3\,dp\,. \quad \ldots\ldots(10)$$

These equations may now be compared with the following arising in Landau's theory:

$$\frac{\partial S}{\partial t}=-\frac{\partial}{\partial x}(Sv_{\mathrm{n}}) \quad \ldots\ldots(11) \qquad -S\frac{\partial T}{\partial x}=\frac{\partial}{\partial t}\left(\frac{\rho_{\mathrm{n}}\rho v_{\mathrm{n}}}{\rho_{\mathrm{s}}}\right) \quad \ldots\ldots(12)$$

In (11) and (12) v_{n} is the 'drift velocity' of the excitations in the x direction. Since by (8)

$$S=-\frac{\partial F}{\partial T}=\frac{4\pi}{3h^3}\int v\frac{\partial f_0}{\partial T}p^3\,dp=-\frac{4\pi}{3Th^3}\int Ev\frac{\partial f_0}{\partial E}p^3\,dp \qquad \ldots\ldots(13)$$

the last step following from the fact that $f_0=f_0(E/T)$, agreement between our equation (9) and Landau's equation of entropy conservation (11) is obtained only if

$$f'=-\tfrac{1}{3}v_{\mathrm{n}}p\,\partial f_0/\partial E\,. \qquad \ldots\ldots(14)$$

* If the particles or excitations are conserved, the left-hand side of (8) is equal to $F-NE_0$, where N is their number and E_0 their degeneracy energy. The argument is unchanged.

Equation (14) shows that the literal interpretation of v_n as 'drift velocity' is not really necessary. Instead, it may just be regarded as a parameter representing the degree of distortion of the distribution function.

Introducing into the right-hand side of (10) Landau's effective mass-density in the form (cf. Dingle 1951, eqn. (4.7), 1952, (79))

$$\rho_n = -\frac{4\pi}{3h^3}\int p^4 \frac{\partial f_0}{\partial E}\,dp = \frac{4\pi}{v_n h^3}\int f' p^3\,dp \qquad \ldots\ldots (15)$$

it is seen that complete agreement between (10) and (12) is achieved only in the limit $\rho_s \to \rho$, i.e. $\rho_n = \rho - \rho_s \to 0$, which requires $T \to 0$. Put another way, our equations (9) and (10) would lead to a propagation velocity given by $c_2^2 = TS^2/C\rho_n$, where C is the specific heat per unit volume, as compared with Landau's relation $c_2^2 = TS^2\rho_s/C\rho\rho_n$ obtained from (11) and (12). The explanation of this discrepancy is probably that any description in terms of the excitations alone, such as that presented here, is adequate only if their effective mass is negligible compared with the inertial mass of the total assembly. Apart from this defect, the present treatment based on Maxwell's equation of transfer is, so far as it goes, essentially equivalent to Landau's more complete theory.

Royal Society Mond Laboratory,
Cambridge.
14th February 1952.

R. B. Dingle.

Dingle, R. B., 1951, *Phil. Mag.*, **42**, 1080; 1952, *Advances in Physics* (*Phil. Mag.* Suppl.), **1**, No. 2, 111.
Jeans, J. H., 1940, *Introduction to the Kinetic Theory of Gases* (Cambridge: University Press).
Landau, L. D., 1941, *J. Phys., U.S.S.R.*, **5**, 71.
Ward, J. C., and Wilks, J., 1952, *Phil. Mag.*, **43**, 48.

Diffusion in Gaseous Helium at Low Temperatures

Progress in recent years in the separation of ^{3}He and measurement of it sproperties have increased interest in theoretical estimates of these properties. Much has already been done in this direction in the calculation of critical constants and vapour pressure (de Boer and Lunbeck 1948, Lunbeck 1950), the equation of state (de Boer, van Kranendonk and Compaan 1950), and viscosity (Buckingham and Temperley 1950, de Boer and Cohen 1951) at low temperatures, where quantal effects are most important. This note adds information about the diffusion coefficient and thermal diffusion ratio in ^{3}He–^{4}He mixtures at 5° K and below.

The calculations use mainly an interatomic potential of the form introduced by Buckingham and Corner (1947) in dealing with the equation of state at higher temperatures. This is $V(r) = -\epsilon f(\sigma)$, $\sigma = r/r_0$ where ϵ, r_0 are respectively the depth and position of the minimum of $V(r)$, and the shape function is given by

$$f(\sigma) = f_1\sigma^{-6}(1+\beta\sigma^{-2}) - f_2\,e^{-\alpha(\sigma-1)}, \qquad \ldots\ldots (1)$$

where α, β are parameters, and $f_1 = \alpha/\{\alpha(1+\beta) - 6 - 8\beta\}$, $f_2 = -1 + (1+\beta)f_1$. Strictly, the above form is used only for σ greater than 1; when $\sigma < 1$ an exponential factor is introduced which has the effect of eliminating gradually the terms in σ^{-6}, σ^{-8}. Although the effect of varying α and β would be interesting, the values $\alpha = 13{\cdot}5$, $\beta = 0{\cdot}2$, known to be reasonably good, have been adhered to in the present work. It has also been assumed that $\epsilon = 14{\cdot}04 \times 10^{-16}$ erg, $r_0 = 2{\cdot}943$ Å, these values being based partly on a comparison with observed second virial coefficients of ^{4}He at low temperatures (Buckingham, Hamilton and Massey 1941). De Boer and his collaborators have used a potential of the usual Lennard-Jones type in their work.

The table contains the following results:

(1) The coefficient of diffusion, D_{12}, for a mixture of ^{3}He and ^{4}He at a pressure of 1 mm Hg. The values are small, but for temperatures above 3° K they are about twice those predicted by classical theory (Hirschfelder, Bird and Spotz 1948). (2) The thermal diffusion ratio k_T for a mixture containing a molar fraction γ_1 of ^{3}He. For potential (1) and $\gamma_1 = 0{\cdot}3$, $0{\cdot}5$,

0·7 results are given in columns (*a*), and it will be seen that the variation with γ_1 is asymmetric, being more heavily weighted on the side $\gamma_1 > 0{\cdot}5$. For comparison, some results obtained using quantal theory for rigid spheres of diameter 2·1 Å are given in column (*b*); also, the classical value for rigid spheres, which is independent of temperature. (3) The theoretical values of the viscosities, $\mu(^3\text{He})$ and $\mu(^4\text{He})$, which were used in the calculations of k_T. The values for ^{3}He were derived from potential (1), and supersede the preliminary results of Buckingham and Temperley (1950); those for ^{4}He are based on a slightly different potential used in earlier work, though the difference is unlikely to be important.

All these represent first order approximations only; second order corrections, though possibly increasing as T becomes very small, and largest in k_T, should not exceed a few per cent.

T (°K)	D_{12} (cm²/sec)	$-k_T \times 10^2$ (*a*) $\gamma_1=0{\cdot}3$	(*a*) 0·5	(*a*) 0·7	(*b*) 0·5	$\mu(^3\text{He})$ (10^{-6} c.g.s.)	$\mu(^4\text{He})$ (10^{-6} c.g.s.)
0·25		−6·9	−9·8	−10·0		2·35	0·52
0·5	0·028	−0·52	−0·68	−0·64	2·86	3·62	1·99
0·75	0·059	+1·25	+1·66	+1·56		4·90	3·25
1·0	0·098	2·16	2·85	2·68	2·17	6·25	3·48
1·25	0·144	2·29	3·03	2·87		7·53	3·61
1·5	0·198	1·99	2·65	2·52	1·98	8·69	3·84
2·0	0·325	1·88	2·49	2·36	1·83	10·3	4·82
2·5	0·478	1·78	2·34	2·20	1·71	11·2	6·05
3·0	0·655	1·69	2·20	2·03	1·65	11·8	7·47
3·5	0·855	1·63	2·09	1·90		12·1	9·08
4·0	1·07	1·60	2·03	1·83		12·5	10·8
4·5	1·32	1·64	2·06	1·83		13·0	12·2
5·0	1·58	1·80	2·22	1·93		13·7	13·0

For rigid spheres (classical theory), $-k_T \times 10^2 = 3{\cdot}09$, $\gamma_1 = 0{\cdot}5$.

It is perhaps worth noting the sudden change in sign of k_T near 0·5° K. The general behaviour of k_T, as might be expected, departs considerably from classical theory at these low temperatures. Thus the calculations of Hirschfelder, Bird and Spotz, using the Lennard-Jones potential, indicate that k_T is positive over a temperature range from about 4° K to 9·5° K (assuming $\epsilon/k \sim 10$° K), and attains a positive maximum of 0·0020 around 6° K.

Full details of this work will be published later. The calculation of transport properties at higher temperatures is also well advanced.

University College, London. R. A. Buckingham.
10th March 1952. R. A. Scriven.

de Boer, J., and Lunbeck, R. J., 1948, *Physica*, **14**, 510.
de Boer, J., van Kranendonk, J., and Compaan, K., 1950, *Physica*, **16**, 545.
de Boer, J., and Cohen, E. G. D., 1951, *Physica*, **17**, 993.
Buckingham, R. A., and Corner, J., 1947, *Proc. Roy. Soc.* A, **189**, 118.
Buckingham, R. A., Hamilton, J., and Massey, H. S. W., 1941, *Proc. Roy. Soc.* A, **179**, 103.
Buckingham, R. A., and Temperley, H. N., 1950, *Phys. Rev.*, **78**, 482.
Hirschfelder, J. O., Bird, R. B., and Spotz, E. L., 1948, *J. Chem. Phys.*, **16**, 986.
Lunbeck, R. J., 1950, *Dissertation*, Amsterdam.

Intensity Distribution of Bremsstrahlung from Beta-Rays

The emission of beta-rays is accompanied by internal bremsstrahlung, external bremsstrahlung and characteristic x-rays. This note is concerned only with the external bremsstrahlung. The intensity distribution, as a function of quantum energy, has been calculated approximately from the theory given by Heitler (1944), and the results have been checked by means of absorption measurements on the bremsstrahlung from ^{32}P.

The intensity distribution of external bremsstrahlung for an electron which has a particular kinetic energy E has been given by Heitler (1944, fig. 14). For moderate energies the shape of the intensity distribution is roughly independent both of the atomic number of the material through which the electron is passing and of the kinetic energy of the electron, and can be represented by the equation

$$I(h\nu) = 4 - 3h\nu/E, \quad (0 \leqslant h\nu \leqslant E, E \text{ being constant}). \qquad \ldots\ldots (1)$$

The intensity of bremsstrahlung at a particular quantum energy $h\nu$, radiated from the whole track of the electron, may be obtained by integrating eqn. (1) with respect to E from the initial kinetic energy E_0 down to $h\nu$; this gives

$$I(h\nu)=E_0\left\{4\left(1-\frac{h\nu}{E_0}\right)-3\frac{h\nu}{E_0}\log\frac{E_0}{h\nu}\right\}. \qquad \ldots\ldots (2)$$

The distribution of eqn. (2) is plotted as curve A in fig. 1, where the function $I(\lambda)$, $(\lambda=h\nu/E_0)$, has been normalized so that the area under the graph, which is the total intensity of bremsstrahlung radiated from the whole track of the electron, is unity. Since the shape of the distribution given by eqn. (2) is independent of the value of E_0, curve A applies to electrons of any initial kinetic energy up to a few MeV. To find the intensity distribution of bremsstrahlung from a radioactive isotope, eqn. (2) must be integrated over the beta-ray spectrum. This has been done numerically for ^{32}P, using the shape of the beta-ray spectrum given by Siegbahn (1946). The resulting intensity is plotted as curve B of fig. 1, where in this case $\lambda=h\nu/E_\beta$ and E_β is the maximum beta-ray energy. Curve B has also been plotted so that the area under the graph, which is the total intensity of bremsstrahlung radiated by the isotope, is unity. Since the shape of curve B is independent of the value of E_β, up to a few MeV, the curve gives the intensity distribution of bremsstrahlung from any isotope whose beta-ray spectrum has the same shape as ^{32}P.

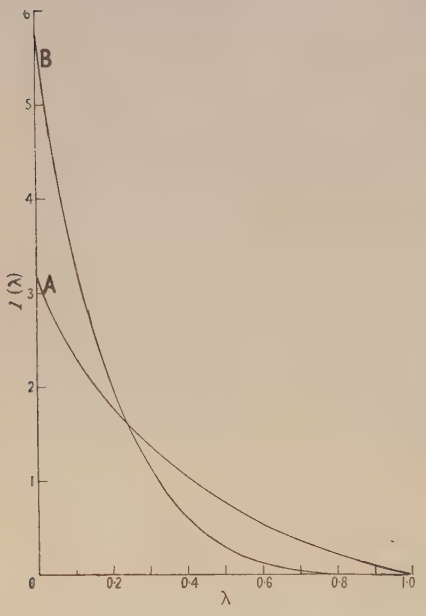

Fig. 1. Intensity distribution of bremsstrahlung from a single electron (curve A : $\lambda=h\nu/E_0$) ; and from a beta-ray spectrum (curve B : $\lambda=h\nu/E_\beta$).

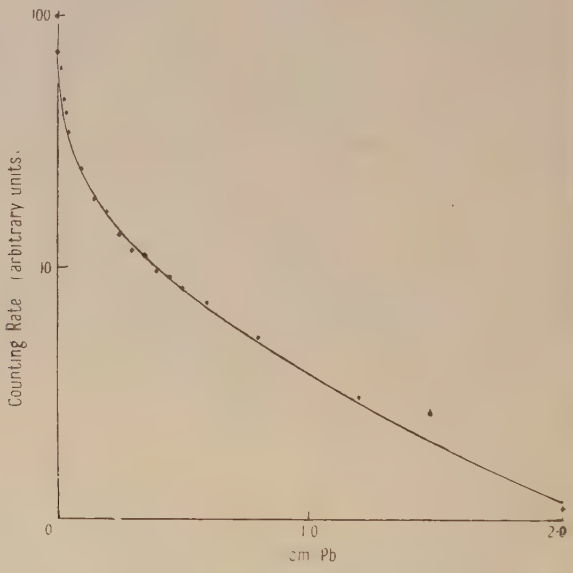

Fig. 2. Absorption in lead of bremsstrahlung from ^{32}P. The curve is calculated from theory, the dots are measured values.

In order to check these calculations, measurements were made of the absorption in lead of the bremsstrahlung from ^{32}P. The geometry of the experiment was good. The source of radiation consisted of 10 g of red phosphorus (B.D.H. ground), irradiated in the pile at Harwell, and contained in a thin-walled brass box. The total radiation from such a source consists of external bremsstrahlung, internal bremsstrahlung and characteristic x-rays, plus any gamma-radiation due to contamination. The total intensity and the intensity distribution of the internal bremsstrahlung has been calculated by Knipp and Uhlenbeck (1936), and measured by Wu (1941) and by Mandanski and Rasetti (1951). For the source used in this experiment the total intensity of the internal bremsstrahlung is about 20% of the intensity of the external bremsstrahlung, and the intensity distribution is not very different from that of curve B. Hence the internal bremsstrahlung will have a negligible effect on the shape of the absorption curve. The characteristic x-rays are so soft that they will be almost

completely absorbed in the wall of the counter. The intensity of gamma-radiation due to contamination was calculated from a chemical analysis of the phosphorus and should have been negligible. However, the first absorption measurements revealed the presence of a strong gamma-ray of about 1·75 MeV quantum energy. Fortunately the contaminating gamma-radiation decayed with a half-life of about 15 hours (it was probably due to ^{24}Na), so that a week later its effect was negligible. The absorption curve in lead was now measured again, with the results shown by the dots in fig. 2. The probable error was 2% in most cases.

The curve of fig. 2 was calculated from the intensity distribution of fig. 1, curve B, taking into account the variation of the counter sensitivity with quantum energy (Renard 1948, down to 0·1 MeV, Saurer 1950, below 0·1 MeV) and the initial filtration of the brass box. The agreement is good beyond 0·5 mm of lead, but the measured points indicate a rather greater proportion of very soft radiation than was calculated.

Radiotherapy Department,
University College Hospital,
London W.C.1.
18th February 1952.

S. J. WYARD.

HEITLER, W., 1944, *The Quantum Theory of Radiation*, 2nd edn. (Oxford: University Press).
KNIPP, J. K., and UHLENBECK, G. E., 1936, *Physica*, **3**, 425.
MANDANSKI, L., and RASETTI, F., 1951, *Phys. Rev.*, **83**, 187.
RENARD, G. A., 1948, *J. Phys. Radium*, **9**, 212.
SAURER, H., 1950, *Helv. Phys. Acta*, **23**, 381.
SIEGBAHN, K., 1946, *Phys. Rev.*, **70**, 127.
WU, CHIEN-SHIUNG, 1941, *Phys. Rev.*, **59**, 481.

REVIEWS OF BOOKS

An Introduction to Experimental Physics, by H. G. JERRARD and D. B. MCNEILL. Pp. 576. (London: Harrap, 1951.) 25*s*.

Anyone who has had the responsibility of organizing an elementary physical laboratory is aware of two important problems: (i) Are students to be provided with manuscript directions appropriate to each experiment and the apparatus which is available for its performance? Or are they to be expected to purchase a textbook of practical physics, the exercises in which approximate fairly closely to what can be done with the available apparatus? (ii) Bearing in mind the limited number of sets of apparatus for a particular exercise, how are the experiments performed by the students to be linked with the theoretical treatment of the subject in the class-room or lecture theatre?

The book under review undoubtedly provides an exhaustive collection of experimental exercises suitable for an intermediate course in physics; but for this very reason, in size and price it compares with several well-known textbooks of theoretical intermediate physics. At a price of twenty-five shillings it is certainly value for money by modern standards; yet it is doubtful whether all the students using a particular laboratory could be expected to possess a copy, in addition to equally expensive and more necessary books which cover the theoretical aspect of the subject. It does not seem, therefore, to be a substitute for 'manuscripts'. Moreover, few students would cover adequately all of its 180 experiments in the time usually available for practical work. Inevitably, therefore, selection is necessary; and the book appears to be more suitable as a volume of reference in the laboratory than as a manual to be possessed by every student.

The problem of linking a student's experimental and theoretical work is met by giving a fairly complete preliminary account of the principles underlying the group of related experiments which form the contents of each particular chapter. Thus the volume is self-contained and on the whole orderly. It seems strange, however, that a fairly full treatment of pendulums, including the compound bar pendulum, in Chapter VIII, should precede the verification of the elementary laws of dynamics by means of Fletcher's trolley in Chapter XIII. This again suggests that the book is most suited to be a work of reference.

Criticism of the book must be made on a number of points of detail. Though the diagrams are clearly drawn, a few are inaccurate or misleading. For instance, fig. 30 suggests an extremely orderly packing of the molecules of a liquid. Surely, unequal, randomly oriented forces could be shown in equilibrium. Fig. 31 shows *two* distinct normals at a single point on a curved liquid surface! The treatment of the telescope (pp. 331–5) suffers in that the diagrams show no rays, other than paraxial rays, passing right through the system. Fig. 300, illustrating the forces on the needle of a dip circle, in two planes at right angles, is obviously in error. The points O, A, C, B should appear in perspective as the corners of a parallelogram. There is also a certain amount of unnecessary duplication of diagrams. For example, 267 repeats 246; 268 repeats 247; 302 repeats 281.

In the section on magnetism and electricity the reviewer feels that a more critical attitude might well have been adopted towards a number of well-known but not very valuable exercises. Hibbert's magnetic balance appears to be somewhat out of place in a modern textbook, particularly without any discussion of the mutual demagnetization of the magnets; and, in any case, the apparatus would be unworkable if the suspended magnet were 'supported at its centre on a knife-edge', as stated (p. 421), or worse still as it is shown in fig. 284. The location of neutral points is discussed without reference to Owen's method except in a short footnote (pp. 410–4). The moments of magnets are compared by the 'sum and difference' method, again without reference to the precaution which is essential in order to avoid demagnetization (p. 428). Ohm's law is 'verified' by voltmeter and ammeter, and only a footnote suggests that the experiment is worthless except as a very elementary illustration of the law (p. 460). The 'sum and difference' method of comparing the e.m.f.'s of cells is given without any reference to the well-known objection to this exercise (p. 481). The Wheatstone net is given in every case without a reversing key (pp. 493–507). Presumably it is only by an oversight that we read on p. 467: "The absolute value of the volt is 10^8 ergs"; while the section in which this statement occurs gives, to say the least, a misleading impression of the present status of the 'international' volt, ampere and ohm.

However, the book is clearly written, well-printed, and stoutly bound. Full use is made of graphical methods of representation, including the plotting of logarithms. The inclusion of 'worked examples' sets a high standard for the student's notebook, which the reviewer hopes will be copied. The defects that are noted above can easily be remedied in a future edition, and the book should find a place in many physical laboratories in schools and colleges, where it will serve a useful purpose as a singularly full and complete textbook of experimental physics.

G. D. Y.

Differential Equations, by H. B. Phillips. Pp. viii + 149. 3rd Edition revised. (New York: Wiley and Sons; London: Chapman and Hall, 1951.) 24*s*.

This is a most attractive introduction to the subject, intended mainly for physicists and engineers. While providing some formal instruction in the solution of simple ordinary differential equations, most emphasis is placed on the setting-up and solution of differential equations arising in Applied Mathematics, Physics, Chemistry, etc., such physical principles as are required being briefly described in the text.

Chapter I deals with those first-order equations which can be solved by separation of the variables, with a wide variety of applications.

Chapter II completes the work on first-order equations, exact, linear and homogeneous equations being discussed. The integrating factor for the general linear equation is merely stated and verified. A direct derivation would take very little extra space. The alternative method of solving the same type of equation given on p. 44 so obviously comes to the same thing that it could well be omitted. The chapter ends with a brief description of simultaneous equations and solution by change of variable.

The simpler types of second-order equation, i.e. those in which x or y is explicitly absent and homogeneous equations, are dealt with in Chapter III. Theoretical discussion is confined to eight pages only, but there are many worked examples, including a section on the motion of dynamical systems of varying mass.

The final chapter treats linear equations of the nth order with constant coefficients in an elementary way, operational methods receiving only a brief mention.

In addition to about seventy illustrative examples worked out in full in the text, there are nearly five hundred exercises, for which answers are provided at the end of the book.

A. N. GORDON.

The Interpretation of X-ray Diffraction Photographs, by N. F. M. Henry, H. Lipson and W. A. Wooster. Pp. ix+258. (London: Macmillan, 1951.) 42*s*.

The appearance of this book marks a stage in the development of x-ray crystallography. A considerable number of books have been written on the subject, but this is the first textbook written specifically for the student pursuing a systematic course of study. X-ray crystallography has become an essential tool in many types of research, both fundamental and applied, and is increasingly used in industry. The need for the training of x-ray crystallographers has been recognized in recent years and steps taken to provide it. This book will be of very great assistance in this task.

The book covers the interpretation of x-ray diffraction effects from crystalline material, but does not deal with space group theory or the derivation of atomic positions from a list of corrected intensities. It has an excellent system of cross reference and a large number of original papers are referred to. The photographs and charts are produced to scale so that the student can carry out each step of the interpretation himself. A number of very useful tables are given in appendices.

It is sufficient recommendation to say that this book is an essential textbook for any serious student of the subject, and, since it has no competitor, the remainder of this review can safely be devoted to suggestions for improvements in the next edition, which is certain to be required very soon.

In the first place there is a certain lack of balance which is possibly due to the book's triple authorship. The interpretation of Laue photographs is dealt with in great detail and occupies 16 pages, together with four more in the chapter on crystal setting. On the other hand, the interpretation of Weissenberg photographs is covered in 14 pages, and the measurement and correction of intensities (including a discussion of structure factor theory) also receives only 14 pages. In the latter case, the geometrical factor for equi-inclination Weissenberg photographs is not considered at all, and, in general, practical details of the methods of correction are dealt with only by references to original papers. In other places the text appears to be condensed to a degree which makes comprehension unnecessarily difficult. In view of the fact that the indexing of Laue photographs is only very rarely required, it is difficult to justify the relative space given to this subject.

The second main criticism concerns the interpretation of oscillation photographs. In the process of setting a crystal, the recognition of salient features of a tilted reciprocal lattice may be a major step. This recognition is facilitated if one is in the habit of viewing the reciprocal lattice and sphere of reflection with the x-ray beam coming towards the observer. In the book under review, however, these are presented with the x-ray beam going away from the observer.

The problems of determining the azimuthal orientation of a crystal and the β-angle of a monoclinic lattice are insufficiently developed. A section on the design and use of camera arcs could well have been included in Chapter 4.

There are two points of presentation which the reviewer would like to see incorporated. The effect of the Laue conditions for diffraction can be most easily visualized by the use of three intersecting cones whose axes coincide with the crystal lattice axes. It seems a pity that this should have been left out.

The second point concerns the use of the reciprocal lattice in interpreting effects due to the ' white ' radiation. The method adopted is to keep the reciprocal lattice fixed and vary the size of the sphere of reflection. However, for some purposes it is desirable to keep the sphere of reflection fixed in size and associate a weighted radial line with each characteristic point of the reciprocal lattice. This line is limited towards the origin by the short wavelength cut-off, and fades out on the other side of the characteristic point. The production of Laue streaks on constant ρ curves, and the measurement of the end positions of a streak in an oscillation photograph on $(90°-\phi)$ curves, can be easily visualized in this way.

In the chapter on fibre photographs the problem of interpreting a complicated fibre diagram, such as is given by some minerals, is not really tackled at all. The starting point for interpretation is given as the ' indexing of the power lines '. In the case of mineral fibres, the occurrence of a fibre photograph is usually the only thing that makes indexing possible at all, and the problem is even then often a difficult one. It is best approached by means of the reciprocal lattice, a concept which is not used in this chapter at all. A further section to the chapter on fibre photographs is certainly required.

The numerous diagrams are almost all excellent. Two or three could have minor improvements to make them more readily understandable.

The book is very well produced and very few misprints have crept into the text.

The index, while not very detailed, is sufficient, if one is prepared to look for a rather general heading and search a few pages of text to find the detailed reference required. This is comparatively simple since the text is divided into small sections which have clear headings.

The points of criticism raised above are comparatively minor ones which are almost inevitable in the first edition of a pioneering book. Future generations of students and teachers of x-ray crystallography will have reason to be grateful to the authors for the care and thoroughness with which they have made available their unrivalled experience in the wide field covered by this book.

J. W. JEFFERY.

Recommendations for Waste Disposals of Phosphorus-32 and Iodine-131 for Medical Users, by U.S. Department of Commerce, National Bureau of Standards. Pp. iv+11. (Washington, D.C.: Government Printing Office.)

CONTENTS FOR SECTION B

PAGE

Dr. H. J. GRENVILLE-WELLS. The Texture of Diamonds used for Counting α, β or γ Particles as found from Divergent-Beam X-Ray Photographs . 313

Dr. J. F. RAFFLE and Mr. E. J. ROBBINS. Non-Linear Amplification in E.M.I. Photomultipliers 320

Prof. R. M. CHAUDHRI and Mr. M. A. BAQUI. On the Measurement of Current Density at the Cathode of a Glow Discharge and Aston's Law at Low Pressures and High Discharge Voltages 324

Dr. K. S. W. CHAMPION. The Theory of Gaseous Arcs: I—The Fundamental Relations for the Positive Columns. 329

Dr. K. S. W. CHAMPION. The Theory of Gaseous Arcs: II—The Energy Balance Equation for the Positive Columns 345

Mr. N. R. LABRUM and Mr. E. K. BIGG. Observations on Radio-Frequency Oscillations in Low-Pressure Electrical Discharges 356

Dr. R. BECHMANN. An Improved Frequency Equation for Contour Modes of Square Plates of Anisotropic Material 368

Dr. R. BECHMANN. Elastic and Piezoelectric Coefficients of Lithium Sulphate Monohydrate 375

Dr. A. F. GIBSON. The Absorption Spectra of Single Crystals of Lead Sulphide, Selenide and Telluride 378

Letters to the Editor:

Dr. E. H. PUTLEY. Electrical Conductivity in the Compounds PbS, PbSe, PbTe 388

Dr. G. O. JONES and Mr. F. F. ROBERTS. The Spontaneous Magnetization of Magnesium Ferrite and Magnesium Ferrite-Aluminate Powders at Low Temperatures 390

Reviews of Books 391

Contents for Section A 394

Abstracts for Section A 395

ABSTRACTS FOR SECTION B

The Texture of Diamonds used for Counting α, β or γ Particles, as found from Divergent-Beam X-Ray Photographs, by H. J. GRENVILLE-WELLS.

ABSTRACT. Since the radiation-counting efficiency of diamonds is a structure-sensitive property, x-ray experiments have been undertaken to see whether it is related to crystal texture. A technique for obtaining divergent beam photographs superimposed on Laue photographs has been developed, and results are given for 28 out of 38 colourless octahedral diamonds (edge 1–3 mm) whose ultra-violet transparency, β-particle counting efficiency and fluorescence are known. The relative strength of the anomalous extra x-ray reflections generally found for comparatively perfect diamonds has also been determined for these 38 specimens. Counting efficiency does not seem to be closely related to texture and, in particular, mosaicity is not a necessary condition.

Non-Linear Amplification in E.M.I. Photomultipliers, by J. F. RAFFLE and E. J. ROBBINS.

ABSTRACT. The output pulse heights obtained from E.M.I. photomultipliers are found not always to be proportional to the quantity of light incident on the photo-surface of the photomultiplier. The photomultiplier ceases to be a linear amplifier of the incident light pulses when the charge density in the multiplier becomes too great.

The relation between pulse height and energy loss of alpha-particles in various fluorescent materials has been determined at low values of charge density.

On the Measurement of Current Density at the Cathode of a Glow Discharge and Aston's Law at Low Pressures and High Discharge Voltages, by R. M. CHAUDHRI and M. A. BAQUI.

ABSTRACT. A method has been described for determining the current density on a plane cathode of a glow discharge over a wide range of pressure and voltage. It is shown that Aston's relation, $V=E+F\sqrt{i}/P$, holds good down to as low a pressure as 2×10^{-2} mm Hg and up to as high a voltage as 3000 volts. The work of the earlier investigators extends up to a voltage of about 1000 volts and a pressure not much below 10^{-1} mm Hg. It is also seen from these experiments that the distribution of current over a plane cathode is a function of the discharge pressure and is in general independent of voltage and current.

The Theory of Gaseous Arcs: I—The Fundamental Relations for the Positive Columns, by K. S. W. CHAMPION.

ABSTRACT. It is postulated that the five fundamental relations, stated by Tonks and Langmuir to be sufficient to describe fully a low pressure positive column, also apply to high pressure positive columns. Previously, only two of these relations had been applied to high pressure columns. A 'natural arc radius' is postulated for low pressure arcs when the boundaries are removed an indefinite distance. Previous theories of low pressure arcs always assumed that the arc completely filled the cross section of its containing vessel and thus did not apply to low pressure arcs in large chambers or arcs at intermediate pressures.

The theory of low pressure arcs with high electron densities in which ionization by stages is important is developed. It is then shown that by taking recombination into account this theory may be applied to intermediate and high pressure arcs with a high degree of ionization. A first approximation is also obtained for the theory of high pressure arcs in which there is a low degree of ionization. All the theory presented includes the effect of a longitudinal magnetic field, and the no-field conditions are included as a special case. It is found that the effects of a magnetic field predicted by the theory are in agreement with experimental observations.

The Theory of Gaseous Arcs: II—The Energy Balance Equation for the Positive Columns, by K. S. W. CHAMPION.

ABSTRACT. The theory of arcs is developed further by investigating the energy balance equation for high pressure positive columns. The energy balance equation put forward by Suits and based on the Nusselt relation is considered and some refinements in his analysis result in better agreement between theory and experiment. This theory only takes into account energy losses due to convection and conduction, but the neglect of radiation losses is justified for a wide range of conditions by reference to experimental values of radiation efficiencies.

The effect of a longitudinal magnetic field on high pressure arcs is then investigated. From the point of view of the energy balance equation the action of a magnetic field is to reduce the contributions of the charged particles to the conduction and convection losses from the column. Horizontal and vertical arcs are considered separately, as the nature of the convection, and hence the effect of a magnetic field, is not the same in the two cases.

The theory predicts that the action of a magnetic field will tend to a limit with sufficiently strong fields, and certain simple relations are deduced which should apply in this case. According to the theory, when the radius of a high pressure arc is reduced by a magnetic field the arc temperature must rise (incidentally, only by a relatively small amount) and the positive column gradient may increase or decrease, depending on certain relations which are specified. There are virtually no experimental data available for these conditions, but the scant data available are in general agreement with the theory.

Observations on Radio-Frequency Oscillations in Low-Pressure Electrical Discharges, by N. R. LABRUM and E. K. BIGG.

ABSTRACT. The generation of high-frequency energy by electrical discharges in air at low pressures has been investigated by observations with several types of discharge tubes, at frequencies near 200 Mc/s and below 2 Mc/s.

Random noise of high intensity was observed in both these frequency ranges, and was found to be associated with a field reversal in the discharge.

Coherent oscillations were also observed at the lower frequencies, and there was evidence that these were the cause of the striations of the positive column.

An Improved Frequency Equation for Contour Modes of Square Plates of Anisotropic Material, by R. BECHMANN.

ABSTRACT. An improved approximation, based on previous work, has been derived for the frequency equation covering the four contour modes of vibration of square plates of anisotropic material. The modes consist of three longitudinal and one shear mode. An X-cut quartz, a Y-cut EDT and Yψ-cut lithium sulphate plates have been used as examples. The equation has been used to determine the elastic coefficients s_{55} and s_{13} of EDT and lithium sulphate monohydrate.

Elastic and Piezoelectric Coefficients of Lithium Sulphate Monohydrate, by R. BECHMANN.

ABSTRACT. A new determination has been made of the elastic and piezoelectric coefficients of lithium sulphate monohydrate and of their temperature coefficients.

The Absorption Spectra of Single Crystals of Lead Sulphide, Selenide and Telluride, by A. F. GIBSON.

ABSTRACT. The absorption spectra of single crystals of PbS, PbSe and PbTe have been examined in the temperature range from 20°K to 600°K. The spectra are characterized by a sharp absorption edge which coincides with the long wavelength limit of photoconductivity in each material. At longer wavelengths the absorption coefficient increases slowly with increasing wavelength, as in germanium and silicon.